Studies in Coherent Control of Optical Processes

A THESIS

submitted for the Award of Ph.D degree of

Mohan Lal Sukhadia University

in the

Faculty of Science

BY

Shubhrangshu Dasgupta

Under the Supervision of

Prof. G.S. Agarwal

Director, Physical Research Laboratory

DEPARTMENT OF QUANTUM OPTICS and QUANTUM INFORMATION

PHYSICAL RESEARCH LABORATORY, AHMEDABAD.

MOHANLAL SUKHADIA UNIVERSITY, UDAIPUR

Year of submission: 2004

CERTIFICATE

This is to certify that the thesis entitled "Studies in Coherent Control of Optical Processes" submitted for the award of the degree of Doctor of Philosophy of Mohanlal Sukhadia University in the faculty of Science is a record of bonafide investigations carried out by Shri. Shubhrangshu Dasgupta under my supervision and guidance.

This is an original piece of work on which no one has been awarded a degree in this University or in any other University.

The literary presentation of the thesis is satisfactory and it is in a form suitable for publication. The work presented in the thesis has been done after registration in this University.

Further, the candidate has put in attendance of more than 200 days in my institution as required under rule 7(b) and thus completed the residential requirement.

Prof. G.S. Agarwal
(SUPERVISOR)

to

the memory of my father

Contents

Acknowledgement

I take this opportunity to express my sincere gratitude to Prof. G. S. Agarwal for his excellent guidance, encouraging support and many valuable suggestions. I have benefited much from his clarity of physical ideas, working on fundamental problems and overall his clear approach in solving the problems. His professional, strict behavior and his exceptional capacity to work on many different areas of the subject always inspires me to take research as a serious part of life.

I would also like to thank all of my colleagues in PRL the academic discussions with whom turned out to be much fruitful in course of my research.

I bid my special thanks to Ashoka, who has poured constant inspiration and motivation in different stages during my research work.

Finally, I thank my parents for their invaluable support, sacrifice, and love all along, without which I could not be here where I am now.

Shubhrangshu Dasgupta

Abstract

In chapter 1.1, the basic theory of radiation-matter interaction is introduced. Some relevant properties of density matrix equations and the derivation of interaction Hamiltonian in dipole approximation are discussed. In chapter 1.2, an overview of the atomic coherence effects, like coherent population trapping, lasing without inversion, electromagnetically induced transparency is presented. Specific emphasis on dispersion management as an important aspect of coherent control is given.

In chapter 2, propagation of a linearly polarized pulse through an anisotropic medium is analyzed. It is shown that the orthogonal pulse components can be separated in time due to application of a resonant control field in suitable transition. The property of electromagnetically induced transparency (EIT) is properly exploited in this context. Demonstration of pulse splitting phenomenon is presented to support the physical prediction. An estimate of the broadening of the pulse component at the output end of the medium is given.

In chapter 3, dependence of the absoprtion coefficient on the direction of magnetic field is analyzed in context of propagation of an unpolarized light in an anisotropic medium. It is shown that using a resonant coherent field, it is possible to create asymmetry in the output intensity of the unpolarized field, for two opposite directions of the applied dc magnetic field. This phenomenon is termed as magnetic field reversal asymmetry (MFRA). Typical parameter zone is identified so that upon reversing the direction of this magnetic field, an opaque medium can be made transparent and vice versa. Effect of atomic velocity on this phenomenon is investigated. It is emphasized that the MFRA is a manifestation of dipole effect and thus much larger in magnitude compared to a similarly looking phenemenon called magneto-chiral anisotropy, which is an effect of higher order moments.

In chapter 4, the effect of nonmonochromaticity of the interacting field on the magneto-optical rotation (MOR) angle is investigated. The linear depen-

dence of the MOR angle on the optical density breaks down for larger values of spectral width of the field. The theoretical results are shown to be in good agreement with a relevant experiment.

In chapter 5, the possibility of non-zero susceptibility at two-photon resonance and of gain in a medium is predicted. This can be understood as an effect of coherence induced by an extra control field in a Λ system. Proper dressed state analysis is provided to show that the gain arises due to population inversion in dressed state basis. Further, large MOR angle can be achieved by applying this extra control field.

In chapter 6, the effect of a classical control field on fidelity of an atomic cloner in a cavity QED situation is investigated. It is shown that the control field can improve the fidelity for long times much above the optimal limit. The proper physical explanation of this effect is given in terms of the Rabi cycling. Further, the question of universality of the cloner driven by the coherent field is addressed. The case of a two-atom cloner is also analyzed.

In appendices, the analysis of the interaction of fields with atoms in the three standard three-level configurations, namely Λ, V, and Ladder system, is provided. Dressed state analysis of each of these configurations is included. The analytical result for broadening of the pulse, propagating through a coherent medium is given.

Chapter 1

Introduction

Optics is one of the most interesting subject by its fundamental nature. Physicists have put plenty of efforts to understand the nature of light. Further, light-matter interaction is another key area of research. After the discovery of laser by Schwallow and Townes in mid-twentieth century, a new era in this area has emerged. Our ability of using the coherent light sources for selective transitions and high tunability of its frequency and energy have extensively contributed to understand various physical processes. By the end of the twentieth century, lasers have found immense applications in all facets of life, namely, bio-science, space science, defence, computing and communication etc. Lasers are used for high precision measurements. In last few decades, further developments in both theoretical and experimental research have taken place in this field. Lasers are becoming key instrument in modifying and controlling the optical properties of matter and spectral properties of the emitted radiation. For example, experiments have been performed to demonstrate subluminal and superluminal group velocities of light pulse inside a coherent medium. Bose-Einstein condensation, control of molecular processes etc. are now possible using the atom-laser interaction. A new field called *coherent control* has thus branched out in the study of light-matter interaction. The present thesis describes various application-oriented aspects of coherent control.

1.1 Interaction of radiation with matter

Most of the natural optical processes can be easily explained in terms of wave nature of light. Since the corpuscular theory of Newton, the understanding of nature of light has been far revolutionized through ages. In present day scenario, light can be treated either classically or quantum-mechanically, depending upon the problems one is interested in. However, in most of the problems we deal with, it suffices to consider only the classical nature of the electromagnetic (em) field. On the other hand, microscopic systems (like atoms or electrons) are to be treated quantum mechanically. Thus we adopt a treatment called *semiclassical* theory of the interaction of light with matter, in which the radiation field is treated classically and the matter is treated as a quantum mechanical particle having discrete energy levels. We describe this theory in the next few subsections.

1.1.1 Classical electromagnetic theory : Classical picture of radiation

We consider propagation of the em field inside a nonmagnetic medium. This propagation can be described by the following four *macroscopic* Maxwell's equations in CGS units [1]:

$$\vec{\nabla}.\vec{D} = 0\,, \tag{1.1a}$$

$$\vec{\nabla}.\vec{B} = 0\,, \tag{1.1b}$$

$$\vec{\nabla}\times\vec{E} = -\frac{1}{c}\frac{\partial\vec{B}}{\partial t}\,, \tag{1.1c}$$

$$\vec{\nabla}\times\vec{H} = \frac{1}{c}\frac{\partial\vec{D}}{\partial t}\,, \tag{1.1d}$$

where $\vec{E}$ and $\vec{B}$ are the macroscopic electric and magnetic induction vectors at certain space-time point $(\vec{r},t)$ and c is the velocity of the em field in vacuum. Here we have assumed that the medium is free of any bound charge and also is non-conducting. Further, there is no free charge in the medium, as well. Thus all the source terms like charge density and current density are zero. It should be mentioned here that the above quantities are macroscopic in the sense they are the average contributions from all the microscopic constituents, namely the tiny

atoms, inside the medium. The above equations are valid for contribution from each atom also, but one requires a quantum mechanical framework for treating them.

The macroscopic displacement vector $\vec{D}$ and the magnetic field vector $\vec{H}$ inside a static nonmagnetic medium are given by

$$\vec{D} = \vec{E} + 4\pi\vec{P} + \cdots \,, \;\; \vec{H} = \vec{B} + \cdots \,, \tag{1.2}$$

where $\vec{P}$ is the macroscopic electric dipole moment per unit volume. The macroscopic electric dipole moment density is very often called as macroscopic polarization. Here we have assumed that the higher order moments are negligible than the dipole moment density $\vec{P}$ in Eq. (1.2). Because the medium is nonmagnetic, we get $\vec{B} = \vec{H}$. Then using the curl equations in the Maxwell's equations, we obtain the following:

$$\vec{\nabla} \times \vec{\nabla} \times \vec{E} + \frac{1}{c^2}\frac{\partial^2}{\partial t^2}(\vec{E} + 4\pi\vec{P}) = 0 \,. \tag{1.3}$$

We consider the medium with no bound charges. Thus, $\vec{\nabla}.\vec{D} = 0$. Writing $\vec{D} = \epsilon\vec{E}$, where ϵ is the electric permittivity tensor and function of field frequency, we get $\vec{\nabla}.\vec{E} = 0$, Thus the above equation reduces to

$$\nabla^2\vec{E} - \frac{1}{c^2}\frac{\partial^2\vec{E}}{\partial t^2} = \frac{4\pi}{c^2}\frac{\partial^2\vec{P}}{\partial t^2} \,. \tag{1.4}$$

Note that the polarization $\vec{P}$ is induced in the medium by the applied electric field $\vec{E}$. In a dielectric medium due to local field effect, this can be expressed as $\vec{P} = \chi\vec{E}$, where χ is a dimensional parameter called *linear susceptibility* of the medium. However, the polarization $\vec{P}$ may have nonlinear dependence on the electric field for large electric field. Thus from (1.2), we can write $\vec{D} = (1 + 4\pi\chi)\vec{E}$, such that $\epsilon = 1 + 4\pi\chi$.

The Eq. (1.4) can be easily solved with certain boundary condition or with certain forms of the electric field. We start with a plane monochromatic wave (with angular frequency ω) propagating in the z-direction in an atomic gas medium. The corresponding electric field can be written as

$$\vec{E}(z,t) = \hat{\epsilon}\mathcal{E}(z,t)e^{ikz - i\omega t} + \text{c.c.} \,, \tag{1.5}$$

where $\hat{\epsilon}$ is the polarization of the field and $\mathcal{E}(z,t)$ is the slowly varying amplitude. Here, it is assumed that the spread of the electric field in the direction transverse to the propagation direction is negligible. The magnetic field component of the em field is very weak in magnitude and we will not consider the effect of that component in the kind of problems to be discussed in this thesis. The polarization that is induced inside the medium by the applied electric field is given by

$$\vec{P}(z,t) = \hat{\epsilon}\mathcal{P}(z,t)e^{ikz-i\omega t} + \text{c.c.}\ , \tag{1.6}$$

Because the bound electron in an atomic medium suffers much larger electrostatic field (due to interaction with the nucleus) than the applied electric field, then the applied electric field can be treated as a perturbation. Thus we can expand the polarization as a power series expansion of the electric field as

$$P(z,t) = \chi^{(1)}E(z,t) + \chi^{(2)}E^2(z,t) + \chi^{(3)}E^3(z,t) + \cdots\ , \tag{1.7}$$

where $\chi^{(n)}$ is the nth order susceptibility. Because a weak field is used in the problems to be discussed in the present thesis, so we limit ourselves upto the linear term above. Further, any physical system requires some time to respond to the excitation. Thus, the polarization at a given time t depends upon polarizations of the medium at earlier times. Then the space component of the linear polarization can be written as

$$P_\alpha(z,t) = \sum_\beta \int_{-\infty}^{t} d\tau \chi^{(1)}_{\alpha\beta}(t-\tau)E_\beta(z,\tau)\ , \tag{1.8}$$

where $\chi^{(1)}_{\alpha\beta}$ represents the linear susceptibility of the medium and is a tensor of rank 3 [1]. If we assume that the field under consideration is a continuous wave, then we can neglect the time-dependence of $\mathcal{E}$. Thus, the above relation reduces to

$$P_\alpha(z,t) = \sum_\beta \chi^{(1)}_{\alpha\beta}(\omega)E_\beta(z)e^{ikz-i\omega t} + \text{c.c.}\ , \tag{1.9}$$

[1] In general, the susceptibility tensor being a tensor of rank 3 has nine components $\chi_{\alpha\beta}$, $\alpha,\beta \in x,y,z$. In our analysis, we have assumed that the light propagates in the z-direction. Thus in (1.8), only $\chi^{(1)}_{zz}$ contributes, because the polarization $P(z,t)$ has the same direction as of $E(z,t)$. It can be shown however that structure of an anisotropic medium permits two different polarization directions with different velocities to propagate in any given direction. As for a given propagation direction of the electric field, two polarization directions are allowed and for each such direction, susceptibilities can have two different values in an anisotropic medium.

where $\chi^{(1)}_{\alpha\beta}(\omega)$ is the Fourier transform of $\chi^{(1)}_{\alpha\beta}(t)$ and is given by

$$\chi^{(1)}_{\alpha\beta}(\omega) = \int_0^\infty dt \chi^{(1)}_{\alpha\beta}(t) e^{-i\omega t} \ . \tag{1.10}$$

Note that the space dependence of the polarization comes only from the electric field, but there is no space dependence of the susceptibility. The time-dependence of the $\chi_{\alpha\beta}$ has been absorbed through Fourier transform. Moreover, we are interested in the long-time behavior of the medium properties, which is well-known as the steady-state behavior. In this time-limit, the time-dependence of the medium properties vanishes.

Now we can consider two different cases : (a) an isotropic medium and (b) an anisotropic medium. In an isotropic medium, the medium responds to the electric field symmetrically in all directions. On the other hand, in an anisotropic medium, the response of the medium becomes different for different directions of polarization of the applied electric field. Thus for an isotropic medium, only the diagonal elements of the susceptibility tensor are nonzero and are equal. But for an anisotropic medium, the tensorial diagonal elements have unequal values, which means that $\chi_{\alpha\alpha} \neq \chi_{\beta\beta}$. Moreover, from Maxwell's equations, it can be shown that this tensor must be symmetric, i.e., $\chi_{\alpha\beta} = \chi_{\beta\alpha}$ [1]. In the present thesis, we concentrate on the anisotropic medium.

Now we again consider the Eq. (1.4), which for an electric field propagating in the z-direction [see Eq. (1.5)] reduces to

$$\frac{\partial^2 \vec{E}}{\partial z^2} - \frac{1}{c^2}\frac{\partial^2 \vec{E}}{\partial t^2} = \frac{4\pi}{c^2}\frac{\partial^2 \vec{P}}{\partial t^2} \ . \tag{1.11}$$

We now consider the following approximations, namely

$$\left|k\frac{\partial \mathcal{E}}{\partial z}\right| \gg \left|\frac{\partial^2 \mathcal{E}}{\partial z^2}\right| \ , \ \left|\omega\frac{\partial \mathcal{E}}{\partial t}\right| \gg \left|\frac{\partial^2 \mathcal{E}}{\partial t^2}\right| \ , \ |\omega^2 \mathcal{P}| \gg \left|\omega\frac{\partial P}{\partial t}\right| \gg \left|\frac{\partial^2 \mathcal{P}}{\partial t^2}\right| \ , \tag{1.12}$$

which are called the slowly varying envelope approximation (SVEA). These mean that the amplitudes of the electric field and polarization are slowly varying both with space coordinate compared to the scale of optical wavelength and with time compared to optical period of the radiation field. Using these approximations and using the plane wave forms (1.5) and (1.6) of the electric field and the correspond-

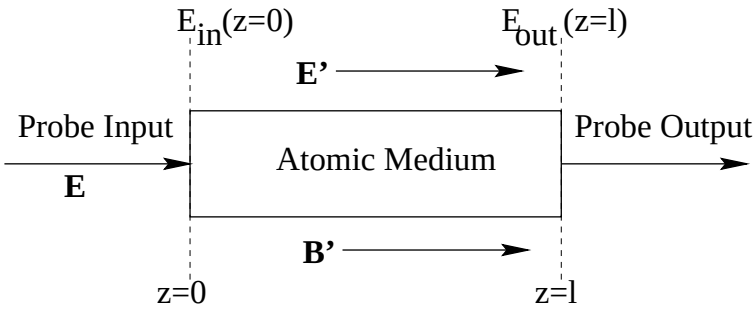

Figure 1.1: Figure representing a dilute atomic medium. The medium is driven by control field **E'** and the external magnetic field **B'**. The property of the medium is modified by the application of these fields. A weak probe field **E** helps to exploit these modifications.

ing linear polarization, respectively in the Eq. (1.11), we obtain,

$$\frac{\partial \mathcal{E}}{\partial z} + \frac{1}{c}\frac{\partial \mathcal{E}}{\partial t} = 2\pi i k \mathcal{P} \ . \tag{1.13}$$

In the steady state, when there is no reasonable time-variation in the electric field, from the above equation, we get,

$$\frac{\partial \mathcal{E}}{\partial z} = 2\pi i k \chi(\omega)\mathcal{E}(\omega, z) \ , \tag{1.14}$$

where we have used $\mathcal{P}(\omega, z) = \chi(\omega)\mathcal{E}(\omega, z)$. Here we have dropped out the tensorial notation and order of the susceptibility for brevity. Here onwards, we will be considering only the linear susceptibility. The solution of the above is now extremely simple and thus the output electric field is given by

$$\vec{E}(z = l) = \hat{\epsilon}\mathcal{E}(\omega, 0)e^{2\pi i k l \chi(\omega)}e^{ikl - i\omega t} + \text{c.c.} \tag{1.15}$$

Clearly the information of the susceptibility lies in the measured output intensity. Thus properly probing the medium, one can get the information of the property of the medium from the output. We are much interested in dilute atomic medium, as shown in Fig. 1.1, in which the atomic density is of the order of 10^{11} atoms cm^{-3}. In this kind of medium, the absolute value of the susceptibility χ becomes much less than unity. Thus, the dielectric constant $\epsilon = 1 + 4\pi\chi = n^2$ yields

$$n = \sqrt{\epsilon} = 1 + 2\pi\chi \ , \tag{1.16}$$

where n is the complex refractive index. From the result (1.15), we thus infer that the linear refractive index $\eta(\omega)$ and the absorption coefficient αl can be defined as

$$\eta(\omega) = 1 + 2\pi \mathrm{Re}[\chi(\omega)] \,, \tag{1.17a}$$

$$\alpha(\omega) l = 4\pi k l \, \mathrm{Im}[\chi(\omega)] \,, \tag{1.17b}$$

such that

$$\vec{E}(z=l) = \hat{\epsilon}\mathcal{E}(0) e^{-\alpha l/2} e^{\frac{i\eta(\omega)\omega}{c} l} e^{-i\omega t} + \text{c.c.} \,, \; I_0(z=l) = I(0) e^{-\alpha l} \,. \tag{1.18}$$

The frequency-dependence of the terms η and α come from the same of the linear susceptibility χ. Two important points are in order. First, measurable quantities η and α depend upon the medium susceptibility. The susceptibility of the medium can be changed by applying strong external coherent electric (or magnetic) field. Thus we can 'coherently control' the properties of the medium. One applies a suitable weak field ("probe field") to probe this change by measuring the quantities like probe absorption spectrum etc. Note that this is possible unless the strong field changes much while propagating through the medium. It is further assumed that the probe field does not change the properties of the medium to any measurable extent. Second, the relation of the term ϵ with the susceptibility provides us an dispersion relation, namely, $k^2(\omega) = \epsilon(\omega)(\omega^2/c^2)$.

1.1.2 Quantum statistical analysis of atoms

So far, we have discussed how the properties of a plane em wave depends upon the atomic properties. We now concentrate on the quantum treatment of the atoms to find how its properties depend on the applied em field. We assume that the atoms have quantized energy levels and we use the standard Dirac's bra-ket notation [2] now onwards.

Density matrix formalism

For a quantum mechanical system with the state $|\psi\rangle$, the dynamics is governed by the Schrödinger equation

$$i\hbar \frac{\partial |\psi\rangle}{\partial t} = H|\psi\rangle \,, \tag{1.19}$$

where, H represents the Hamiltonian of the system. This equation is exactly solvable, if the initial state of the system is precisely known. But for an atomic vapor cell, where many atoms reside and obey only the Maxwell's distribution of velocity at a given temperature, it is impossible to know the exact state of the either atom. Thus, a quantum statistical theory of the atoms is warranted.

Any arbitrary quantum state $|\psi\rangle$ can be expanded in terms of the orthonormal basis states $\{|i\rangle\}$ as $|\psi\rangle = \sum_i c_i|i\rangle$, where $\sum_i |c_i|^2 = 1$. This state is called a pure state [3]. The density operator (or density matrix) ρ is defined as $\rho = |\psi\rangle\langle\psi|$. The matrix element of ρ in $\{|i\rangle\}$ basis is given by $\rho_{ij} = \langle i|\rho|j\rangle = c_i^* c_j$. Some of the important properties of the density operator ρ are now in order: (1) Tr(ρ)=1, which indicates the conservation of probability. (2) The expectation value of any arbitrary operator A can be written as

$$\langle A\rangle = \langle\psi|A|\psi\rangle = \mathrm{Tr}(\rho A)\ . \tag{1.20}$$

(3) $\mathrm{Tr}(\rho^2) \leq 1$, where the equality sign holds only for a pure state. (4) ρ is hermitian and positive definite. We should mention that the designation of a single isolated quantum system either by an arbitrary state $|\psi\rangle$ or by the corresponding density operator ρ are equivalent.

In certain situations (as in the case of atomic vapor cell), one may have an ensemble of such identical systems $|\psi_i\rangle$. Then one cannot exactly know the state of the system. What one is left with is only a set of certain probabilities $\{p_i\}$ to be in the states $\{|\psi_i\rangle\}$. Clearly the wave-function approach is not suitable. In this case, one not only need to take the quantum mechanical average (1.20), but also the ensemble average over all the identical systems that have been similarly prepared:

$$\langle A\rangle = \sum_i \langle\psi_i|A|\psi_i\rangle = \mathrm{Tr}(\rho A)\ , \tag{1.21}$$

where the density operator ρ is defined as

$$\rho = \sum_i p_i|\psi_i\rangle\langle\psi_i|\ , \sum_i p_i = 1\ . \tag{1.22}$$

The matrix elements ρ_{ij} in the basis $\{|i\rangle\}$ are now given by $\sum_k p_k c_i^{k^*} c_j^k$. In this case, one can easily find that $\mathrm{Tr}(\rho^2) < 1$.

Before proceeding further, let us discuss the physical interpretation of the density matrix. The diagonal element ρ_{ii} of this matrix represents the ensemble-averaged probability that the system is in the energy eigenstate $|i\rangle$ (eigenstate of the Hamiltonian H, when there is no perturbation) and is often called as the 'population' in the $|i\rangle$ state. The off-diagonal term ρ_{ij} of the density operator represents the coherence between the levels $|i\rangle$ and $|j\rangle$. For a coherent superposition of the states $|i\rangle$ and $|j\rangle$, clearly $\rho_{ij} \equiv c_i^* c_j$ becomes non-zero. Moreover, for an ensemble of atomic states, ρ_{ij} is given by the ensemble average of such terms $c_i^{k^*} c_j^k$. Thus, there arises a possibility of destructive interference to make the coherence zero, as all the cross terms like $c_i^{k^*} c_j^k$ are complex in nature. If $\rho_{ij} \neq 0$, then some kind of coherent addition of interference terms exists. In the subsequent part of this thesis, we calculate the 'population' of the atomic levels $|i\rangle$ and the coherence between the levels $|i\rangle$ and $|j\rangle$ for different kinds of atomic models, in presence of external fields.

It is clear from the above discussion that irrespective of the exact nature of the system, we always can use the density matrix approach in a more general sense. The dynamics of the system is governed by the following Liouville equation:

$$\dot{\rho} = -\frac{i}{\hbar}[H, \rho] \; . \tag{1.23}$$

This equation can easily be derived for a pure state from the Schrödinger equation. Note that the Schrödinger equation is very difficult to work with for an ensemble of identical systems. On the other hand, Eq. (1.23) is quite general in nature, because it can be applied in treating the system irrespective of its state. Moreover, it gives both the quantum-mechanical as well as the statistical information of the system.

However, the above Liouville equation is not quite realistic. In any physical system, there lies a spectrum of incoherent processes, namely the spontaneous emission of the excited atoms, Doppler effect, collisional mechanism etc. These give rise to broadening of the atomic levels. One always has to incorporate these in the Liouville equation. Thus we obtain our working equation as follows.

$$\dot{\rho} = -\frac{i}{\hbar}[H, \rho] + \mathcal{L}\rho \; , \tag{1.24}$$

where $\mathcal{L}$ represents the matrix containing decay terms. The explicit form of this matrix can be derived using rigorous master equation formalism [4]. We provide the relevant form of this matrix in Appendix A.

1.1.3 Interaction between classical fields and atoms

In this part of the section, we describe the interaction of radiation with atoms. We use the classical picture of the radiation and quantum mechanical picture of the atoms. Thus the analysis described here is essentially semiclassical in nature.

Electric dipole approximation

Consider an electron of mass m and charge e situated at a distance $\vec{r}$ from the nucleus (assumed to be motionless) and bound to it by a potential $V(r)$ [5]. This electron is interacting with a plane em wave and the quantum mechanical Hamiltonian for this interaction can be written as

$$H = \frac{1}{2m}\left[\vec{P} - e\vec{A}(\vec{r},t)\right]^2 + eU(\vec{r},t) + V(r)\ , \tag{1.25}$$

where $\vec{A}(\vec{r},t)$ and $U(\vec{r},t)$ are the vector and scalar potentials, respectively, for the external field and $\vec{P}$ is the momentum operator for the electron. In the following, we first derive this equation from a gauge invariance point of view.

The dynamics of a free electron is governed by the equation

$$H|\psi\rangle = i\hbar\frac{\partial|\psi\rangle}{\partial t}\ ,\ H = -\frac{\hbar^2}{2m}\vec{\nabla}^2\ . \tag{1.26}$$

If $\psi(\vec{r},t)$ is a solution of the above equation, then $\psi(\vec{r},t)\exp(i\xi)$ is also a solution which does not change the probability density, where ξ is an arbitrary phase. But if one allows the phase to vary locally, i.e., to be a function of space and time variables,

$$\psi(\vec{r},t) \rightarrow \psi(\vec{r},t)e^{i\xi(\vec{r},t)}\ , \tag{1.27}$$

then though the probability density does not change, the Schrödinger equation no longer is satisfied. Now to satisfy the local gauge (phase) invariance, the Schrödinger equation must be modified by adding new terms in (1.26). Then the new Hamiltonian takes the following form:

$$H = \left\{-\frac{\hbar^2}{2m}\left[\vec{\nabla} - i\frac{e}{\hbar}\vec{A}(\vec{r},t)\right]^2 + eU(\vec{r},t)\right\}\ . \tag{1.28}$$

where $\vec{A}(\vec{r},t)$ and $U(\vec{r},t)$ are the functions which must be inserted into (1.26) if we want to be able to make the transformation (1.27) and to keep the Schrödinger equation gauge-independent. These are given by

$$\begin{aligned} \vec{A}(\vec{r},t) &\longrightarrow \vec{A}(\vec{r},t) + \frac{\hbar}{e}\nabla\chi(\vec{r},t) \ , \\ U(\vec{r},t) &\longrightarrow U(\vec{r},t) - \frac{\hbar}{e}\frac{\partial\chi(\vec{r},t)}{\partial t} \ . \end{aligned} \tag{1.29}$$

Clearly, the $\vec{A}(\vec{r},t)$ and $U(\vec{r},t)$ are the gauge-dependent potentials. Now inserting the potential $V(r)$ into the expression (1.28), we get the intended Hamiltonian (1.25) for a bound electron.

Now let us assume that the electron is bound to the nucleus (assumed to be static) which is situated at $\vec{r}_0$. Thus the vector potential is given by $\vec{A}(\vec{r}_0+\vec{r},t)$. Now we consider the *dipole approximation* $\vec{k}.\vec{r} \ll 1$ such that $\vec{A}(\vec{r}_0+\vec{r},t)$ can be written as $\vec{A}(\vec{r}_0,t)$. Then the new Hamiltonian reads as

$$H = \left\{ -\frac{\hbar^2}{2m}\left[\vec{\nabla} - i\frac{e}{\hbar}\vec{A}(\vec{r}_0,t)\right]^2 + V(r)\right\} \ , \tag{1.30}$$

where we have used the radiation gauge such that $U(\vec{r},t)=0$ and $\vec{\nabla}.\vec{A}=0$. By defining a new wave function

$$\phi(\vec{r},t) = \psi(\vec{r},t)\exp\left[\frac{-ie}{\hbar}\vec{A}(\vec{r}_0,t)\right] \ , \tag{1.31}$$

and using the above Hamiltonian H in (1.19), we lead to the following equation:

$$\left\{\left[\frac{p^2}{2m}+V(r)\right] - e\vec{r}.\vec{E}(\vec{r}_0,t)\right\}\phi(\vec{r},t) = i\hbar\dot{\phi}(\vec{r},t) \ , \tag{1.32}$$

where we have used the relations $\vec{E} = -\partial\vec{A}/\partial t$ (see [1]) and $\vec{p} = -i\hbar\vec{\nabla}$. The square bracketed term in the above equation is the unperturbed Hamiltonian of the bound electron. On the other hand, the second term $H_1 = -\vec{d}.\vec{E}(\vec{r}_0,t)$, where $\vec{d} = e\vec{r}$, is the perturbation term that is given in terms of gauge independent field $\vec{E}$. We shall use this Hamiltonian for further studies of atom-field interaction. We should mention here that another form of the perturabation part $\vec{p}.\vec{A}$ is well-known. However, it can be proved that these two forms of the Hamiltonian are equivalent, only upto a gauge trasformation (For detailed analysis, see [6]).

Note that the dipole approximation amounts to neglecting the terms like $\vec{k}.\vec{r}$ compared to unity. This refers to the assumption that the Bohr radius (typical

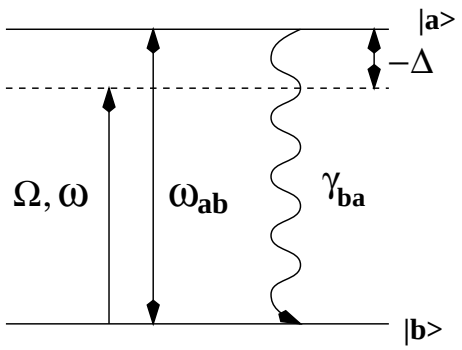

Figure 1.2: Level diagram for two-level system

dimension of the atom) is much smaller than the wavelength λ of the interacting field. Thus, the electric field remains nearly constant within the atomic length scale.

1.2 Atomic coherence effects

Coherence in atomic systems is a manifestation of the coherent superposition of atomic levels. This can be created by using external fields. In the following, we show how this coherence is created and manipulated. We use the density matrix formalism.

In the context of interaction of atoms with radiation, only few energy levels of the atom are relevant. Because, the monochromatic radiation [2] can be resonant or near-resonant to only a few levels, the atom can be treated as a two-level, three-level atom and so on, accordingly. The other off-resonant levels remain irrelevant in all practical calculations.

1.2.1 Two-level problem

We start with a two-level atom with the excited state $|a\rangle$ and the ground state $|b\rangle$ [see Fig. 1.2]. The quantum mechanical Hamiltonian of this atom can be written

[2] In practice, radiation with a single frequency is not achievable. However, if the spectral width of the radiation becomes much smaller than the natural line-width of the level, then the radiation can be treated practically as a monochromatic light and all the present analysis will be relevant.

as

$$H_0 = \hbar\omega_a|a\rangle\langle a| + \hbar\omega_b|b\rangle\langle b| \equiv \hbar\omega_{ab}|a\rangle\langle a| \ , \tag{1.33}$$

where ω_a and ω_b are the absolute energy eigenvalues of the corresponding levels. The last part of the above equation has been written assuming that the zero of the energy lies in the state $|b\rangle$. Thus ω_{ab} gives the relative energy of the state $|a\rangle$. The dipole moment operator can be written as

$$\vec{d} = \vec{d}_{ab}|a\rangle\langle b| + \text{h.c.} \ , \tag{1.34}$$

where the diagonal elements of $\vec{d}$ are zero due to parity reasons[3]. Let the atom interact with a monochromatic electric field given by

$$\vec{E}(\vec{r},t) = \hat{\epsilon}\mathcal{E}e^{i\vec{k}.\vec{r}-i\omega t} + \text{c.c.} \tag{1.35}$$

where, ω is the angular frequency of the field. Then the interaction Hamiltonian using the dipole approximation can be written as

$$H_1 = -\vec{d}.\vec{E} = -\hbar(\Omega e^{-i\omega t}|a\rangle\langle b| + \Omega'^{*}e^{i\omega t}|a\rangle\langle b| + \Omega' e^{-i\omega t}|b\rangle\langle a| + \Omega^{*}e^{i\omega t}|b\rangle\langle a|) \tag{1.36}$$

where

$$\Omega = \frac{\vec{d}_{ab}.\vec{\mathcal{E}}}{\hbar}e^{i\vec{k}.\vec{r}} \ \ ; \Omega' = \frac{\vec{d}_{ba}.\vec{\mathcal{E}}}{\hbar}e^{i\vec{k}.\vec{r}} \ . \tag{1.37}$$

The spatial dependence of the Ω's can be neglected if we consider the atoms to be static and $a_0 \ll \lambda$ (case of dipole approximation). However, for moving atoms, the Ω's can be spatially dependent. The entire Hamiltonian for the atom+radiation interaction is written as $H = H_0 + H_1$. We now apply an unitary transformation $|\psi\rangle = e^{-i\omega|a\rangle\langle a|t}|\phi\rangle$ to the Schrödinger equation (1.19), so that the transformed equation becomes

$$i\hbar\frac{\partial|\phi\rangle}{\partial t} = H_{\text{eff}}|\phi\rangle \ , \ H_{\text{eff}} = \hbar\left[-\Delta|a\rangle\langle a| - (|\Omega| + \Omega'^{*}e^{2i\omega t})|a\rangle\langle b| + \text{h.c.}\right] \tag{1.38}$$

where, $\Delta = \omega - \omega_{ab}$ is the field detuning from the $|a\rangle \leftrightarrow |b\rangle$ transition. Note that the expression for H_{eff} contains two terms - one oscillating in frequency 2ω (which are

[3]The matrix element of the dipole moment operator between the same levels or between the same parity [defined by $(-1)^l$] involves an odd function in space coordinate. Thus the matrix elements becomes zero while taking the relevant integration.

anti-resonant terms) and the other one is dc. For a cw laser in optical domain, $\Omega' \ll 2\omega$. Only for high-intensity laser fields, Ω' can be comparable to 2ω. As we are interested in ordinary light in optical domain, the anti-resonant components can be neglected. This approximation is called rotating wave approximation (RWA) [7]. Further, as one measures any quantum-mechanical observable for finite time, the time-averaged contribution of the off-resonant term (which is highly oscillating) becomes negligible for any practical purpose. Note that by using RWA, one can remove the explicit time-dependence of the Hamiltonian. Finally, the effective Hamiltonian for a two-level system interacting with plane em field becomes

$$H_{\rm eff} = -\hbar \left[\Delta |a\rangle\langle a| + |\Omega||a\rangle\langle b| + |\Omega||b\rangle\langle a|\right] \ . \tag{1.39}$$

Now using the Liouville equation (1.23) and using the effective Hamiltonian $H_{\rm eff}$ under RWA, we find the following equations of atomic density matrix elements:

$$\dot{\tilde{\rho}}_{aa} = -\dot{\tilde{\rho}}_{bb} = i(\Omega\tilde{\rho}_{ba} - \Omega^*\tilde{\rho}_{ab}) \ , \ \dot{\tilde{\rho}}_{ab} = -i\Delta\tilde{\rho}_{ab} - i\Omega(\rho_{aa} - \rho_{bb}) \ , \tag{1.40}$$

where $\tilde{\rho}$ is the density matrix in rotating frame.

The same equations could be obtained by imposing RWA on the density matrix elements instead of on the wave function, as in (1.38). Using the entire Hamiltonian $H = H_0 + H_1$ in Eq. (1.23) and then making a transformation like

$$\rho_{\alpha\alpha} \to \tilde{\rho}_{\alpha\alpha} \ , \ \rho_{ab} \to \tilde{\rho}_{ab} e^{-i\omega t} \ , \tag{1.41}$$

we could obtain the above equations. We should comment here that though we are obtaining the same equations, making RWA on the wave function and on the density matrix elements are not equivalent. Rather, the former one is more revealing as it provides the proper account of the vacuum shift (so-called Lamb shift) [4].

The above density matrix equations can be solved exactly, assuming that all the atoms reside initially in the level $|b\rangle$, i.e., $\rho_{bb}(t=0) = 1$. The solution is

$$\tilde{\rho}_{bb} - \tilde{\rho}_{aa} = \frac{\Delta^2}{\Omega_R^2} + \frac{4|\Omega|^2}{\Omega_R^2}\cos(\Omega_R t) \ , \ \tilde{\rho}_{bb} + \tilde{\rho}_{aa} = 1 \ , \tag{1.42}$$

$$\rho_{ab} = \frac{\Omega}{2\Omega_R^2}\left[-2\Delta e^{-i\omega t} - (\Omega_R - \Delta)e^{-i(\omega+\Omega_R)t} + (\Omega_R + \Delta)e^{-i(\omega-\Omega_R)t}\right] \tag{1.43}$$

where, $\Omega_R^2 = \Delta^2 + 4|\Omega|^2$. Note that the atomic inversion (population difference between the two levels) oscillates sinusoidally with a frequency Ω_R. If the field is in resonance, i.e., if $\Delta = 0$, then the frequency of this oscillation becomes $2|\Omega|$. If the detuning increases, the frequency of oscillation increases, but the amplitude decreases. This oscillation is called Rabi oscillation due to historical reason [4] and the corresponding frequency is called the Rabi frequency. An analysis of two-level atom and its interaction with classical fields has been given in [7]. Some other reviews on two-level atom can be found also in [9, 10].

So far we did not consider the decay process involved in an atomic system. In fact, the decay mechanism brings the Rabi oscillation to a dynamic steady state. The population of the excited levels decay spontaneously and the coherence between any two levels decay at a rate defined by the spontaneous emission rate of the levels involved. We add the phenomenological decay terms to the Liouville equation (1.23) so as to use the master equation (1.24) and find the following equations:

$$\dot{\tilde{\rho}}_{aa} = i(\Omega\tilde{\rho}_{ba} - \Omega^*\tilde{\rho}_{ab}) - \gamma_{ba}\tilde{\rho}_{aa}, \tag{1.44}$$

$$\dot{\tilde{\rho}}_{bb} = i(\Omega^*\tilde{\rho}_{ab} - \Omega\tilde{\rho}_{ba}) + \gamma_{ba}\tilde{\rho}_{aa}, \tag{1.45}$$

$$\dot{\tilde{\rho}}_{ab} = i\Delta\tilde{\rho}_{ab} - i\Omega(\rho_{aa} - \rho_{bb}) - \Gamma_{ab}\tilde{\rho}_{ab}, \tag{1.46}$$

$$\dot{\tilde{\rho}}_{ba} = -i\Delta\tilde{\rho}_{ba} + i\Omega^*(\tilde{\rho}_{aa} - \tilde{\rho}_{bb}) - \Gamma_{ab}\tilde{\rho}_{ba}, \tag{1.47}$$

where $\Gamma_{ab} = \frac{1}{2}\gamma_{ba} + \gamma_{coll}$ is the decay rate of the coherence $\tilde{\rho}_{ab}$, γ_{ba} is the spontaneous decay rate from the level $|a\rangle$ to $|b\rangle$, and $\gamma_{\rm coll}$ is the collisional decay rate (see Appendix E for details).

Due to presence of the spontaneous emission process, the Rabi oscillation gradually damps. One thus attains a steady state in a time-limit much longer than the spontaneous life time ($= 1/\gamma_{ba}$) of the level $|a\rangle$. Then the time-variation of the density matrix elements ceases to exist. Thus the above equations become a

[4] I. I. Rabi (1937) discovered that the probability of a spin-1/2 particle oscillates between its two possible spin states with the radio-frequency of the applied magnetic field [8].

set of simple algebraic equations. We solve them to obtain the following:

$$\tilde{\rho}_{aa} = \frac{2|\Omega|^2\Gamma_{ab}}{\gamma_{ba}(\Delta^2+\Gamma_{ab}^2)+4|\Omega|^2\Gamma_{ab}}, \quad \tilde{\rho}_{bb}=1-\tilde{\rho}_{aa}\ , \tag{1.48}$$

$$\tilde{\rho}_{ab} = \frac{i\Omega\gamma_{ba}(i\Delta+\Gamma_{ab})}{\gamma_{ba}(\Delta^2+\Gamma_{ab}^2)+4|\Omega|^2\Gamma_{ab}}. \tag{1.49}$$

In the following, we discuss different aspects of the steady state coherence $\tilde{\rho}_{ab}$.

It is known that, quantum mechanically, the expectation value of the dipole moment is written as

$$\langle\vec{d}\rangle = \mathrm{Tr}\{\rho\vec{d}\} = \mathrm{Tr}\left\{\rho\sum_{i\neq j}\vec{d}_{ij}|i\rangle\langle j|\right\} = \rho_{ij}\vec{d}_{ji}\ . \tag{1.50}$$

Thus the α-th component of the polarization density $\vec{\mathcal{P}}=N\langle\vec{d}\rangle$, N being the number density of the atomic medium, can be written as

$$\begin{aligned}
\mathcal{P}_\alpha &= N\rho_{ij}d_{ji}^{(\alpha)} \\
\text{or,}\quad d_{ij}^{(\alpha)}\mathcal{P}_\alpha &= N\rho_{ij}|d_{ij}^{(\alpha)}|^2 \\
\text{or,}\quad d_{ij}^{(\alpha)}\chi_{\alpha\beta}^{(1)}(\omega)\mathcal{E}_\beta &= N\rho_{ij}|d_{ij}^{(\alpha)}|^2 \\
\text{or,}\quad \hbar\chi_{\alpha\beta}^{(1)}(\omega)\Omega_{ij}^{(\alpha)}(\omega) &= N\rho_{ij}|d_{ij}^{(\alpha)}|^2 \\
\text{or,}\quad \chi_{\alpha\beta}^{(1)}(\omega) &= N\frac{\rho_{ij}|d_{ij}^{(\alpha)}|^2}{\hbar\Omega_{ij}^{(\alpha)}}\ .
\end{aligned} \tag{1.51}$$

Thus we could attain a relation between the coherence ρ_{ij} between two levels and the first order susceptibility $\chi_{\alpha\beta}^{(1)}$ of the medium. Using this general relation, we can write the susceptibility of the two-level system under consideration. This is given by

$$\chi(\omega)=\frac{N|d_{ab}|^2}{\hbar\Omega}\tilde{\rho}_{ab}=\frac{N|d_{ab}|^2}{\hbar}\frac{i\gamma_{ba}(i\Delta+\Gamma_{ab})}{\gamma_{ba}(\Delta^2+\Gamma_{ab}^2)+4|\Omega|^2\Gamma_{ab}}. \tag{1.52}$$

Note that the imaginary part of the above susceptibility, which gives the absorption profile [Eq. (1.17b)], is Lorentzian in nature. This is given by

$$\begin{aligned}
\mathrm{Im}(\chi) &= \frac{N|d_{ab}|^2}{\hbar}\frac{\gamma_{ba}\Gamma_{ab}}{\gamma_{ba}(\Delta^2+\Gamma_{ab}^2)+4|\Omega|^2\Gamma_{ab}} \\
&= \frac{N|d_{ab}|^2}{\hbar}.\frac{\Gamma_{ab}\pi}{\gamma_c}\frac{\gamma_c/\pi}{\Delta^2+\gamma_c^2}\ , \qquad \gamma_c=\sqrt{\Gamma_{ab}^2+\frac{4|\Omega|^2\Gamma_{ab}}{\gamma_{ba}}}\ .
\end{aligned} \tag{1.53}$$

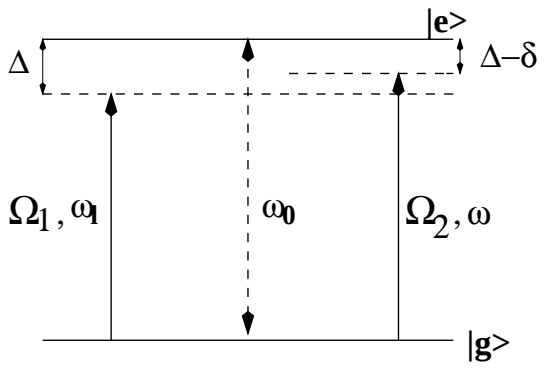

Figure 1.3: Driven two-level system probed by an weak field.

Here γ_c is the line width of the Lorentzian absorption spectrum (absorption profile in the frequency domain). The width has a dependence on the Rabi frequency of the interacting field. This result explains the power broadening of the atomic levels. The position and the width of the absorption peak could be obtained by finding the pole of the absorption profile. Because the function is analytic in the upper half of the complex Δ-plane [11], this pole is given by

$$\Delta = i\sqrt{\Gamma_{ab}^2 + 4|\Omega|^2(\Gamma_{ab}/\gamma_{ba})}\ , \tag{1.54}$$

which represents a single absorption peak at $\Delta = 0$ with a width equal to $[\Gamma_{ab}^2 + 4|\Omega|^2(\Gamma_{ab}/\gamma_{ba})]^{1/2}$, which is the same as γ_c above.

Further, the real part of the susceptibility provides the dispersion profile of the medium and is given by

$$\mathrm{Re}(\chi) = \frac{N|d_{ab}|^2}{\hbar}\frac{-\gamma_{ba}\Delta}{\gamma_{ba}(\Delta^2 + \Gamma_{ab}^2) + 4|\Omega|^2\Gamma_{ab}}\ . \tag{1.55}$$

Note that at $\Delta = 0$, the dispersion vanishes. Also, the slope of the dispersion in Δ-domain is negative at the resonance, which refers to the anomalous dispersion. Thus we infer that, it is the applied electric field, which induces the coherence between the atomic levels. This coherence makes the medium highly absorptive and anomalously dispersive in nature. We next show that this coherence (or susceptibility) can be modified and new effects can arise due to usage of extra control fields.

1.2.2 Driven two-level problem

We now consider the effect of an external strong field ("control" field) of angular frequency ω_l

$$\vec{E}_p = \vec{\mathcal{E}}_p e^{-i\omega_l t} + \vec{\mathcal{E}}_p^* e^{i\omega_l t} \tag{1.56}$$

on the atomic properties of a two-level system as shown in Fig. 1.3. We apply a weak field with angular frequency ω

$$\vec{E} = \vec{\mathcal{E}} e^{-i\omega t} + \vec{\mathcal{E}}^* e^{i\omega t} \tag{1.57}$$

to probe this effect. The Hamiltonian of the system under the action of these fields in dipole approximation can be written as

$$\begin{aligned} H &= H_0 + H_1 \\ &= \hbar\omega_0 |a\rangle\langle a| - \hbar[\Omega_1 e^{-i\omega_l t}|a\rangle\langle b| + \Omega_1' e^{-i\omega_l t}|b\rangle\langle a| + \Omega_2 e^{-i\omega t}|a\rangle\langle b| + \Omega_2' e^{-i\omega t}|b\rangle\langle a| + \text{h.c.}] \,, \end{aligned} \tag{1.58}$$

where,

$$\Omega_1 = \frac{\vec{d}_{ab}.\vec{\mathcal{E}}_p}{\hbar}, \;\; \Omega_1' = \frac{\vec{d}_{ba}.\vec{\mathcal{E}}_p}{\hbar}, \;\; \Omega_2 = \frac{\vec{d}_{ab}.\vec{\mathcal{E}}}{\hbar}, \text{ and } \Omega_2' = \frac{\vec{d}_{ba}.\vec{\mathcal{E}}}{\hbar}. \tag{1.59}$$

Here ω_0 is the atomic frequency and we have assumed the energy of the level $|b\rangle$ to be zero. Using the Liouville equation and making the RWA, we obtain the following density matrix equations:

$$\dot{\tilde{\rho}}_{aa} = -\gamma_{ba}\tilde{\rho}_{aa} + i(\Omega_1 + \Omega_2 e^{-i\delta t})\tilde{\rho}_{ba} - i(\Omega_1^* + \Omega_2^* e^{i\delta t})\tilde{\rho}_{ab}, \tag{1.60}$$

$$\dot{\tilde{\rho}}_{bb} = -\dot{\tilde{\rho}}_{aa}, \tag{1.61}$$

$$\dot{\tilde{\rho}}_{ab} = -(i\Delta + \Gamma_{ab})\tilde{\rho}_{ab} + i(\Omega_1 + \Omega_2 e^{-i\delta t})(\tilde{\rho}_{bb} - \tilde{\rho}_{aa}), \tag{1.62}$$

$$\dot{\tilde{\rho}}_{ba} = (i\Delta - \Gamma_{ab}) - i(\Omega_1^* + \Omega_2^* e^{i\delta t})(\tilde{\rho}_{bb} - \tilde{\rho}_{aa}), \tag{1.63}$$

where the transformation $\tilde{\rho}_{ab} = \rho_{ab} e^{i\omega_l t}$ has been used and the detunings and the decay rates have been defined as

$$\Delta = \omega_0 - \omega_l, \;\; \text{and} \;\; \delta = \omega - \omega_l, \;\; \Gamma_{ab} = \frac{1}{2}\gamma_{ba} + \gamma_{coll}. \tag{1.64}$$

We are treating the field with Rabi frequency $2\Omega_2$ as the weak probe field and that with Rabi frequency $2\Omega_1$ as strong pump field. Thus the above equations can be solved in a perturbative method in terms of probe field. We expand the density matrix elements $\tilde{\rho}_{\alpha\beta}$ upto the first order of Ω_2 as

$$\tilde{\rho}_{\alpha\beta} = \tilde{\rho}^{(0)}_{\alpha\beta} + \tilde{\rho}^{(+)}_{\alpha\beta}\Omega_2 e^{-i\delta t} + \tilde{\rho}^{(-)}_{\alpha\beta}\Omega_2^* e^{i\delta t}. \tag{1.65}$$

Substituting this in the density matrix equations, we equate the coefficients of $\Omega_2 e^{-i\delta t}$, $\Omega_2^* e^{i\delta t}$ and the constant terms. Thus we obtain the following solutions for all the relevant coefficients as follows:

$$\tilde{\rho}^{(0)}_{aa} = \frac{2|\Omega_1|^2\Gamma_{ab}}{\gamma_{ba}(\Delta^2+\Gamma_{ab}^2)+4|\Omega_1|^2\Gamma_{ab}}, \tag{1.66}$$

$$\tilde{\rho}^{(0)}_{ab} = \frac{i\Omega_1\gamma_{ab}(\Delta^2+\Gamma_{ab}^2)}{(i\Delta+\Gamma_{ab})[\gamma_{ba}(\Delta^2+\Gamma_{ab}^2)+4|\Omega_1|^2\Gamma_{ab}]}, \tag{1.67}$$

$$\begin{aligned}\tilde{\rho}^{(+)}_{ab} &= \frac{[\{(\gamma_{ba}-i\delta)(\Gamma_{ab}-i\Delta)-2|\Omega_1|^2\}\{\Gamma_{ab}-i(\delta+\Delta)\}-2|\Omega_1|^2(\Gamma_{ab}-i\Delta)]}{\{-4|\Omega_1|^2(\Gamma_{ab}-i\delta)+(\gamma_{ba}-i\delta)(i\Gamma_{ab}+\delta-\Delta)(i\Gamma_{ab}+\delta-\Delta)\}} \\ &\quad\times\frac{\gamma_{ba}(\Delta-i\Gamma_{ab})}{\{4|\Omega_1|^2\Gamma_{ab}+\gamma_{ba}(\Gamma_{ab}^2+\Delta^2)\}},\end{aligned} \tag{1.68}$$

$$\tilde{\rho}^{(-)}_{ab} = -\frac{2|\Omega_1|^2\gamma_{ba}(\Gamma_{ab}-i\Delta)(2\Gamma_{ab}+i\delta)}{\{4|\Omega_1|^2\Gamma_{ab}+\gamma_{ba}(\Gamma_{ab}^2+\Delta^2)\}[4|\Omega_1|^2(-i\Gamma_{ab}+\delta)+(-i\gamma_{ba}+\delta)\{(\Gamma_{ab}+i\delta)^2+\Delta^2\}]}, \tag{1.69}$$

$$\tilde{\rho}^{(+)}_{aa} = \frac{i\tilde{\rho}^{(0)}_{ba}+i\Omega_1\tilde{\rho}^{(+)}_{ba}-i\Omega_1^*\tilde{\rho}^{(+)}_{ab}}{\gamma_{ba}-i\delta}, \tag{1.70}$$

$$\tilde{\rho}^{(-)}_{aa} = \frac{-i\tilde{\rho}^{(0)}_{ab}+i\Omega_1\tilde{\rho}^{(-)}_{ba}-i\Omega_1^*\tilde{\rho}^{(-)}_{ab}}{\gamma_{ba}+i\delta}, \tag{1.71}$$

$$\tag{1.72}$$

and $\tilde{\rho}^{(0)}_{ba} = \tilde{\rho}^{(0)*}_{ab}$, $\tilde{\rho}^{(\pm)}_{ba} = \tilde{\rho}^{(\mp)*}_{ab}$.

We should mention here that the effect of intense laser field on a two-level system was first dealt with by Mollow [12]. He studied the resonance fluorescence spectrum from a two-level atom driven by a monochromatic strong source of light. Using a semiclassical calculation, he showed a triplet structure (at the frequencies ω_l and $\omega_l \pm \Omega_1$) in the power spectrum of light scattered by the two-level atom. This structure is known as Mollow triplet. Note that, the similar result can be attained from the solution for the coherence ρ_{ab} in (1.40), which shows that the dipole will exhibit induced oscillation in the frequencies $\omega \pm \Omega_R$ apart from the

frequency ω. Thus the fluorescence spectrum will have new frequency side-bands corresponding to $\omega \pm \Omega_R$. However, a strong control field ($\Omega_1 \gg \gamma_{ab}$) is necessary for these sidebands to appear, which is the same situation we dealt with in the above analysis. The Mollow triplet was experimentally verified by Hartig *et al.* [13] and Grove *et al.* [14].

Mollow further has shown that the stimulated absorption and emission spectrum of the probe become asymmetric due to this coherence [15]. He observed gain of the probe in certain probe frequencies. The probe field gets amplified at $\omega = \omega_l - \Omega_1$ and gets absorbed at $\omega = \omega_l + \Omega_1$, when $\Delta > 0$. The reverse occurs when $\Delta < 0$. The gain is not due to any intuitive population inversion between the levels $|a\rangle$ and $|b\rangle$. Rather, the gain arises due to the probe coherence $\tilde{\rho}_{ab}$ induced by the pump field, as we calculated above. Mollow's work has stimulated a series of theoretical [16] and experimental [17] investigations. This gain can show lasing action also [18]. We should note further that in the absorption spectra, a dispersive feature appears around $\omega \approx \omega_l$ which is related to stimulated Rayleigh scattering. Agarwal has discussed its origin in much details [19]. The gain associated with this has been utilized for optical parametric oscillator [20]. We should note that classical fields lead to many other interesting effects in a two-level atom. For example, strong bichromatic field interacting with a two-level atom gives rise to complicated Rabi splitting [21, 22]. Rabi sideband can be generated by four-wave parametric interaction [23]. Even population trapping state can exist when a two-level atom is driven by frequency modulated field [24]. Agarwal has developed a complete theory for quantum statistical treatment of the spontaneous emission in a collection of two-level atoms, and even in multilevel atoms [4, 25]. We will consider multilevel atoms in the following.

1.2.3 Coherent control in Multilevel systems

The idea of coherence developed in the earlier section will now be extended to multilevel systems, especially to three-level systems. Increasing the number of the levels in atoms provides much more freedom in possible configurations and in number of new effects. Depending on the level structure and dipole allowed transitions, there can be three types of three-level systems, as shown in Fig. 1.4.

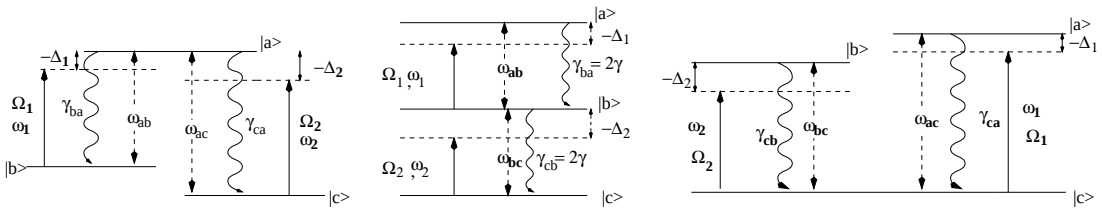

Figure 1.4: Three different configurations of three-level atomic system: Λ, Ξ, and V.

The detailed analysis of these configurations have been given in Appendices B, C, D. In the following we discuss some interesting optical phenomena occuring in these three-level systems.

Coherent Population Trapping

The development of monochromatic and tunable laser sources has boosted numerous high-resolution spectroscopic studies in these three-level structures. Out of these, the coherent population trapping (CPT) has been extensively studied in literature. Alzetta *et al.* have observed a decrease in fluorescence emission from Sodium atoms driven by two laser fields [26]. This was the first observation of CPT. At the same time, Whitley and Stroud studied CPT theoretically [27] and Grey *et al.* has done an experiment on Sodium atoms to verify the ideas [28]. It has been shown that when two resonant fields interact with two coupled atomic transitions, then the atomic population gets trapped in certain state. Physically, an atomic coherence arises due to the applied radiation such that the atomic evolution is out of phase with the radiation and destructive interference occurs between these two to meet a situation of no absorption. CPT is much important in coherent control studies because this exploits the macroscopic (observable) effect of coherence between the atomic states. Though in the absence of any spontaneous relaxation processes, all the three configurations as shown in Fig. 1.4 are equivalent, for relevant purpose the Λ configuration is the most suitable one for study of CPT. This is because, the population gets trapped in the two ground states, lifetime of which is very large. A theory of Lambda system interacting with two coherent fields of arbitrary strengths has been developed by Cohen-Tannoudji and Reynaud using dressed state approach [29] and by Agarwal and Jha [30] using master equation approach. We provide a qualitative analysis of CPT in this

part of the present thesis.

Let us consider two laser fields of frequency ω_1 and ω_2 interacting with the transition $|a\rangle \leftrightarrow |b\rangle$ and $|a\rangle \leftrightarrow |c\rangle$, respectively. The Hamiltonian of this system in dipole approximation can be written as (B.2) [see Appendix B]. Using RWA, we obtain the effective Hamiltonian (B.9) which can be diagonalized. Under condition of two-photon resonance ($\Delta_1 = \Delta_2$), one of the eigenvalues of this Hamiltonian is found to be zero. The corresponding eigenstate is given by

$$|NC\rangle = \frac{1}{\Omega}[\Omega_1|c\rangle - \Omega_2|b\rangle], \quad \Omega = \sqrt{\Omega_1^2 + \Omega_2^2}, \tag{1.73}$$

such that $H_{\text{eff}}|NC\rangle = 0$. (Note that we are not assuming the either field much stronger than the other, as one often does in the study of EIT). This state is called CPT state or dark state, which is uncoupled from the applied field and does not evolve further [31]. To understand the process of CPT, one has to consider the relaxation processes which are always present in an atom. The spontaneous emission from the level $|a\rangle$ constantly populates the state $|NC\rangle$. As this state remains uncoupled form the interacting fields, at long time limit (at time much longer than the spontaneous life-time of the level $|a\rangle$) the population gets trapped in the state $|NC\rangle$, irrespective of the initial condition. On the other hand, the interacting fields couple the state $|a\rangle$ with the state

$$|C\rangle = \frac{1}{\Omega}[\Omega_1|b\rangle + \Omega_2|c\rangle] \tag{1.74}$$

with an effective Rabi frequency Ω. CPT can also be understood as the destructive interference between two different excitation pathways [28, 32]. Note that the CPT state $|NC\rangle$ involves the states which are long-lived. However, in presence of atomic collisions, Doppler effects etc., broadening of these levels occur and thus the CPT state does not remain stable. The population further decays from this state. Several progress have been made to explore the effect of these broadening processes on CPT. Phase fluctuation of the interacting fields are also known to affect the stability of CPT state [33]. Truly speaking it is very difficult to find a *closed*[5] system in nature. The simplest model of a Lambda system is the $J = 1 \leftrightarrow J = 1$ with circularly polarized fields. More general level schemes have been

[5]If the excited levels decay only to the coupled ground states, then the system is said to be a closed one. Otherwise it is an open system.

investigated in the context of CPT [34]. It is shown that if there is one more ground level than the excited levels, then CPT can occur. Different other systems like molecular systems [35], atoms with excited continuum [36], dense atomic systems [37] etc. have been investigated also. CPT in open systems [38] and in the system driven by large magnetic field [39] have also been reported.

Besides different aspects of CPT, many applications of CPT have also been explored. It has found immense application in metrology [40], laser cooling [41], and in generation of microwave field [42]. Time-dependent CPT state has been extensively utilized in the study of adiabatic population transfer [43]. Harshawardhan and Agarwal have reported the use of CPT in optical bistability [44]. Use of quantized fields give rise to novel field properties under trapping conditions [45].

CPT has a close bearing with some other phenomena like electromagnetically induced transparency (EIT), lasing without inversion (LWI), enhancement of refractive index etc. We provide a brief discussion of these in the following.

Electromagnetically induced transparency : EIT

According to quantum mechanics, if several transition amplitudes (or several pathways) co-exist for any specific transition process, then these transition amplitudes can interfere with each other either constructively of destructively. We have already mentioned that CPT can occur for destructive interference of two different pathways. Fano interference is another example of this quantum interference process. Similar kind of destructive interference occurs in the process of EIT. The phenomenon that an otherwise optically opaque atomic medium can be made transparent to a weak probe field by using a strong control field is referred to EIT.

EIT was first demonstrated by Harris and coworkers in a Lambda-type system in atomic vapor of Strontium [46]. The control field at resonance ($\lambda = 570.3$ nm) was applied on the $|a\rangle \leftrightarrow |b\rangle$ transition, whereas the probe field ($\lambda = 337.1$ nm) was applied in the transition $|a\rangle \leftrightarrow |c\rangle$. The probe laser has an intensity about 10^3 times less than the control laser. Thus the state $|c\rangle$ will be the effective dark state, as $\Omega_1 \gg \Omega_2$ [see Eq. (1.73)]. Note that here lies the difference between the basic mechanisms of CPT and EIT. In CPT, both the interacting fields dress the ground levels and the CPT can be explained in terms of interference due to

both the fields. But in EIT, only stronger field dresses the two levels $|a\rangle$ and $|b\rangle$ which it couples. The other state $|c\rangle$, which is a ground state remains practically unaffected by this strong control field. Thus EIT is understood by the interference between transition from this state to the dressed states, given by

$$|\pm\rangle = \frac{1}{\sqrt{2}}(|a\rangle \pm |b\rangle) \ . \tag{1.75}$$

In Raman resonance condition (two-photon resonance condition : $\Delta_1 = \Delta_2$), the transition amplitudes for the $|\pm\rangle \leftrightarrow |c\rangle$ interfere destructively. Then an absorption minimum arises in the absorption spectra of the probe Ω_2. The population gets trapped in the level $|c\rangle$ at the Raman resonance frequency of the weak probe field. Thus the medium appears transparent to the probe. This situation is called EIT. Further, the absorption in the transitions $|c\rangle \rightarrow |\pm\rangle$ give rise to new resonances at the frequencies $\omega_2 = \omega_{ab} \pm \Omega_1$. These absorption peaks are known as Autler-Townes doublet [47]. The dip in the absorption at the frequency $\omega_2 = \omega_{ab}$ between these two peaks corresponds to EIT dip. We should mention that the first observation of this doublet in optical domain was reported by Hertz *et al.* [48]. Agarwal has shown that EIT spectra can be interpreted through Lorentzian contributions from the new resonances and dispersive contributions from interference terms [49]. Moreover, it should be emphasized that not only a small field, but also a small control field (of the order of the decay rate of the excited level) is sufficient for EIT to occur [50].

There have been several demonstrations of EIT in different kinds of level schemes [51, 52, 53, 54, 55, 56, 57, 58]. EIT is best obtained in Lambda type of configuration, whereas in the other standard three-level configurations (namely V and Ladder schemes), one does not get complete transparency. A comparison of these configurations has been studied in somewhat different context [53]. EIT has been observed in different kinds of media, e.g., in laser-cooled samples [56], in plasma [59], in solid samples [57], and in sample kept in cavities [53]. Agarwal and Boyd have applied the EIT in controlling the band-gap in dielectric media [60]. EIT has been shown to be useful as a coherent switch also [61]. Dependence of EIT on phase [62] and on the polarization [63] of the interacting fields have also been explored.

EIT has found immense application in isotope separation [64], controlling optical bistability [44], electromagnetically induced grating [65]. Laser pulse matching and soliton like propagation which have applications in optical communication, can be observed in EIT-like situation [66]. Agarwal has extended this issue to quantum regime to show matching in photon statistics [67]. Agarwal and Harshawardhan have generalized the idea to achieve control of two-photon processes [68]. Photon switching at a single photon level has been proposed by Harris and Yamamoto using a similar idea [69]. Recently two-photon switching has been observed by Yan *et al.* [70]. Many review articles on EIT now exist in the literature [71].

Lasing without inversion : LWI

Lasing occurs due to population inversion between the relevant levels. Interestingly, one can get lasing even without population inversion in the relevant levels. This can be achieved by using the atomic coherence. Thus, LWI has created a lot of attention after its advent by Kocharovskaya and Khanin [72] and Harris [73]. The authors in Ref. [72] have found that ultra-short pulses get amplified due to CPT even without any inversion in the atomic levels in a Lambda system. Harris observed that decay from discrete states to an identical continuum causes an absorption in absorption, whereas the stimulated emission spectra remains unaffected. Thus there creates an asymmetry between the absorption and emission spectra. Hence, there arises a possibility of LWI. Imamoglu and Harris have shown that the similar kind of effects can be produced by using a control field [74]. On the other hand, Scully and coworkers have proposed that coherent superposition of the ground levels of a Lambda system can give rise to LWI [75]. Agarwal has shown that a laser based on LWI exhibits ultra-narrow line-widths due to quenching of spontaneous emission [76].

After the discovery of LWI, several theoretical proposals and experimental verifications have been reported. The first experimental indication of gain without inversion (GWI) was in a four-level model [77]. In this work, in $3S_{1/2} \leftrightarrow 3P_{1/2}$ transition in Na, atomic coherence among the ground hyperfine levels $F = 1$ and $F = 2$ have been created giving rise to gain of a probe field along $3S_{1/2} \leftrightarrow 3P_{1/2}$ transition. This work was based on the model proposed by Narducci *et al.* [78],

but the experiment did not have concrete evidence that the gain was in fact without inversion. Nevertheless, the results did show atomic coherence effect. The first unambiguous demonstration of GWI was given by Fry *et al.* in a Λ system in Na [79]. It has been found that though there is no inversion in bare basis, there exists inversion in dressed basis. In some cases, there exists no population inversion even in any basis. Some of the experimental observations based on this have been reported in ^{87}Rb (V configuration) [80] and in ^{23}Na (Λ configuration) [81]. Agarwal explained that LWI in this case is due to the coherence of the dressed states [82]. Menon and Agarwal have shown that LWI can be observed in a Λ system due to cross-coupling of control and probe fields [83]. Many reviews exist in the literature on LWI [84].

Dispersion management : Harmonic Generation

So far we have discussed the coherent control of the absorption of the probe field. Applying the interacting field, one can also manipulate the dispersive property of the medium. It is known that one can generate different harmonics of the incident frequency using several available nonlinear optical techniques, which is associated with large nonlinear susceptibility. On the other hand, in context of atomic vapors interacting with coherent fields, one also can generate large nonlinear susceptibility at resonance condition. But both the dispersion and absorption are very much high in this case. To probe the dispersive property of the medium, one would like to have less absorption and as much as high dispersion. Here lies the basic goal of dispersion management. The first work in this context was done by Tewari and Agarwal to show harmonic generation using strong saturating field [85]. This field can change the phase matching condition in the four-wave mixing process and radiation in vacuum-ultraviolet region can be enhanced by orders of magnitude. Harris *et al.* have shown that EIT results in destructive interference in linear susceptibility and constructive interference in third order susceptibility [86]. As the efficiency of four-wave mixing depends upon the ratio of the susceptibilities of the third order and the first order, thus any reduction of first order susceptibility will cause the efficiency to increase. In fact, both the proposals were closely related and the large efficiency arises from the same mechanism [87].

A series of demonstration have been reported in context of harmonic genera-

tion using coherent control. Hakuta and coworkers have achieved resonantly enhanced second harmonics accompanied with reduced absorption in 2s↔2p transition of Hydrogen [88]. This work demonstrated that EIT is possible with dc field, also. Zhang *et al.* demonstrated sum-frequency generation at the frequency 103 nm in VUV region from the 2s↔3p transition strongly coupled with a laser [89]. Phase matching induced by control field was observed in an off-resonant scheme of four-wave mixing in ^{208}Pb [90]. In this work, transparency has a little role in enhancement due to large detuning. In another experiment CPT is shown to play the major role in generating new frequencies [91]. Many other experiments exploiting the nonlinear coherence effects include observation of giant Kerr nonlinearity [92], efficient phase conjugation [93], nonlinear two-photon spectroscopy in optically dense media [94].

Dispersion management : Ultra-high refractive index

The real part of the dispersion gives the refractive index. In atomic vapor, refractive index is, in general, high at resonance associated with large absorption. In EIT, one obtains vanishing absorption as well as vanishing dispersion. Using atomic coherence effects and quantum interference, Scully and coworkers have shown that in some spectral region, refractive index can be kept large, but the absorption can be suppressed [95]. This has been experimentally verified by Zibrov *et al.* in Rb vapor [96]. Using a different technique, Kocharovskaya and coworkers have shown that large refractive index associated with zero absorption can be achieved by suppressing the spontaneous emission using control fields [97]. This happens in a situation where the ground states have a larger energy than the Stark-shifted levels, which are created due to application of the control field.

Dispersion management : Magnetometry

The frequency dependence of the dispersion in EIT condition can be employed in measuring very feeble magnetic field. It can be shown that in the vicinity of probe resonance, the phase shift of the probe field is proportional to the two-photon detuning. This phase change can be measured using such a medium in the Mach-Zehnder interferometer. Scully and Fleischhauer have shown that two-photon detuning of the order of 10^{-5} Hz can be detected using this technique [98]. This has immense application in determining frequency standard. Even

very small Zeeman splitting due to weak magnetic field can be measured by this technique. In [98], it is shown that magnetic field of the order of pico-Gauss can be detected, which otherwise would require large superconducting devices.

Dispersion management : Manipulation of group velocities

Recently, atomic coherence effects have been demonstrated in a series of theoretical and experimental investigation in manipulation of group velocities. Historically, concept of group velocity has been extensively studied by Brillouin in his famous book [99]. The group velocity is defined by [see Eq. (A.15)]

$$v_g = \frac{c}{\eta(\omega) + \omega \frac{d\eta}{d\omega}} \,, \tag{1.76}$$

where $\eta = 1 + 2\pi \mathrm{Re}[\chi(\omega)]$ is the linear refractive index. We describe how to derive this formula in Appendix A in general and in Appendix E for propagation of a cw pulse through a dilute atomic vapor medium. Near the EIT window, both the real and imaginary parts of the susceptibility almost vanish. Thus the group velocity is entirely determined by the slope of the real part of the susceptibility χ. If it is large enough, then the group velocity can be reduced. One thus defines a slow light, group velocity of which is much less than the velocity c of light in vacuum. The positive slope ($d\eta/d\omega > 0$) is referred to as normal dispersion. Thus normal dispersion is responsible in slowing the group velocity. The amount of this slope depends upon the width of the EIT window. Narrow EIT windows can be created by using very small control field. Thus group velocity can be controlled using the coherent control technique. However, in atomic vapors, the inelastic collision with the wall, Doppler broadening etc. may suppress the EIT effect, in presence of weak control field. Harris *et al.* have shown that for a large control field (intensity $\sim$ 283 kW cm^{-2}) group velocity can be reduced to $c/250$ in EIT window [100]. Kasapi *et al.* have investigated the propagation dynamics of the optical pulses inside an optically thick medium and have shown that the group velocity can be reduced to $c/165$ [101]. They have used strong control field also ($\sim$ 200 kW cm^{-2}) with the probe of intensity of the same order. However, due to recent developments in experimental techniques, one can attain slow group velocity using weak control field also. In the first experiment of this kind, Hau *et al.* have been able to reduce the group velocity to 17 m s^{-1} in a Sodium Bose

condensate medium using a weak control field (power $\sim$ 1 mW cm^{-2}) [102]. Even in hot gases [103] and vapors in room temperature [104], one can create slow group velocities, by using anti-relaxation coating on the wall of the vapor cell to suppress collisional effects. In [104], a group velocity of 8 ms^{-1} has been reported. Schmidt *et al.* have shown that group velocity can be reduced below $c/3000$ in a CPT condition [105]. In a Raman scheme, one can achieve extremely slow propagation even without satisfying any EIT condition [106]. Xiao *et al.* have shown that in a Ladder system (where EIT is not complete, see Appendix C), one can achieve a reduction $\sim c/13.2$ [107]. Large group delay (i.e., slow group velocity) has been reported in photonic band edge [108] and in solid medium like Ruby crystal also [109]. Slow light pulses in moving media have been investigated [110, 111, 112]. Entanglement of slow photons has also been reported [113].

Extending the idea of coherent manipulation of group velocity, Fleischhauer and Lukin have shown that the light pulses in quantum domain can be decelerated and even *trapped* inside a medium [114]. This is done by transfering the quantum correlations from light field to collective atomic states. This stored quantum information can be transferred back to the light fields. Thus this process has potential application in quantum information processing. Further Lukin *et al.* have shown that this procedure can help in producing entanglement in atomic ensembles, in creating atomic squeezed states, and in teleportation of atomic states [115]. In a different development, Liu *et al.* have been successful to *halt* the light pulses in an atomic medium and to make it useful in information processing [116]. On the other hand, Phillips *et al.* have independently demonstrated that the light field can be stored in atomic vapor [117]. Kocharovskaya and coworkers have used hot atoms to stop the light inside the medium [118]. Grobe *et al.* have interpreted that in adiabatic limit, storage of light refers to transfer of the information of the light field to the ground state coherence of the atom [119].

So far we have discussed the slowing and stopping of light pulse. From the expression of group velocity v_g, one can see that it is 'in principle' possible to enhance the group velocity *larger than* c. This can be done in a situation, when the medium shows *anomalous* dispersion (i.e., $d\eta/d\omega < 0$). There are a lot of theoretical studies [120, 121] on this issue. Specifically, in [121], the conditions that

an amplifying medium would show superluminality, have been derived. The first demonstration of superluminality in an absorbing medium have been reported by Chu and Wong [122] to verify the prediction of [120]. In degenerate two-level configuration of Rb atoms, a negative group velocity $\sim -c/23000$ has been reported [123]. Superluminous soliton is possible in a Brillouin fiber ring laser also [124]. Chiao and coworkers have proposed experiments in the present context in a detuned high-gain medium [125, 126]. However, the most interesting contribution came from Wang *et al.* who have demonstrated the superluminal propagation (with a group velocity $\sim -c/310$) of a Gaussian pulse in a *resonant gain medium* [127]. The ultracold atoms [128] and photonic band gap [129] also have been shown to be useful to exhibit superluminal behavior. A lot of theoretical studies inside inverted medium [130], in bandpass filter [131], in a medium with gain doublet [132] etc. have been performed. We should emphasize here that the observed superluminal behavior does not conflict with the basic assumptions of relativity as well as with causality. The information cannot be transferred superluminally [133, 134], as this behavior is proved to be a manifestation of pulse reshaping inside the medium. Further, the theory of relativity demands the velocity of light not to exceed c in a vacuum, while, the superluminality have been demonstrated inside a medium.

More interestingly, some proposals have been recently made to obtain both subluminal and superluminal propagation in the same medium. Phase control of group velocity has been reported in this regard [135]. By changing the power of control field, Kim *et al.* have shown that it is possible to change the superluminal group velocity to subluminal one [136]. Agarwal and coworkers have proposed a 'microwave knob' to continuously change the group velocities from subluminal to superluminal and vice versa [137]. By changing the dye concentration, and thereby, the optical density of the medium, Talukder *et al.* could be able to control the group velocity of the medium [138].

Dispersion management : Magneto-optical rotation

When a linearly polarized light passes through a medium in the direction of magnetic field, it experiences a rotation of polarization, called magneto-optical rotation (MOR). This was first formulated by Faraday [139, 140]. The MOR angle

can be written as

$$\theta = \pi k l \mathrm{Re}(\chi_- - \chi_+) \ , \tag{1.77}$$

in case of a non-attenuating medium, where k is the wave number of the electric field, l is the length of the medium, and $\chi_\pm$ are the linear susceptibilities of the medium for the right or left circularly polarized components of the input field (see Chapter 4 for derivation of the above expression). In conventional Faraday rotation, the rotation angle is extremely small, and is difficult to measure. One can see from the above equation that the larger the asymmetry between the χ's, the larger the MOR. As we have discussed earlier and will show in the following part of this thesis, coherent field can create large dispersion at even atomic resonance. Thus large asymmetry in the susceptibilities can be achieved. Thus in principle, it suffices to use even dilute medium (N is small) to attain large MOR angle [141]. There have been a lot of theoretical [142, 143] and experimental studies [144] which discussed the usage of atomic coherence to enhance the MOR. Effect of magnetic field and strong electric field on MOR have been studied by Budker and coworkers [145]. Large atomic coherence in *optically thick* atomic vapor can also enhance the MOR [146]. The authors in [146] have utilized the idea to improve the signal-to-noise ratio. Effect of Doppler broadening on MOR has been investigated [147]. Further studies in saturated medium (case of strong electric field) [148] and for arbitrary direction of magnetic field [149] have been reported. In saturated medium, nonlinear MOR (NMOR) comes into picture. Using the idea of enhancement of refractive index using atomic coherence and NMOR, Scully and coworkers have investigated the possibility of high-precision magnetometry in optically thick cell both theoretically [98, 150] and experimentally [146, 151]. Budker *et al.* have used anti-relaxation paraffin coating to reduce the Doppler effect in a Rb vapor cell in study of high-precision magnetometry [145, 152]. Cold atoms have also been employed to reduce the ground state relaxation in study of NMOR [153, 154]. MOR has been utilized in radiation trapping in an optically thick atomic vapor [155] and in group velocity studies in an optically dilute medium [156]. It has been shown by Patnaik and Agarwal that even laser field alone can create the above asymmetry and optical rotation can be controlled as

well as enhanced applying a control field only [157]. Recently MOR has been extensively reviewed by Budker *et al.* [158].

1.3 Outline of this Thesis

Different chapters in this thesis develop the framework and models for laser field-induced coherence effect in anisotropic systems. We predict many new interesting effects arising due to application of coherent control field. The motivation and important results of these chapters are briefly discussed below.

Chapter 2: In an anisotropic medium, the orthogonal polarization components of a linearly polarized pulse have different susceptibilities. Thus, they travel through the medium with different group velocities. But at the resonance of the either component, its absorption becomes very large. In this chapter, we show that applying a resonant laser field, it is possible to create EIT at the resonance of the either. In this condition, both the components have different group velocities but negligible absorption. Thus it is possible to split them so that they come out of the medium at different times. We demonstrated this effect numerically in context of propagation of a Gaussian pulse through the medium. An analytical estimate of the broadening of the pulse component at the output end of the medium is given.

Chapter 3: When an unpolarized light propagates through an anisotropic medium, the output intensity becomes the same irrespective of the direction of the applied dc magnetic field. However, if one drives the medium with a resonant electric field in suitable transition, then the susceptibilities of the polarization components of the field get modified. Then the output field intensities become different for two opposite directions of the magnetic field. We can find a typical parameter zone, such that the absorption coefficient can be switched from nearly zero to nearly unity or vice versa by just reversing the magnetic field. Thus we show the coherent control of the medium absorption. We show that the large asymmetry in the output intensities can also be created in a Doppler-broadened medium. We note that similar kind of effect, called magneto-chiral anisotropy, exists, which is an effect of the higher order moments, and thus too small in

magnitude to detect. On the other hand, we show that magnetic field reversal asymmetry, as we discuss, is an effect of dipole moments and thus quite easy to detect experimentally.

Chapter 4: It is known that the MOR angle depends upon the optical density in a linear fashion. This is true for a near monochromatic light. But, for a sufficiently nonmonochromatic light, nonlinear dependence of the MOR angle on the optical density occurs. This has been observed in a related experiment. We provide an theoretical explanation of this effect. The theoretical results are shown to be in good agreement with the experimental results. We further investigate the effect of the applied magnetic field in this context.

Chapter 5: In an EIT situation which occurs in a standard Λ configuration, there arises situations like zero absorption and zero dispersion of the medium. We show that, coupling a noninteracting level with an extra control field in this configuration, one can obtain non-zero absorption associated with zero absorprtion. Further, in certain probe frequency region, the medium exhibits gain behavior. These results are understood as a coherence effect induced by the control field. The gain behavior can be explained in terms of population inversion in dressed state basis. We further show that large MOR angles are possible to attain, by applying control field.

Chapter 6: An excited atom in V-configuration, interacting with a two-mode cavity can serve as a quantum cloner of a photon in either mode. The stimulated emission emits a second photon, which can serve as a clone of the initial one. The fidelity of this process is reduced due to simultaneous existence of spontaneous emission in the other mode. Our motivation is to enhance the fidelity beyond the optimal limit. This is possible by applying a coherent field to couple the excited states to an upper metastable state, so that the population can be cycled in that transition for longer time. Thus the relative probability of the stimulated emission is enhanced, so that the fidelity of quantum cloning is also enhanced. We investigate the effect of two atoms in this context. We further show that the universality of the cloning process breaks down by the applied control field.

Chapter 2

Coherent medium as a polarization splitter of pulses

So far we have discussed the basic analysis of the interaction of radiation field with atom. We explained the concept of various coherent control effects, namely EIT, dispersion management and so on. Using the concept of EIT, we show in the following, how an anisotropic coherent medium can be used to separate out two polarization components of a pulse.

2.1 Anisotropic medium

As we have explained in the previous chapter, in an anisotropic medium, different polarization components for a given direction of propagation of the electric field have different susceptibilities, In other words, the response of the system becomes different for different polarization directions. It is well known that an applied magnetic field makes an isotropic medium anisotropic. Note that the long-known Faraday effect [139] is a manifestation of the anisotropy of the medium. In this process, the polarization of a cw field is rotated, if this field propagates through the anisotropic medium along the direction of the magnetic field. We already referred to this process as MOR in the previous chapter. Though, it is now known that even the control field alone can create anisotropy, we make use of magnetic field for this in the present context.

Consider the propagation of a linearly polarized laser pulse through an anisotropic

medium of length l. A pulse is a coherent superposition of many monochromatic plane waves, which are given by the Eq. (2.1). We assume a linearly polarized pulse which is given by

$$\vec{E}(z,t) = \hat{x}\int_{-\infty}^{\infty} \mathcal{E}(\omega)\exp\left\{i\omega\left(\frac{z}{c}-t\right)\right\}d\omega + \text{c.c.}, \tag{2.1}$$

where we assume that the pulse has a small spectral width. Note that because, a pulse consists of many Fourier components, its amplitude becomes frequency-dependent. In time-domain, this pulse has certain temporal profile also, as we will discuss in details later on in this chapter.

The amplitude $\hat{x}\mathcal{E}$ can be resolved in terms of two circular components

$$\hat{x}\mathcal{E} = \hat{\epsilon}_+\mathcal{E}_+ + \hat{\epsilon}_-\mathcal{E}_-, \quad \mathcal{E}_\pm = \mathcal{E}/\sqrt{2}, \tag{2.2}$$

where, unit orthogonal polarization vectors $\hat{\epsilon}_\pm$ correspond to $\sigma^\pm$ (we use the convention that $\sigma_\pm$ correspond to left circular and right circular polarization, respectively) polarizations, and are given by

$$\hat{\epsilon}_\pm = \frac{1}{\sqrt{2}}(\hat{x} \pm i\hat{y}). \tag{2.3}$$

The induced polarization in the medium due to the interaction with the linearly polarized probe can be expressed accordingly as

$$\vec{P}(z,t) = \hat{\epsilon}_+P_+(z,t) + \hat{\epsilon}_-P_-(z,t), \tag{2.4}$$

where,

$$P_\pm(z,t) = \int_{-\infty}^{\infty}\chi_\pm(\omega)\mathcal{E}_\pm(z,\omega)e^{-i\omega t}d\omega. \tag{2.5}$$

Here, $\chi_\pm(\omega)$ are the complex susceptibilities for the two circularly polarized components inside the medium for a given frequency ω.

If we assume that the density N of the medium is small so that the back reflections are negligible (i.e., a case when $4\pi|\chi_\pm| \ll 1$), then the field at the output can be written as

$$\begin{aligned}\vec{E}(l,t) &\equiv \hat{\epsilon}_+\int_{-\infty}^{+\infty} d\omega\ \mathcal{E}_+(\omega)\exp\left\{i\omega\left(\frac{l}{c}-t\right)+\frac{2\pi i\omega l}{c}\chi_+(\omega)\right\} \\ &+ \hat{\epsilon}_-\int_{-\infty}^{+\infty} d\omega\ \mathcal{E}_-(\omega)\exp\left\{i\omega\left(\frac{l}{c}-t\right)+\frac{2\pi i\omega l}{c}\chi_-(\omega)\right\}.\end{aligned} \tag{2.6}$$

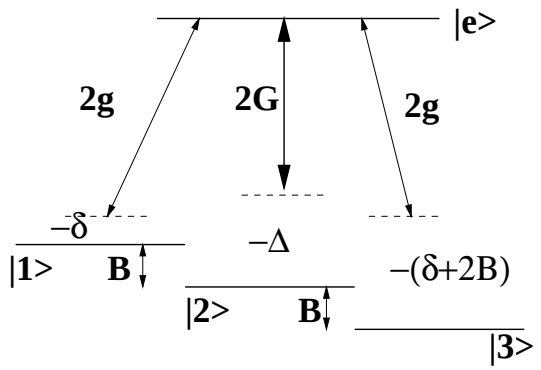

Figure 2.1: The level configuration for splitting of a linearly polarized pulse. The $\sigma^{\pm}$ components of the input pulse with respective Rabi frequencies $2g_1$ and $2g_2$ interact with the $|e\rangle \leftrightarrow |1\rangle$ and $|e\rangle \leftrightarrow |3\rangle$ transitions, respectively. The pump field with Rabi frequency $2G$ is applied in the $|e\rangle \leftrightarrow |2\rangle$ transition.

Clearly the two components of the pulse travel with different group velocities $v_g^{\pm}$ inside the medium which are given by

$$v_g^{\pm} = c/n_g^{\pm} \tag{2.7}$$

where the group indices $n_g^{\pm}$ are given by (see Appendix E)

$$n_g^{\pm} \approx 1 + 2\pi\chi_{\pm}(\omega) + 2\pi\omega\frac{\partial\chi_{\pm}(\omega)}{\partial\omega}, \tag{2.8}$$

where the expression (2.8) is to be evaluated at the central frequency ω_0 of the pulse.

2.2 Model configuration

We will now demonstrate how the ideas of coherent control can be used to separate temporally the two components of a linearly polarized pulse given by the expression (2.1). This is possible if one can produce large anisotropy between n_g^+ and n_g^-. We consider a generic four-level model as shown in Fig. 2.1 for this purpose. The relevant energy-levels are found in many systems such as in ^{23}Na [159], ^{7}Li [160], and Pr:YSO [161]. The upper level $|e\rangle$ which is a $|m_F = 0\rangle$ state is coupled to the ground levels $|1\rangle(m_F = +1)$ and $|3\rangle(m_F = -1)$ by a $\hat{x}$-polarized laser probe, given by (2.1). The orthogonal components of the probe with σ_- and σ_+ polarizations interact with $|e\rangle \leftrightarrow |1\rangle$ and $|e\rangle \leftrightarrow |3\rangle$ transitions, respectively. The

degeneracy of the ground level has been removed by applying a static magnetic field of strength B in the direction of the propagation (parallel to $\vec{k}$) of the applied laser fields, as in the case of Faraday effect [139, 140]. Thus the medium becomes anisotropic. Note that Renzoni *et al.* [38] used the same atomic configuration to investigate the possibility of coherent population trapping using cw field of arbitrary intensities. In a dressed state approach they have shown that the long-interaction-time-evolution of the system can be completely characterized by the effective line-width of the noncoupled state.

We should mention here that the following analysis is performed for the ^{23}Na atoms. Because the Landé g-factor of the ground levels is negative in this case, thus the level $|1\rangle \equiv m_F = +1$ ($|3\rangle \equiv m_F = -1$) shifts upwards (downwards) upon application of the magnetic field (see Appendix F).

2.3 Analysis

In the previous chapter, we have described the detailed method to treat the interaction of an atom with monochromatic field. For a pulse, we start with the similar treatment and assume the frequency dependence of the pulse later on. Thus, in dipole approximation, the Hamiltonian for the system under consideration can be written as

$$H = \hbar[\omega_{e3}|e\rangle\langle e| + \omega_{13}|1\rangle\langle 1|] - (\vec{d}_{e1}|e\rangle\langle 1| + \vec{d}_{e3}|e\rangle\langle 3|).(\vec{\mathcal{E}}e^{-i\omega t} + \text{c.c.}) \ . \tag{2.9}$$

We use the Liouville equation (1.24) and obtain the following equations for the density matrix elements using RWA:

$$\begin{aligned}
\dot{\tilde{\rho}}_{ee} &= -(\gamma_{1e} + \gamma_{3e})\tilde{\rho}_{ee} + i[g_1\tilde{\rho}_{1e} + g_2\tilde{\rho}_{3e} - \text{c.c.}] \ , \\
\dot{\tilde{\rho}}_{11} &= -\gamma_{1e}\tilde{\rho}_{ee} + i[g_1^*\tilde{\rho}_{e1} - \text{c.c.}] \ , \\
\dot{\tilde{\rho}}_{e1} &= (i\delta - \Gamma_{e1})\tilde{\rho}_{e1} + i[g_1(\tilde{\rho}_{11} - \tilde{\rho}_{ee}) + g_2\tilde{\rho}_{31}] \ , \\
\dot{\tilde{\rho}}_{e3} &= [i(\delta + 2B) - \Gamma_{e3}]\tilde{\rho}_{e3} + i[g_1\tilde{\rho}_{13} + g_2(\tilde{\rho}_{33} - \tilde{\rho}_{ee})] \ , \\
\dot{\tilde{\rho}}_{13} &= -[2iB + \Gamma_{13}]\tilde{\rho}_{13} + i[g_1^*\tilde{\rho}_{e3} - g_2\tilde{\rho}_{1e}] \ ,
\end{aligned} \tag{2.10}$$

where the g_1 and g_2 are half of the Rabi frequencies of the $\sigma_{\mp}$ components of the input field, as shown in the figure. These are defined as

$$2g_1 = 2\frac{\vec{d}_{e1}.\hat{x}\mathcal{E}}{\hbar} = \frac{D\mathcal{E}_-}{\hbar}; \quad 2g_2 = 2\frac{\vec{d}_{e3}.\hat{x}\mathcal{E}}{\hbar} = -\frac{D\mathcal{E}_+}{\hbar}, \tag{2.11}$$

where, D is the magnitude of the dipole moment matrix element between the levels $|e\rangle$ and $|1\rangle$ and is proportional to the reduced matrix elements for the relevant $|F_e, m_F = 0\rangle \leftrightarrow |F_g, m_F = \pm 1\rangle$ transitions and can be calculated using the Wigner-Eckert theorem for the hyperfine levels [see Appendix F].

The probe field detuning is defined as $\delta = \omega - \omega_{e1}$, ω_{e1} being the atomic transition frequency between the levels $|e\rangle$ and $|1\rangle$. The parameters $\gamma_{\alpha\beta}$ denote the spontaneous decay rate from the level $|\beta\rangle$ to $|\alpha\rangle$ and $\Gamma_{\alpha\beta}$ denotes the decay rate of the coherence between the levels $|\alpha\rangle$ and $|\beta\rangle$. Note that in the above equations, we have ignored the decay of the level $|e\rangle$ to the level $|2\rangle$ (a case when the system could be an open system). These equations can be solved in steady state. Assuming the fields to be weak enough so that the system behaves like a linear medium, we can use the perturbative method as described in Appendix A. Thus, we obtain the following solutions for the susceptibilities of the $\sigma_{\pm}$ components of the probe:

$$\chi_+(\omega) = \left(\frac{ND^2}{\hbar\Gamma}\right)\frac{-i\Gamma}{2[i(\delta+2B)-\Gamma]}; \quad \chi_-(\omega) = \left(\frac{ND^2}{\hbar\Gamma}\right)\frac{-i\Gamma}{2(i\delta-\Gamma)}, \tag{2.12}$$

where N is the atomic number density of the medium. Here we have considered $\Gamma_{ej} = \Gamma$ $(j \in 1, 3)$ without loss of generalization.

The results we have obtained in (2.12) refer to two-level problems in the transitions of $\sigma_{\pm}$. Thus, at its resonance, either component suffers large absorption [large Im(χ)] and large normal dispersion (referring to slow group velocity). The other component at this frequency suffers less absorption due to off-resonance from the corresponding transition[1] as well as almost flat dispersion, i.e., $\partial\chi/\partial\omega \approx 0$ (leading to no change of the group velocity from that in the vacuum). Thus both the components would come out from the medium at different times due to different group velocities inside the medium. But due to large absorption of the resonant component inside the medium, only the off-resonant

[1]Both the components have the same frequency as they are derived from the same x-polarized light field.

component survives till the output end. Thus the system under consideration could be termed as a polarizing medium, but not as a polarization splitter.

The requirement for splitting of the pulse into its two polarization components is that the absorption of both the components must be much less so that both of them will come out of the medium almost unattenuated. On the other hand, the difference between their group velocities must be sufficiently large so as to resolve them in time domain (i.e., the time separation of them at the end point of the medium must be larger than the width of the pulse). We should emphasize that the time-separation is to be calculated between the peaks of the pulse components. This requires large asymmetry between $\chi_{\pm}$. This could be done using large magnetic field [see Eq. (2.12)], which however would create Paschen-Back splitting in both the excited and ground state manifold. To circumvent these difficulties, one can employ a control electric field with suitable polarization and frequency to make use of EIT. We apply a coherent cw field on the transition $|e\rangle \leftrightarrow |2\rangle$ ($F_g = 0, m_F = 0$)

$$\vec{E}_c(z,t) = \vec{\mathcal{E}}_c(z)e^{-i\omega_c t} + \text{c.c.} \tag{2.13}$$

Thus the equations (2.10) become modified. We take the decay from the level $|e\rangle$ to $|2\rangle$ into account now. The new density matrix equations can be solved analytically in steady state assuming the Rabi frequency of the control field $2G = 2\vec{d}_{e2}.\vec{\mathcal{E}}_c/\hbar$ to be much larger than the Rabi frequencies $2g_i$ of the $\sigma_{\pm}$ components. The susceptibilities of these components get modified by the control field and are given by

$$\bar{\chi}_+(\omega) = \left(\frac{ND^2}{\hbar\Gamma}\right)\frac{1}{2}\frac{-i\Gamma[i(\delta+2B-\Delta)-\Gamma_{23}]}{[i(\delta+2B)-\Gamma][i(\delta+2B-\Delta)-\Gamma_{23}]+|G|^2}, \tag{2.14a}$$

$$\bar{\chi}_-(\omega) = \left(\frac{ND^2}{\hbar\Gamma}\right)\frac{1}{2}\frac{-i\Gamma[i(\delta-\Delta)-\Gamma_{12}]}{(i\delta-\Gamma)[i(\delta-\Delta)-\Gamma_{12}]+|G|^2}, \tag{2.14b}$$

where $\Delta = \omega_c - \omega_{e2}$ is the detuning of the control field from the corresponding transition.

2.3.1 Numerical analysis

These susceptibilities in units of $ND^2/\hbar\Gamma$ have been plotted with respect to probe detuning δ/Γ in the Fig. 2.2. We have used the parameters for ^{23}Na vapor with the

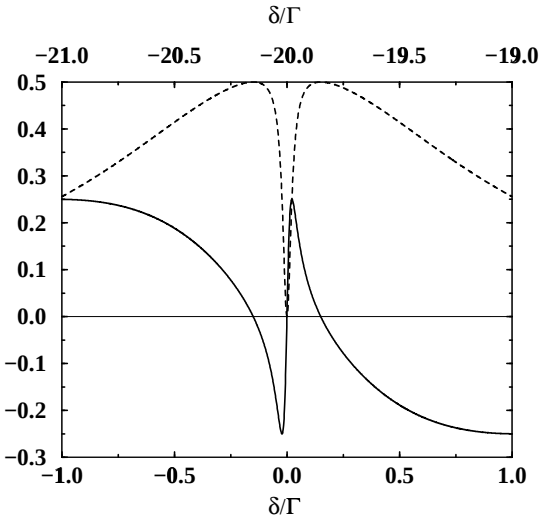

Figure 2.2: The variations of real (solid line) and imaginary (dotted line) parts of the susceptibilities $\bar{\chi}_+$ [upper tick-labels in x-axis] and $\bar{\chi}_-$ [lower tick-labels in x-axis] in units of $ND^2/\hbar\Gamma$ with probe detuning δ/Γ are plotted here. The parameters used are $G = 0.15\Gamma$, and $\Delta = 0$. All the other parameters are explained in the text. At the EIT window $\delta = \Delta = 0$ of the σ_- component, the Im$[\bar{\chi}_+]$ attains a value of 3.38×10^{-7}.

spontaneous decay rate of the level $|e\rangle$ (the A-coefficient) $A = 6.2 \times 10^7$, s^{-1}[2], the wavelength for the ground to excited level transition $\lambda = 5890$ Å[3], density of atoms in the medium $N = 2.2 \times 10^{11}$ atoms cm^{-3}. We have assumed a Zeeman splitting of $B = 10\Gamma$ for the present case, which corresponds to a magnetic field of amplitude ~ 70 G (see Appendix F), For ^{23}Na, Γ can be calculated to be 6γ, where $\gamma = A/12$. Because the transition between the ground levels are not dipole-allowed, there is no spontaneous decay between them. Further, we have assumed that there is no collisional relaxation and Dopler-broadening between the levels such that $\Gamma_{12} = \Gamma_{13} = \Gamma_{23} = 0$.

[2]This is the decay rate from the level $2P_{1/2}$ to the ground level $2S_{1/2}$. The treatment of the decay rate requires caution if these levels get resolved as in our case. Here $A = \sum_i \gamma_{ie}$ to take into account all the dacays from the upper level.

[3]The corresponding angular frequency is $2\pi\times$ 5.1 $\times 10^{14}$ Hz, whereas, the detuning we consider in this kind of problem becomes of the order of 10^6 Hz, which is much less than the transition frequency.

2.3.2 Explanation

Now onwards in this chapter, we assume that the electric field amplitude to have certain frequency profile. This pulse has certain central frequency, same as ω we have introduced in (2.1) and the amplitude of the pulse at this frequency is maximum.

From Fig. 2.1, it is clear that upon application of the control field, either component sees a Λ configuration for $(2g_i, 2G)$ field combination. Thus they experience EIT at respective resonances, i.e., at the detunings $\delta = \Delta$ (for σ_- component) and $\delta = \Delta - 2B$ (for σ_+ component).

The lower tick-labels in the x-axis in Fig. 2.2 shows that when $\delta = \Delta$, i.e., when the central frequency of the pulse is near-resonance with the $|e\rangle \leftrightarrow |1\rangle$ transition, the σ_- component shows a normal dispersive nature, which corresponds to a slow group velocity v_g^-; whereas the dispersion of the σ_+ component shows a flatter behavior in frequency domain, which means that this component will propagate with a group velocity not too different from its velocity c in vacuum. Note that because the σ_+ component is far detuned, its absorption through the medium is small ($\mathrm{Im}[\bar{\chi}_+(\delta = \Delta)] \sim 3.38 \times 10^{-7}$ for the chosen parameters). The medium will appear transparent to the σ_- component also, because this satisfies the condition of EIT in the Λ-type sector comprising of the levels $|e\rangle, |1\rangle$ and $|2\rangle$ of the configuration in Fig. 2.1. A similar situation prevails when $\delta = \Delta - 2B$, i.e., when the input pulse has a central frequency which is near-resonance with the $|e\rangle \leftrightarrow |3\rangle$ transition [upper tick-labels in x-axis; Fig. 2.2]. In that case, the σ_- component would propagate faster than the other [σ_+ component will satisfy the condition of EIT with the pump in the $|e\rangle \leftrightarrow |2\rangle$ transition and thereby experiences slow group velocities]. However both the components still propagate with negligible absorptions. In either case, because of the difference in group velocities inside the medium, the two circularly polarized components will come out of the medium at different times, without being absorbed significantly. Thus, the medium separates the two polarization components of the input pulse temporally. We have shown the response of the medium for the off-resonant control field in the Fig. 2.3 under the EIT condition $\delta = \Delta$. For this condition n_g^- attains a value of 3.92×10^6, whereas n_g^+ depends on the value of Δ. But still n_g^+ remains much less than n_g^-.

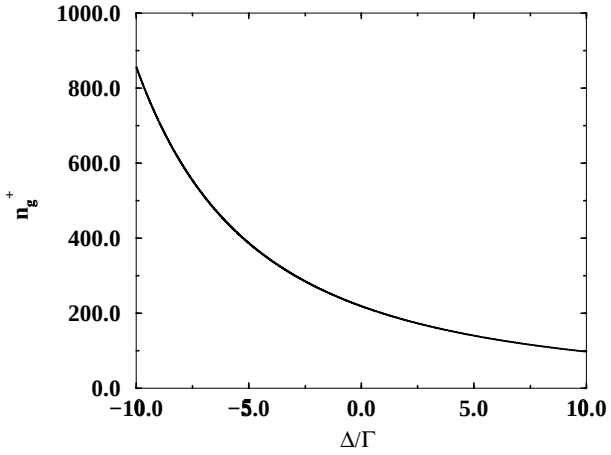

Figure 2.3: This figure shows the variation of n_g^+ with the pump detuning Δ/Γ at the EIT window $\delta = \Delta$ of σ_- component. The parameters used here are $N = 2.2 \times 10^{11}$ atoms cm^{-3}, $\lambda = 5890$ Å, and $\Gamma = 3.1 \times 10^7$ s^{-1}. All the other parameters are the same as in the Fig. 2.2. Here n_g^- remains constant at a value $\sim 3.92 \times 10^6$.

Thus the group velocities have significant difference in order of magnitude.

Further, we have compared the time-difference between the pulse components at the end point of the medium of length $l = 1$ cm. In Fig. 2.4, we have plotted the variation of temporal separation $\Gamma(t_+ - t_-)$ between the two polarization-components of the pulse with the probe-detuning δ/Γ. Here $t_\pm = l/v_g^\pm$ are the times taken by the $\sigma_\pm$ components to travel through the medium. We assumed that the peak of the pulse enters into the medium at time $t = 0$ and the pump is in resonance (i.e., $\Delta = 0$). The maximum time separation between two components is found to be about -130 μs. This occurs at $\delta = 0$, i.e., when the pulse is in resonance in its central frequency with the $|e\rangle \leftrightarrow |1\rangle$ transition as well as with the pump. The negative sign appearing here refers to the fact that the σ_+ component takes less time than the σ_- component, as expected. Clearly we can reverse the role of σ_+ and σ_- by working at $\delta = \Delta - 2B$.

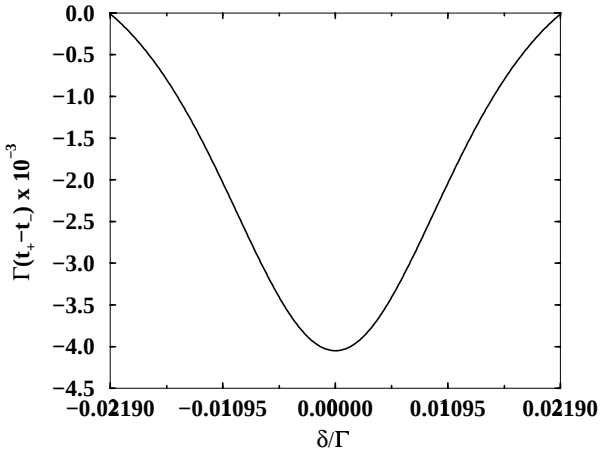

Figure 2.4: The variations of temporal separation between the two pulses with the probe detuning δ/Γ are shown here. The parameters used here are $l = 1$ cm and $\Delta = 0$. All the other parameters are the same as in the Fig. 2.3. Note that the σ_+ component moves faster inside the medium than the σ_- component around the EIT window $\delta = \Delta$.

2.3.3 Verification

We next confirm these results by studying the propagation of a Gaussian pulse through the medium [see Fig. 2.5(a)]. We choose its normalized envelop as follows:

$$\mathcal{E}(\omega) = \mathcal{E}_0 \frac{1}{\sigma\sqrt{\pi}} \exp\left[-\omega^2/\sigma^2\right]; \qquad \mathcal{E}(t) = \mathcal{E}_0 \exp\left(-\sigma^2 t^2/4\right). \tag{2.15}$$

where, σ gives the width of the pulse in frequency domain. To avoid unwanted absorption of the frequency components of the pulse, which are off-resonant, one has to choose a narrow-band pulse (small σ), so that it remains well within the EIT window. For our numerical calculation, we choose $\sigma = 2\pi \times 4.775$ kHz which is much less than width of the EIT window (cf. $\Gamma = 3.1 \times 10^7$ s^{-1}). Next using Eqs. (2.6) and (2.14), we evaluate numerically the output pulse and show the results in the Fig. 2.5(b). Clearly the pulse-components are well resolved in time-domain. This means that the peak-to-peak separation between the pulses is much larger than the temporal width of the pulses (Note that the width of any Gaussian pulse can be calculated in terms of the separation of times at which the pulse amplitude reduces to $1/e$ times its maximum value).

In Fig. 2.5(b), it is observed that the amplitude of the σ_+ component is much

reduced. It suffers from broadening also. This is due to substantial absorption of this component through the medium, for our specific choice of number density and central frequency of the pulse. If we would use less number density, the absorption would be less accordingly. On the other hand, the σ_- component also suffers from the absorption, even though we have chosen sufficiently small width of the pulse in frequency domain, so that the off-resonant components would not get absorbed much. We can trace out the reason of this from the following. We evaluate the envelop of this component at the end-point of the medium.

$$\mathcal{E}_-(l,t) = \mathcal{E}_0 \frac{\sigma'}{\sigma} \exp\left[-\frac{\sigma'^2}{4}\left(t - \frac{l}{v_g^-}\right)^2\right]; \tag{2.16}$$

$$\sigma' = \frac{\sigma}{\sqrt{1-i\kappa}}, \qquad \kappa = \frac{\sigma^2 l}{2c}\left[\frac{d^2}{d\omega^2}\left\{\omega\left[1+2\pi\chi_-(\omega)\right]\right\}\right]_{\omega=\omega_0}.$$

Detailed derivation of the above formula is given in the Appendix E. The intensity of the σ_- component thus gets reduced by $\mathrm{Im}(\kappa)$ [see Appendix E]. From the expression of κ, it is clear that the second order derivative of the susceptibility is the main contributing factor for this reduction. The reduction in amplitude as seen in the Fig. 2.5(b) is in conformity with it as $\mathrm{Im}(\kappa)$ is about 0.15 for the chosen parameters. Despite absorption, the two components are still *well separated in time*. The time separation between the two peaks in Fig. 2.5(b) is of the order of 4000 in units of $1/\Gamma$, which is in agreement with the value given in the Fig. 2.4 which is based on the calculation of group velocities. The time separation can in principle be made larger if we increase the density of the medium. However, the latter option would make the absorption of σ_+ quite large leading essentially to an output pulse which is primarily σ^- polarized, i.e., the medium would act like a polarizing medium. The results that are shown in the present chapter are quite optimum in terms of the chosen parameters. Any major change in the parameters would degrade the time-separation so that one cannot resolve the pulse components properly.

We have investigated the above effect in a different atomic system, where the configuration of the kind as shown in Fig. 2.1 is available. For example, in ^{7}Li [160] (nuclear spin $I = 3/2$), we identify the level $|e\rangle$ with the $2\mathrm{P}_{3/2}, F = 3, m_F = 0$ state and the ground levels ($|1\rangle, |2\rangle$, ad $|3\rangle$) with the $2\mathrm{S}_{1/2}, F = 2, m_F = -1, 0, +1$

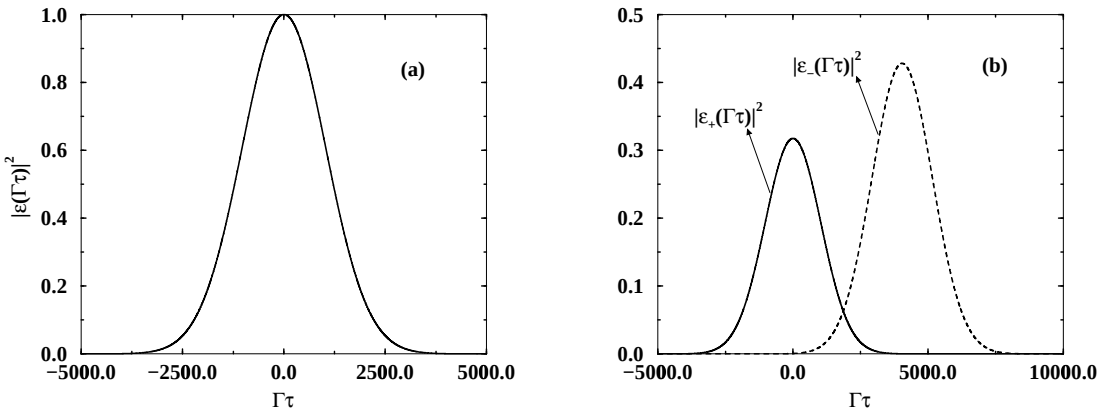

Figure 2.5: (a) This displays the input Gaussian pulse in time-domain with a width of $2\pi \times 4.775$ kHz; $|\mathcal{E}_+|^2 = |\mathcal{E}_-|^2 = |\mathcal{E}|^2/2$. (b) The two orthogonal components of the linearly polarized input probe pulse at the output of the medium are displayed here. It also demonstrates the temporal separation between them for $\delta = \Delta$. The solid line shows the σ_+ component and the dashed curve refers to the σ_- component. The parameters used here are the same as in the Fig. 2.3 and $\tau = t - l/c$.

state. In this configuration, the transition wavelength is $\lambda = 670.96$ nm. Because the Landé g-factor of the ground hyperfine levels is positive, the sublevel $m_F = -1$ shifts upwards. The result for pulse separation in this case can thus be obtained by changing B to $-B$. For this configuration, we have calculated the time-separation between the two pulse components keeping the other parameters, e.g., length of the medium l, atomic number density N etc. the same. We found that the time-separation $t_+ - t_-$ is $+282.5\mu$s. This means that the σ_- component will come out earlier than the σ_+ component for $\delta = \Delta$.

Chapter 3

Laser induced magneto-chiral anisotropy

So far in the previous chapters, we have described the propagation of polarized pulse through an atomic medium. In this chapter, we describe an interesting situation considering the incident field to be unpolarized.

3.1 Magneto-chiral anisotropy

The situation we will be describing in this chapter has large resemblance with the phenomena like natural optical activity [140] (discovered by Arago, 1811) and the magneto-chiral anisotropy (MCA) which occur in many systems in nature [162, 163, 164]. We already mentioned that the MOR refers to the difference in refraction between the two circular components. On the other hand, the NOA involves in a difference in absorption in 'chiral' media. However, the physical origin of these two are completely different. The MOR is a consequence of breaking of symmetry of the susceptibilities of the circular components by a magnetic field. But the NOA is a result of nonlocal optical response in a media which lacks all mirror symmetries.

There are several media in which under certain conditions both the time-reversal and mirror symmetries break down. A newer effect called the MCA arises in that case. Its existence can be appreciated by the following arguments. We expand the dielectric tensor of a chiral media subjected to the magnetic field to the first order in $\vec{k}$ and $\vec{B}$ as [165]

$$\varepsilon_{ij}(\omega, \vec{k}, \vec{B}) = \varepsilon_{ij}(\omega) + \alpha_{ijl}k_l + \beta_{ijl}(\omega)B_l + \gamma_{ijlm}(\omega)k_l B_m \ , \tag{3.1}$$

where the tensors α and β describe the NOA and the magneto-optical activity, respectively. Here ω is the optical frequency. For high symmetry media like gases, liquids, cubic or uniaxial crystals with the optical axis parallel to the applied magnetic field etc., the above can be simplified as

$$\varepsilon_{\pm}(\omega, \vec{k}, \vec{B}) = \varepsilon(\omega) \pm \alpha_{\mathrm{NOA}}(\omega)k \pm \beta_{\mathrm{MOR}}(\omega)B + \gamma_{\mathrm{MCA}}\vec{k}.\vec{B} \ , \tag{3.2}$$

where $\varepsilon_{\pm}$ are the relative dielectric constants for the left and right circularly polarized components ($\sigma_{\pm}$). The material parameters α, β, γ and ε are all generally complex-valued. The magneto-chiral anisotropy is basically represented by the fourth term in the above expression. It depends upon the *relative orientation* of $\vec{k}$ and $\vec{B}$ and hence the name. It is independent of the polarization also.

There have been a large number of theoretical and experimental investigation on MCA. After an implicit prediction of the MCA [166], the existence of the MCA in crystals was reported by Portigal and Burstein [165] who showed that two enantiomers (mirror images) of a chiral molecule can be discriminated as a consequence of MCA. Later, for molecules several predictions of MCA in absorption [167] and in refraction [168] have been made. A detailed theory of MCA, both dichroism (asymmetry in absorption) and birefringence (asymmetry in refractive index) in molecules have been developed by Barron and Vrbancich [169]. The first experiment on magneto-chiral dichroism was reported by Rikken and Raupach [163], whereas several papers have investigated magneto-chiral birefringence [170]. These later experiments were unsuccessful to measure the change in refractive index upto the correct order, as theory predicts [167]. Vallet *et al.* [164] have been able to correct this discrepancy and measured the change in refractive index upto order of 10^{-10}, as predicted. The MCA has been observed in electrical conductors also [171]. Further using the magneto-chiral effect, selectivity of the either enantiomer has been demonstrated recently by Rikken and Raupach [172]. In their experiment, chiral molecules interact with unpolarized light, and they have investigated the effect of the magnetic field on this interaction. So far we have given a brief relevant discussion of the effect of MCA.

In the present work, we describe how one can create asymmetry in the output intensity upon reversal of magnetic field as an effect of coherent control. Thus this

is quite similar in the effect (as the MCA in absorption refers to the sensitiveness of the output intensity on the direction of the magnetic field), but very much differs in the physical content. The experimental techniques to verify MCA are quite cumbersome, as the effect itself is very small to measure. This smallness arises from the fact the the MCA is a manifestation of the simultaneous effects of magnetic dipole and electric quadrupole moments. On the other hand, the present work should be understood as a electric dipole effect. As dipole effect is very large in order of magnitude than the higher order multipole moments, the asymmetry discussed in this work will be much larger and easily measurable. Thus we can distinguish it from the MCA that arises from a term in polarization which is a product of B and k [see Eq. 3.2].

3.1.1 Magnetic field reversal symmetry

Let us first describe what does it mean by magnetic field reversal symmetry. In this chapter, we will be dealing with a monochromatic field which can be written in the form

$$\vec{E} \equiv (\mathcal{E}_+\hat{\epsilon}_+ + \mathcal{E}_-\hat{\epsilon}_-)e^{ikz-i\omega t} + \text{c.c.}, \tag{3.3}$$

where $\hat{\epsilon}_\pm$ is given by (2.3) and

$$\mathcal{E}_\pm = \left(\frac{\mathcal{E}_x \mp i\mathcal{E}_y}{\sqrt{2}}\right), \quad k = \frac{\omega}{c}. \tag{3.4}$$

Note that there are no Fourier components in the expression for $\vec{E}$ above, as we are not considering any pulse here. The output field thus can be written as

$$\vec{E}_0 = \vec{\mathcal{E}}_0 e^{ikz-i\omega t} + \text{c.c.}, \tag{3.5}$$

where

$$\vec{\mathcal{E}}_0 = \mathcal{E}_+\hat{\epsilon}_+ e^{2\pi ikl\chi_+} + \mathcal{E}_-\hat{\epsilon}_- e^{2\pi ikl\chi_-}. \tag{3.6}$$

For an unpolarized field, there is random phase difference between the amplitudes $\mathcal{E}_x$ and $\mathcal{E}_y$. Further the intensities (observable quantity) along any two orthogonal directions $(\hat{n}, \hat{n}_\perp)$ are equal. This means

$$\langle \mathcal{E}_x^* \mathcal{E}_y \rangle = 0, \quad \langle \mathcal{E}_x^* \mathcal{E}_x \rangle = \langle \mathcal{E}_y^* \mathcal{E}_y \rangle = \frac{I}{2}, \tag{3.7}$$

I being the intensity of the incident field. From Eqs. (3.4)-(3.7), we can evaluate the output intensity $I_0 = \langle|\vec{\mathcal{E}}_0|^2\rangle$:

$$\begin{aligned} I_0 &\equiv \frac{I}{2}\left[|e^{2\pi ikl\chi_+}|^2 + |e^{2\pi ikl\chi_-}|^2\right] \\ &= \frac{I}{2}\left[\exp\left\{-4\pi kl\mathrm{Im}(\chi_+)\right\} + \exp\left\{-4\pi kl\mathrm{Im}(\chi_-)\right\}\right]. \end{aligned} \tag{3.8}$$

Note that the real part of $\chi_\pm$ contributing to the phase of the field only does not appear in the square moduli of the pulses. Clearly the output intensity is a symmetric function of χ_+ and χ_-. The medium we are considering is an anisotropic one, being subjected to a dc magnetic field. In most cases, one can find a situation, where the susceptibilities $\chi_\pm$ obey the following relation when the direction of the magnetic field is reversed

$$\chi_\pm(B) = \chi_\mp(-B). \tag{3.9}$$

Here $-B$ stands for the amplitude for the reversed magnetic field. Then from (3.8), we find that for an unpolarized input field

$$I_0(B) = I_0(-B). \tag{3.10}$$

i.e., the output intensity remains the same irrespective of whether the magnetic field is parallel or antiparallel to the direction of propagation of the electromagnetic field as long as (3.9) is satisfied. This situation is referred to as magnetic field reversal symmetry.

In this chapter we investigate how this symmetry can be broken down, i.e., we are aiming at a situation when $I_0(B) \neq I_0(-B)$. We are calling this effect as magnetic field reversal asymmetry (MFRA). Thus, the transmission of unpolarized light through an otherwise isotropic medium can be made sensitive to the direction of the magnetic field. In what follows would be perhaps the first demonstration of the dependence of transmission of the unpolarized light on the direction of B in an *atomic vapor*.

3.2 Large magnetic field reversal asymmetry using EIT

3.2.1 A qualitative idea

Consider the following scenario. Let us consider first the case when $\vec{B}$ is applied parallel to the direction of propagation of the electromagnetic field. Suppose the control field is applied such that the medium appears transparent to the σ_+ component of the unpolarized light, i.e., $\mathrm{Im}[\chi_+(B)] \approx 0$ due to outset of EIT. For magnetic field bigger than the typical linewidth (of the relevant atomic levels), the component σ_- is off-resonant. Thus σ_- exhibits very little absorption $\mathrm{Im}(\chi_-) \approx 0$. Under such conditions, Eq. (3.8) shows that the transmitted intensity $\approx I$. Now if the direction of the magnetic field is reversed, then we easily find the situation when σ_+ component becomes off-resonant from the corresponding transition, i.e., $\mathrm{Im}(\chi_+) \approx 0$, whereas the σ_- component can become resonant and suffers large absorption, i.e., exhibits large $\mathrm{Im}(\chi_-)$. Thus only the σ_+ component survives the medium. This gives rise to an intensity $\sim I/2$. Thus the transmittivity reduces by a factor $1/2$ upon reversal of the magnetic field. It is thus clear how coherent fields can be used to create large MFRA.

3.2.2 Atomic configuration

We now demonstrate the feasibility of these ideas. We consider a configuration [see Fig. 3.1] which can be found, for example, in hyperfine levels of ^{23}Na [173]. The level $|g\rangle$ ($|3^2S_{1/2}; F = 1, m_F = 0\rangle$) is coupled to the upper level $|e_-\rangle$ ($|3^2P_{1/2}; F = 2, m_F = -1\rangle$) and $|e_+\rangle$ ($|3^2P_{1/2}; F = 2, m_F = +1\rangle$) by the σ_- and σ_+ components of the probe field, respectively. Thus the system is equivalent to two coupled two-level systems. The susceptibilities for the two components of the probe acting on the transitions $|g\rangle \leftrightarrow |e_-\rangle$ and $|g\rangle \leftrightarrow |e_+\rangle$ can be easily calculated as

$$\chi_-(B) = \frac{-i\gamma\alpha_0}{i(\delta - B) - \Gamma_{e_-g}}\,, \tag{3.11a}$$

$$\chi_+(B) = \frac{-i\gamma\alpha_0}{i(\delta + B) - \Gamma_{e_+g}}\,, \delta \equiv \omega - \omega_{e_+g}(B = 0)\,, \tag{3.11b}$$

where, α_0 is given by $N|\vec{d}|^2/\hbar\gamma$ and is related to the absorption in the line-center for $B = 0$. It should be borne in mind that B represents the Zeeman splitting of

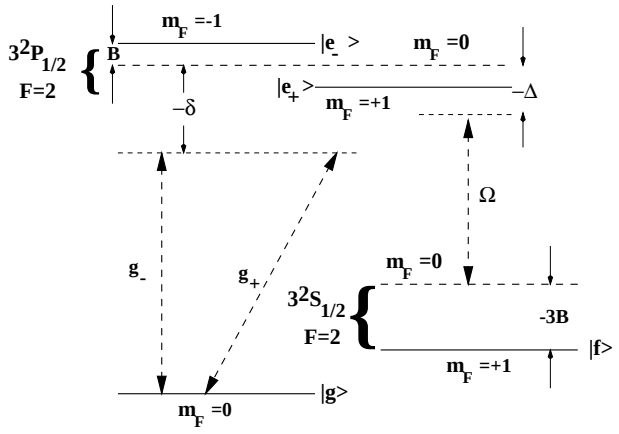

Figure 3.1: The ^{23}Na hyperfine level configuration is shown here. Here, $B > 0$ is the applied magnetic field strength, $2g_{\pm}$ are the probe Rabi frequencies for the $\sigma_{\pm}$ components, and Ω is the half of the pump Rabi frequency. The respective detunings $\delta = [\omega_p - \omega_{e_+g}(B = 0)]$ and Δ for the probe and pump fields are defined with respect to the energy separation between the levels $(|3^2P_{1/2}; F = 2, m_F = 0\rangle, |g\rangle)$ and $(|3^2P_{1/2}; F = 2, m_F = 0\rangle, |3^2S_{1/2}; F = 2, m_F = 0\rangle)$, respectively. Changing the direction of the magnetic field interchanges the positions of $|e_-\rangle$ and $|e_+\rangle$. Besides, the level $|f\rangle$ moves above the dashed line for $|3^2S_{1/2}; F = 2, m_F = 0\rangle$.

the level $m_F = -1$. Thus B has the unit of frequency. Here 2γ is the spontaneous decay rate from the level $|e_-\rangle$, $\Gamma_{e_{\mp}g} = \gamma$ is the decay rate of the off-diagonal density matrix elements between the levels $|e_{\mp}\rangle$ and $|g\rangle$, N is the atomic number density, $|\vec{d}|$ is the dipole moment matrix element between the levels $|e_-\rangle$ and $|g\rangle$, and δ is the detuning of the probe field from the $|g\rangle \leftrightarrow |3^2P_{1/2}; F = 2, m_F = 0\rangle$ transition. We consider B to be a positive quantity. Thus a reversed magnetic field will be represented by $-B$. The detuning δ would always be defined with respect to the levels in the absence of the magnetic field. It is interesting to note that though $\chi_+(B) \neq \chi_-(B)$, the relation (3.10) holds for all δ [see Eqs. (3.8) and (3.11)]. Also note that the condition (3.9) holds in this case.Thus to breakdown the magnetic field reversal symmetry, one has to breakdown the above symmetry (3.9) of the susceptibilities $\chi_{\pm}$.

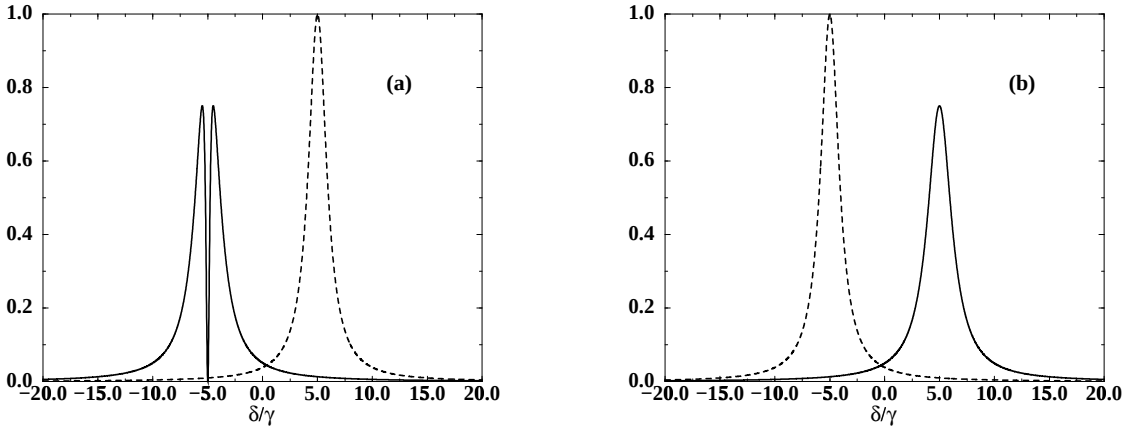

Figure 3.2: The variation of imaginary parts of the susceptibilities $\bar{\chi}_+$ (solid curve) and $\bar{\chi}_-$ (dashed curve) in units of α_0 with probe detuning δ/γ are shown for the $\bar{\chi}_\pm(B)$ [(a)] and $\bar{\chi}_\pm(-B)$ [(b)]. The parameters used here are $\Omega = 0.5\gamma$, $B = 5\gamma$ corresponding to 105 G, $\Gamma_{e_+g} = 4\gamma/3$, $\Gamma_{fg} = 0$, $\Gamma_{e_-g} = \gamma$, and $\Delta = 2B$.

3.2.3 How one can obtain the asymmetry ?

To create a large asymmetry between the output intensities $I_0(B)$ and $I_0(-B)$, we now apply a π-polarized coherent control field

$$\vec{E}_p(t) = \vec{\mathcal{E}}_p e^{-i\omega_p t} + \text{c.c.} \tag{3.12}$$

on the transition $|e_+\rangle \leftrightarrow |f\rangle$ ($|3^2S_{1/2}; F = 2, m_F = +1\rangle$). This modifies the susceptibility χ_+ of the σ_+ component to

$$\begin{aligned} \bar{\chi}_+(B) &= \frac{-i\gamma\alpha_0[i(\delta - \Delta + 3B) - \Gamma_{fg}]}{[i(\delta + B) - \Gamma_{e_+g}][i(\delta - \Delta + 3B) - \Gamma_{fg}] + |\Omega|^2}, \\ \Delta &= \omega_p - \omega_{e_+f}(B = 0). \end{aligned} \tag{3.13}$$

Here, $\Delta = 2B$ is the detuning of the pump field from the transition $|3^2P_{1/2}; F = 2, m_F = 0\rangle \leftrightarrow |3^2S_{1/2}; F = 2, m_F = 0\rangle$ transition [see Fig. 3.1], $\Omega = \vec{d}_{e_+f}.\vec{\mathcal{E}}_p/\hbar$ is the half of the pump Rabi frequency. The parameter Γ_{fg} represents the collisional dephasing between the states $|f\rangle$ and $|g\rangle$. In what follows we use $\Gamma_{fg} = 0$, i.e., we are assuming no collisional relaxation in the medium. Here $\Gamma_{e_-g} = \gamma$ and $\Gamma_{e_+g} = 4\gamma/3$, taking all the spontaneous decays from the upper levels into consideration. The level $|f\rangle$ is Zeeman separated from the level $|3^2S_{1/2}; F = 2, m_F = 0\rangle$ by an amount

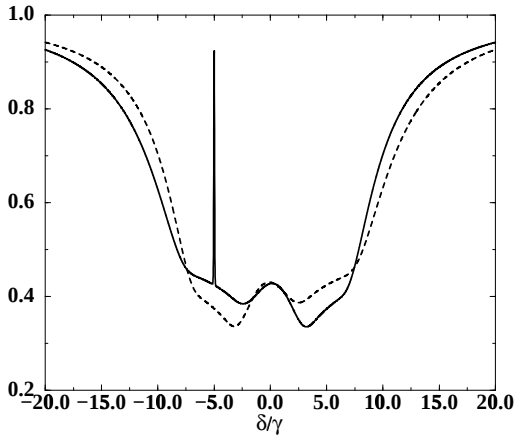

Figure 3.3: This figure shows the variation of the transmittivity $T(B)$ (solid curve) and $T(-B)$ (dashed curve) with respect to probe field detuning δ/γ. The parameters used here are $N = 10^{10}$ atoms cm^{-3}, $\lambda = 589$ nm, and $L = 1$ cm. All the other parameters used are the same as in Fig. 3.2.

of $3B$, whereas the levels $|e_{\pm}\rangle$ are separated by an amount $\mp B$. All these Zeeman separations can be calculated by using the Landé g-factors of the corresponding manifolds[1]. The susceptibility $\bar{\chi}_-$ remains the same as in (3.11a). Thus one could create large asymmetry between the susceptibilities $\chi_{\pm}$. Clearly the equality (3.9) no longer holds. Note that in presence of the control field, the response of the system is equivalent to a two-level system comprised of $(|e_-\rangle, |g\rangle)$ [for σ_- component] and a Λ-system [for σ_+ component] comprised of $(|e_+\rangle, |f\rangle, |g\rangle)$ connected via the common level $|g\rangle$.

It is clear that applying a coherent pump field, one can generate an EIT window at $\delta = -B$ (cf., $\Delta = 2B$) for the σ_+ component [Im $(\bar{\chi}_+) = 0$] in the relevant Λ-type sector comprising of the levels $|g\rangle, |e_+\rangle$, and $|f\rangle$. On the other hand, the absorption peak of the σ_- component occurs at $\delta = B$. Thus, this component suffers a little absorption [Im $(\bar{\chi}_-) \approx 0$] at $\delta = -B$ as the field is far detuned from the $|e_-\rangle \leftrightarrow |g\rangle$ transition as long as we choose the magnetic field much larger than the width of the transition [see Fig. 3.2(a)]. Thus the unpolarized probe field travels through the medium almost unattenuated. The transmittivity $T(B) = I_0(B)/I$ becomes

[1]For $|e_{\pm}\rangle$ manifold $g_F = 1/6$ and for the level $|f\rangle$, $g_F = -1/2$; see Appendix F

almost unity at $\delta = -B$ as obvious from Eq. (3.8) [see Fig. 3.3].

If now the direction of the magnetic field is reversed ($B \to -B$), the level $|e_{\pm}\rangle$ exchange their positions, whereas the level $|f\rangle$ also shifts upwards above the corresponding $m_F = 0$ level. The corresponding susceptibilities for σ_- and σ_+ polarizations become

$$\bar{\chi}_-(-B) = \frac{-i\gamma\alpha_0}{i(\delta + B) - \Gamma_{e_-g}}\,, \tag{3.14a}$$

$$\bar{\chi}_+(-B) = \frac{-i\gamma\alpha_0[i(\delta - \Delta - 3B) - \Gamma_{fg}]}{[i(\delta - B) - \Gamma_{e_+g}][i(\delta - \Delta - 3B) - \Gamma_{fg}] + |\Omega|^2}\,. \tag{3.14b}$$

We continue to take the quantization axis as defined by the direction of the propagation of the electromagnetic field. This means that we are keeping the direction of the electric field $\vec{k}$ the same and only reversing the direction of the magnetic field. Clearly now at $\delta = -B$, $\bar{\chi}_-(-B)$ has absorption peak and σ_- component of the probe will be absorbed. If we continue to use $\Delta = 2B$, i.e., if we keep the control laser frequency fixed while we change the direction of the magnetic field, then $\bar{\chi}_+(-B)$ exhibits resonances at $\delta = 3B \pm \sqrt{4B^2 + \Omega^2}$, both of which are far away from the point $\delta = -B$ unless we choose $\Omega^2 = 12B^2$ (a case we discuss later). Clearly, for $\delta = -B$ and $\Omega^2 \neq 12B^2$, the σ_+ component of the probe will suffer very little absorption. This is in contrast to the behavior of the σ_- component which will be attenuated by the medium. Thus the output field would essentially have the contribution from the σ_+ component only. The transmittivity $T(-B) = I_0(-B)/I$ of the medium decreases to about $1/2$. Thus by using EIT we can produce the result $T(B) \approx 2T(-B)$, i.e., we can alter the transmittivity of the medium by just reversing direction of the magnetic field. The equality (3.10) no longer is valid and the medium behaves like a magneto-chiral medium. This becomes quite clear from the Fig. 3.3, at $\delta = -B$.

3.2.4 Magnetic switching of transmission of an atomic medium

A quite different result is obtained by choosing the parameter region differently. We can find a condition when the absorption peak of both the $\sigma_{\mp}$ components coincide with each other. For the case when the magnetic field is applied in the opposite to the direction of propagation, the absorption peaks of the $\sigma_{\mp}$ compo-

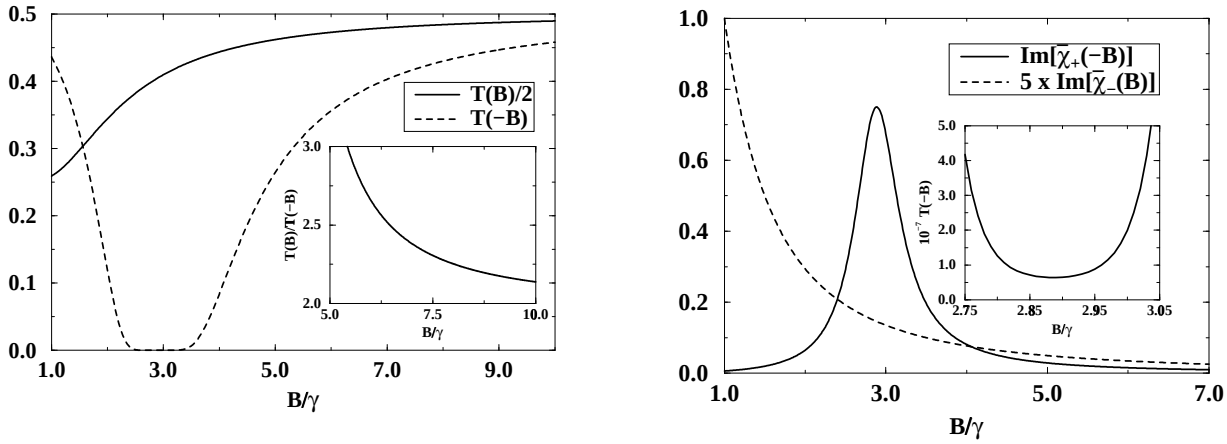

Figure 3.4: (a)The transmittivities $T(B)$ and $T(-B)$ calculated at the value $\delta = -B$ is plotted here with respect to B/γ, for $\Omega = 10\gamma$ and $\Delta = 2B$. The inset shows the magnetic field dependence of the ratio $T(B)/T(-B)$ for the same parameters. All the other parameters are the same as in Fig. 3.3. (b)The variation of the imaginary parts of the susceptibilities $\bar{\chi}_+(-B)$ and $\bar{\chi}_-(B)$ in units of α_0 with the magnetic field B/γ for $\delta = -B$. The inset shows the variation $T(-B)$ with B in the vicinity of $\Omega = 2\sqrt{3}B$. The parameters used here are the same as in Fig. 3.4(a).

nents occur at $\delta = -B$ and $\delta = 3B \pm \sqrt{4B^2 + \Omega^2}$, for a specific choice of pump detuning $\Delta = 2B$. Equating them, we find a relation

$$\Omega = 2\sqrt{3}B \ . \tag{3.15}$$

Clearly, for this value of pump Rabi frequency, the σ_- component gets attenuated due to resonance with the corresponding transition. Moreover, the σ_+ component also gets absorbed significantly. This is the case of antiparallel orientation of $\vec{B}$ and $\vec{k}$. Thus $T(-B)$ becomes insignificant compared to $T(B)$ as shown in Fig. 3.4(a). For larger values of B, the result is shown in the inset. Here $T(B)/T(-B)$ is in the range 2 to 3. The case displayed in Fig. 3.4(a) is quite an unusual one. Such a large dichroism (asymmetry in absorption of two polarization components) of unpolarized light is the result of the application of a coherent control field whose parameters are chosen suitably. Clearly, this effect can be viewed as a process in which an optically transparent dilute atomic medium becomes opaque ($T(-B) \ll T(B)$) and vice versa by just reversing the magnetic field direction. We may call it a magnetic switch of transmittivity of the unpolarized light.

The behavior shown in the Fig. 3.4(a) is easily understood from the magnitudes

of the imaginary parts of the susceptibilities $\bar{\chi}_{\pm}(\pm B)$. In the parameter domain under consideration, $\mathrm{Im}[\bar{\chi}_{+}(B)] = 0$ due to EIT and $\mathrm{Im}[\bar{\chi}_{-}(-B)] = \alpha_0$, because the σ_{-} component is on resonance for $\vec{B}$ antiparallel to the direction of propagation. Further as shown in the Fig. 3.4(a), in the region around $\Omega = 2\sqrt{3}B$, $\mathrm{Im}[\bar{\chi}_{-}(B)] \ll \mathrm{Im}[\bar{\chi}_{+}(-B)]$. Thus both σ_{-} and σ_{+} components are absorbed if $\vec{B}$ is antiparallel to $\vec{k}$ (the absorption peaks of the components coincide with each other), making the medium opaque as shown in the inset of Fig. 3.4(a). The opacity disappears if direction of $\vec{B}$ is reversed (see Fig. 3.4(a), solid curve). For values of B away from the equality $\Omega = 2\sqrt{3}B$, $\mathrm{Im}[\bar{\chi}_{+}(-B)]$ decreases leading to a sharp increase in the transmission $T(-B)$.

3.2.5 Question of time-reversal symmetry

We already have mentioned that in the process of MCA, the time-reversal symmetry (TRS) breaks down. In fact, the magnetic field reversal interchanges the positions of the Zeeman sublevels. This has close resemblance with the time-reversal [174]. Thus it is sufficient to examine the symmetry properties of the Hamiltonian under the transformation $B \to -B$, in the present case. We note from the Fig. 3.1 that the unperturbed Hamiltonian in the absence of the control field is

$$H_0 = (-\delta - B)|e_+\rangle\langle e_+| + (-\delta + B)|e_-\rangle\langle e_-|. \tag{3.16}$$

A transformation $B \to -B$ is like interchanging the states $|e_+\rangle$ and $|e_-\rangle$. Thus any physical result which involves states $|e_{\pm}\rangle$ symmetrically will not change by changing the direction of $\vec{B}$. This is the case with the transmission (3.8). Next when we apply the control field Ω, then the unperturbed Hamiltonian is

$$\begin{aligned} H_0 \;=\; & (-\delta - B)|e_+\rangle\langle e_+| + (-\delta + B)|e_-\rangle\langle e_-| \\ & +(-\delta + \Delta - 3B)|f\rangle\langle f| + \Omega(|e_+\rangle\langle f| + |f\rangle\langle e_+|). \end{aligned} \tag{3.17}$$

The states $|e_+\rangle$ and $|f\rangle$ are mixed by the control field with an amount of mixing that is independent on the magnetic field. Clearly we have lost the symmetry property of H_0 and hence of the transmission (3.8). It is easily seen that (3.16) has the TRS (i.e., symmetry under the transformations $B \to -B$ and $|e_{\pm}\rangle \to |e_{\mp}\rangle$

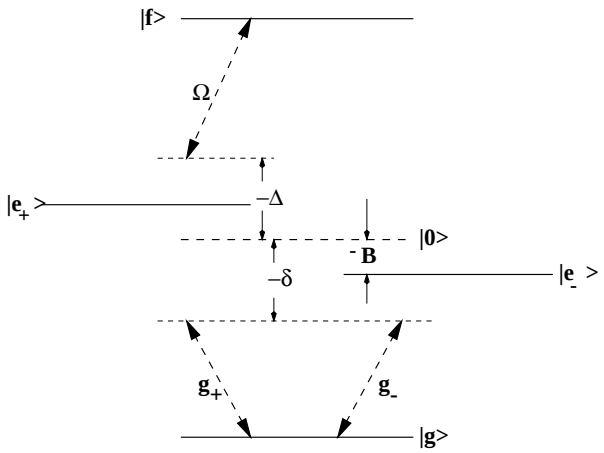

Figure 3.5: The ^{40}Ca level configuration has been shown here. Here, $2g_{\pm}$ are the probe Rabi frequencies for the $\sigma_{\pm}$ components, B is the magnetic field strength, Ω is the half of the pump Rabi frequency, δ and Δ are the respective detuning for the probe and the pump fields. These detunings are defined with respect to the energy separation between the levels $(|0\rangle, |g\rangle)$ and $(|0\rangle, |f\rangle)$, respectively.

as well) whereas (3.17) has no such symmetry. Thus in terms of the TRS, the MCA and MFRA are analogous to each other.

3.3 Large magnetic field reversal asymmetry in ladder system

It may be recalled that there are many different situations where pump cannot be applied in a Lambda configuration. This, say, for example, is the case for ^{40}Ca. The relevant level configuration is shown in Fig. 3.5 [144]. The level $|g\rangle$ $(|4s^2; j = 0, m_j = 0\rangle)$ is coupled to $|e_+\rangle$ $(|4s4p; j = 1, m_j = +1\rangle)$ and $|e_-\rangle$ $(|4s4p; j = 1, m_j = -1\rangle)$ via the σ_+ and σ_- components of the input unpolarized probe field, respectively. In this configuration, the susceptibilities of the two circularly polarized components of the probe are given by

$$\begin{aligned} \chi_+(B) &= \frac{-i\gamma\alpha_0}{i(\delta - B) - \gamma}\,, \\ \chi_-(B) &= \frac{-i\gamma\alpha_0}{i(\delta + B) - \gamma}\,, \ \delta = \omega - \omega_{e_- g}(B = 0)\,, \end{aligned} \tag{3.18}$$

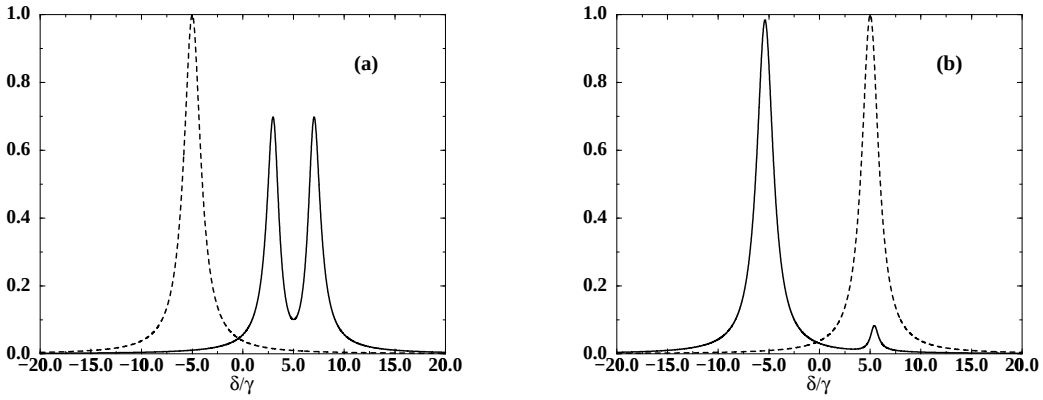

Figure 3.6: The variation of imaginary parts of the susceptibilities $\bar{\chi}_+$ (solid curve) and $\bar{\chi}_-$ (dashed curve) in units of α_0 with respective to the probe detuning δ/γ are shown here for $\bar{\chi}_\pm(B)$ [(a)] and $\bar{\chi}_\pm(-B)$ [(b)]. The parameters used here are $\Omega = 0.5\gamma$, $B = 5\gamma$ corresponding to 123 G, $\Gamma = 0.45\gamma$, and $\Delta = -B$.

where, $\alpha_0 = N|\vec{d}|^2/\hbar\gamma$, N is the number density of the medium, δ is the detuning of the probe field with respect to the $|g\rangle \leftrightarrow |0\rangle$ ($|4s4p; j = 1, m_j = 0\rangle$) transition, $|\vec{d}|$ is the magnitude of the dipole moment matrix element between the levels $|e_+\rangle$ and $|g\rangle$, and 2γ is the decay rate from the levels $|e_+\rangle$ and $|e_-\rangle$ to the level $|g\rangle$. Note that $\chi_\pm$ satisfy the condition (3.9). This clearly predicts perfect symmetry in the transmittivity of the medium upon reversal of the direction of the magnetic field, irrespective of δ.

We will now show how one can use a coherent control field to create asymmetry between $T(B)$ and $T(-B)$. We apply a coherent pump (3.12) to couple $|e_+\rangle$ with a higher excited level $|f\rangle$ ($|4p^2; j = 0, m_j = 0\rangle$) with Rabi frequency $2\Omega = 2\vec{d}_{fe_+}.\vec{\mathcal{E}}_p/\hbar$. This helps to create a ladder configuration for the σ_+ component in the $(|g\rangle, |e_+\rangle, |f\rangle)$, while the σ_- component interacts with an effective two-level configuration, at least upto the first order of the probe field. The susceptibility for σ_+ component now changes to [157]

$$\begin{aligned} \bar{\chi}_+(B) &= \frac{-i\gamma\alpha_0[i(\Delta+\delta)-\Gamma]}{[i(\delta-B)-\gamma][i(\Delta+\delta)-\Gamma]+|\Omega|^2}, \\ \Delta &= \omega_p - \omega_{fe_+}(B=0), \end{aligned} \tag{3.19}$$

where, $\Gamma = 0.5(\lambda_{e_+g}/\lambda_{fe_+})^3\gamma = 0.45\gamma$ is the spontaneous decay rate of the upper level $|f\rangle$ [cf., $\lambda_{e_+g} = 422.7$ nm and $\lambda_{fe_+} = 551.3$ nm], $\lambda_{\alpha\beta}$ is the wavelength of the

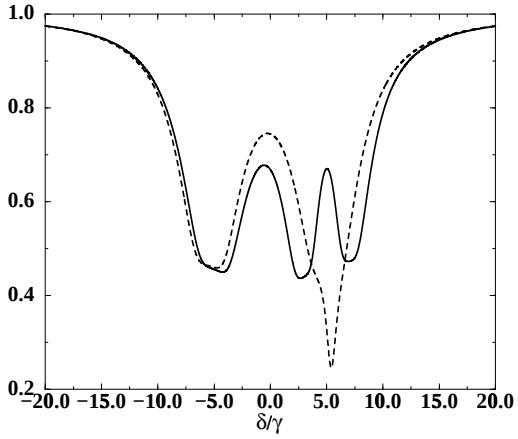

Figure 3.7: The variation for the transmittivities $T(B)$ (solid curve) and $T(-B)$ (dashed curve) with the probe detuning δ/γ are shown in this figure. The parameters used here are $N = 10^{10}$ atoms cm^{-3}, $\lambda_{e+g} = 422.7$ nm, $L = 1$ cm, and the other parameters are the same as in Fig. 3.6.

transition between $|\alpha\rangle$ and $|\beta\rangle$, $\Delta = -B$ is the detuning of the pump field from the $|f\rangle \leftrightarrow |0\rangle$ transition [see Fig. 3.5]. Thus a transparency dip in the absorption profile of the σ_+ component is generated at $\delta = B$ (which is a condition of two-photon resonance from the level $|g\rangle$ to the level $|f\rangle$; $\delta + \Delta = 0$). On the other hand, as the σ_- component remains far-detuned from the corresponding transition, as shown in Fig. 3.6(a), its absorption is much less at $\delta = B$. Note that the transparency for σ_+ is not total which is in contrast to a Lambda system. We display in the Fig. 3.7 the behavior of the transmittivity $T(B)$ of the medium as a function of the detuning. At $\delta = B$, the transmittivity becomes large.

Now upon reversal of the magnetic field direction, the σ_+ component gets detuned from corresponding transition and thereby suffers little absorption. But the σ_- component, being resonant with the corresponding transition, gets largely attenuated inside the medium. This is clear from the Fig. 3.6(b). Thus the contribution to the transmittivity $T(-B)$ comes primarily from the σ_+ component. The Fig. 3.7 exhibits the behavior of $T(-B)$ as the frequency of the probe is changed. In the region of two-photon resonance (EIT), $T(B)$ is several times $T(-B)$. Note that in the present configuration also, one could create MFRA using the notion of

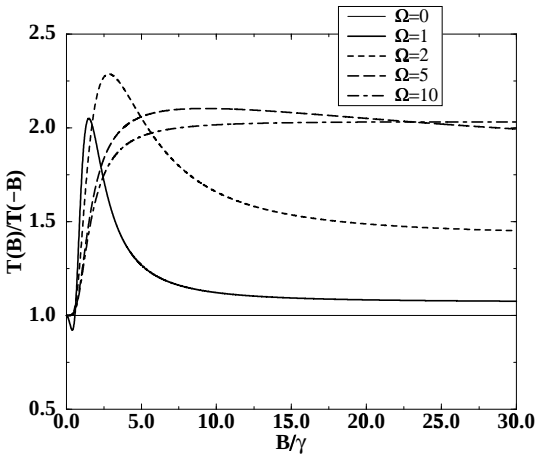

Figure 3.8: The variation of the ratio $T(B)/T(-B)$ calculated at $\delta = B$ with the magnetic field strengths B/γ are shown in this figure for different values of Ω. All the parameters are the same as in Fig. 3.7.

coherent control.

In Fig. 3.8, we have shown how the ratio $T(B)/T(-B)$ calculated at $\delta = B$ is modified with change in the magnitude of the applied magnetic field for different control field Rabi frequencies. Note that for large B and Ω, this ratio approaches the value of two, though for intermediate values it can even exceed two.

3.4 Effect of Doppler broadening in MFRA

We next consider the effects of Doppler broadening on the MFRA in the level configuration in Fig. 3.1. We would like to find parameter regions where $T(B)$ and $T(-B)$ could differ significantly.

Maxwell-Boltzmann velocity distribution function is based on the assumption that in any gaseous sample, the atoms are moving in random direction and with random velocities. The velocity distribution function is Gaussian in nature, the width of which depends upon the temperature of the sample. In the present context, in the presence of the moving atoms, the atom *sees* that the frequency of the electric field is shifted by an amount $\vec{k}.\vec{v}$, where $\vec{v}$ is the velocity of the atoms itself. If the atomic moves opposite to or along the direction of propagation of the

interacting field, then the frequency shift of the field would be $\mp k_z v_z$, assuming that the field is propagating in the z-direction. Thus the detuning of the field would be shifted accordingly. In the present case, the detuning of the pump becomes $\Delta_v = 2B + k_p v_z$, where v_z is the component of the atomic velocity in the direction of the propagation of the electric fields, where k_p is the wave vector amplitude of the pump field. We assume that the pump field propagates in the same direction $\vec{k}_p$ as the probe field wave vector $\vec{k}$ and we further take k and k_p to be approximately equal.

We calculate the Doppler-averaged susceptibilities through the following relation:

$$\langle \bar{\chi}_{\pm}(v_z) \rangle = \int_{-\infty}^{\infty} \bar{\chi}_{\pm}(v_z) \sigma_D(v_z) dv_z, \tag{3.20}$$

where,

$$\sigma_D(v_z) = \frac{1}{\sqrt{2\pi\omega_D^2}} e^{-v_z^2/2\omega_D^2} \tag{3.21}$$

is the Maxwell-Boltzmann velocity distribution at a temperature T with the width $\omega_D = \sqrt{K_B T/M}$, K_B is the Boltzmann constant, and M is the mass of an atom.

The integration (3.20) results in a complex error function [175] (see Appendix G). The result could be interesting in mathematical term. However, to have a physical understanding, we integrate (3.20) by approximating σ_D by a Lorentzian $\sigma_L(v_z)$ of the width $\tilde{\omega}_D = 2\omega_D \ln 2$. This method has been developed by Kash *et al.* [103], who have used the notion that the area under a normalized Gaussian and a normalized Lorentzian is the same, if the width is chosen appropriately. This Lorentzian is given by

$$\sigma_L(v_z) = \frac{\tilde{\omega}_D/\pi}{v_z^2 + \tilde{\omega}_D^2}. \tag{3.22}$$

Using this profile in lieu of σ_D, the integration above is analytically possible without any mathematical jargon. One has to use the method of residues. Noting that the profile σ_L has two complex poles at $v_z = \pm i\tilde{\omega}_D$, and writing the expressions for $\bar{\chi}_{\pm}(\delta_v)$ in form of

$$\bar{\chi}_{\pm} = \frac{-\gamma\alpha_0/k}{v_z - v_{\pm}}\,, \tag{3.23}$$

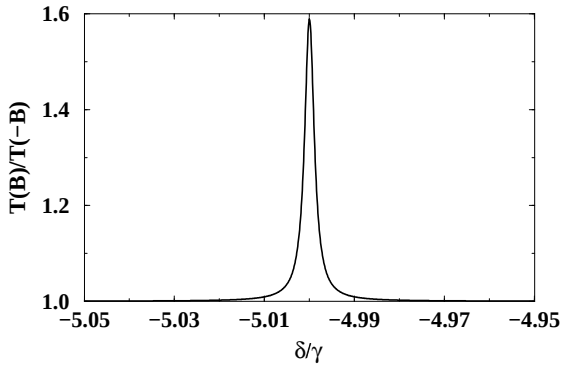

Figure 3.9: The variation in $T(B)/T(-B)$ with the probe detuning δ/γ in a 6 cm Doppler-broadened medium. All the other parameters are the same as in Fig. 3.4(a). Note that $T(B)$ is the transmission for $\vec{B}$ parallel to $\vec{k}$.

we are led to the following results:

$$\langle \bar{\chi}_{\pm}(v_z) \rangle = \frac{\gamma \alpha_0}{k(v_{\pm} - i\tilde{\omega}_D)}, \tag{3.24}$$

where,

$$\begin{aligned} v_+ &= \frac{i\{[i(\delta + B) - \Gamma_{e_+ g}]P + |\Omega|^2\}}{kP}; \\ P &= i(\delta - \Delta + 3B) - \Gamma_{fg}, \\ v_- &= \frac{i[i(\delta - B) - \Gamma_{e_- g}]}{k}. \end{aligned} \tag{3.25}$$

Here we have used the expressions (3.11a) and (3.13) for $\bar{\chi}_{\pm}(v_z)$. These susceptibilities (3.24) are used to calculate the transmittivities at the point $\delta = -B$. In Fig. 3.9 we have shown the corresponding variation of $T(B)$ and $T(-B)$ with δ/γ. We find that the ratio $T(B)/T(-B)$ increases to a value ~ 1.6, for a 6 cm medium. It is clear that, if we choose a longer medium in this case, the MFRA will be further enhanced. We have actually also carried out numerically the integration (3.20). For the parameters of the Fig. 3.9, the results do not change substantially.

Chapter 4

Magneto-optical rotation of spectrally impure fields and its nonlinear dependence on optical density

We have already mentioned that the MOR angle is proportional to the number density of the medium. Thus, increasing the number density of the medium helps in achieving large rotation angles. Recently, very large rotation angles ($\sim 150^0$) in a cold sample have been reported [154]. In this experiment, optical densities of the order of $10 - 20$ were achieved. This experiment also reported a very interesting result, viz., the departure from the linear dependence of the rotation angle on the optical density. This departure has been ascribed to the nonmonochromatic nature of the input laser. The standard MOR theory does not explain this nonlinear behavior. In this chapter, we provide a complete theory of this in a quantitative manner. We will discuss the dependence of the rotation angle on the spectral profile of the input laser. We present a first principle calculation of this dependence.

4.1 Magneto-optical rotation

4.1.1 Basic equations

We consider a plane polarized probe field given by the Eq. (3.3), propagating through an anisotropic medium in the z-direction. Thus the polarization induced

in the atomic medium due to this probe field is given by

$$\vec{\mathcal{P}} = [\mathcal{E}_+\chi_+\hat{\epsilon}_+ + \mathcal{E}_-\chi_-\hat{\epsilon}_-]\, e^{ikz-i\omega t} + \text{c.c.}\,. \tag{4.1}$$

Here $\chi_\pm$ are the susceptibilities of the two circular components $\sigma_\pm$ ($\equiv \hat{\epsilon}_\pm$). Clearly, when the incident probe passes through the medium, different polarization components evolve according to its own susceptibility. The dynamics is governed by the equation (1.4). We assume that $\mathcal{E}_\pm$ and $\chi_\pm$ are independent of time. Thus substituting (4.1) in (1.4) and invoking the SVEA [see Eq. (1.12)] we obtain the following first order differential equations:

$$\begin{aligned} \frac{\partial \mathcal{E}_+}{\partial z} &= 2\pi i k \chi_+ \mathcal{E}_+ \,, \\ \frac{\partial \mathcal{E}_-}{\partial z} &= 2\pi i k \chi_- \mathcal{E}_- \,. \end{aligned} \tag{4.2}$$

Here we have assumed that the medium is so dilute that $|4\pi\chi_\pm| \ll 1$. In general $\chi_\pm$ are the functions of $\mathcal{E}_\pm$. However we consider a weak probe, thus $\chi_\pm$ are independent of $\mathcal{E}_\pm$. The solutions of the above equations can be easily written as

$$\mathcal{E}_\pm(l) = \mathcal{E}_\pm(0)\exp[2\pi i k l \chi_\pm]\,. \tag{4.3}$$

Thus we get the output field (3.6), where l is the length of the medium along z direction. For an x-polarized light, we can write $\mathcal{E}_\pm(0) = \mathcal{E}_0/\sqrt{2}$. Thereby the output field can be rewritten as

$$\begin{aligned} \vec{\mathcal{E}}_l &= \frac{\mathcal{E}_0}{\sqrt{2}}\left[\hat{\epsilon}_+ e^{2\pi i k l \chi_+} + \hat{\epsilon}_- e^{2\pi i k l \chi_-}\right] \,, \\ &= \frac{\mathcal{E}_0}{2}\left[\hat{x}\left\{e^{2\pi i k l \chi_+} + e^{2\pi i k l \chi_-}\right\} + i\hat{y}\left\{e^{2\pi i k l \chi_+} - e^{2\pi i k l \chi_-}\right\}\right] \,. \end{aligned} \tag{4.4}$$

If we assume that the absorption of the $\sigma_\pm$ components to be small or equal, then the ratio of the field-amplitudes in the polarization direction $\hat{y}$ and $\hat{x}$ is given by

$$\frac{\mathcal{E}_y}{\mathcal{E}_x} = \tan\theta = \tan\left[\pi k l \text{Re}(\chi_- - \chi_+)\right] \,. \tag{4.5}$$

Thus the rotation of polarization of an x-polarized incident probe is given by the angle

$$\theta = \pi k l \text{Re}(\chi_- - \chi_+) \,. \tag{4.6}$$

This rotation is referred to as MOR, as we have mentioned in the Introduction.

Because the susceptibilities $\chi_{\pm}$ are proportional to the number density N, thus the MOR angle θ in turn is proportional to the optical density α defined by

$$\alpha = \frac{3\lambda^2}{2\pi} N l \ , \tag{4.7}$$

where λ is the wavelength of the input field. Clearly, it is expected that an increase in number density would lead to large rotation angle. However, because of onset of absorption for large N, the standard theory of MOR that is developed for a nonattenuating medium becomes invalid. In fact, the input field no longer remains linearly polarized after passing through such an absorbing medium. Thus the medium becomes both circularly birefringent (difference in dispersion) and circularly dichroic (difference in absorption). The output field becomes elliptically polarized under the action of such an medium. To treat this kind of situation, we adopt the Stokes' formalism.

4.1.2 Stokes formalism

To fully characterize the polarization state of the output field, one has to use the Stokes parameters [176]. The four Stokes parameters for an electric field are designated by S_α ($\alpha \in 0, 1, 2, 3$) and can be defined as follows:

$$S_0 = I_{||} + I_{\perp} \ , \tag{4.8a}$$

$$S_1 = I_{||} - I_{\perp} \ , \tag{4.8b}$$

$$S_2 = I_{45^o} - I_{-45^o} \ , \tag{4.8c}$$

$$S_3 = I_{\sigma_+} - I_{\sigma_-} \ , \tag{4.8d}$$

where, $I_{\hat{n}} = |\hat{n}.\vec{E}_l|^2$ is the measured intensity along the polarization direction $\hat{n}$. Then the output polarization state can be characterized by the following three quantities:

$$P = \frac{\sqrt{S_1^2 + S_2^2 + S_3^2}}{S_0} \ , \tag{4.9a}$$

$$\tan 2\theta = \frac{S_2}{S_1} \quad (0 \leqslant \theta < \pi) \ , \tag{4.9b}$$

$$\tan 2\phi = \frac{S_3}{S_0 P} \quad (-\pi/4 < \phi \leqslant \pi/4) \ , \tag{4.9c}$$

where, P is the degree of polarization, i.e., the ratio of the intensities of the polarized component to the unpolarized one, θ is the MOR angle of the input field and is measured between the major axis of the ellipse and the x-axis, ϕ provides the ellipticity of polarization through the relation $e = \tan\phi$. For a fully polarized light $P = 1$ and for an unpolarized light $P = 0$.

From Eq. (3.5) one can express the output intensities along different polarization directions in the following way:

$$I_{\parallel}(\omega) = |\hat{x}.\vec{\mathcal{E}}_l|^2 = \frac{I_o}{4}|e^{2\pi ikl\chi_+} + e^{2\pi ikl\chi_-}|^2 , \tag{4.10a}$$

$$I_{\perp}(\omega) = |\hat{y}.\vec{\mathcal{E}}_l|^2 = \frac{I_o}{4}|e^{2\pi ikl\chi_+} - e^{2\pi ikl\chi_-}|^2 , \tag{4.10b}$$

$$\begin{aligned} I_{\pm 45^o}(\omega) &= \left|\frac{\hat{x} \pm \hat{y}}{\sqrt{2}}.\vec{\mathcal{E}}_l\right|^2 \\ &= \frac{I_o}{8}|(1 \pm i)e^{2\pi ikl\chi_+} + (1 \mp i)e^{2\pi ikl\chi_-}|^2 , \end{aligned} \tag{4.10c}$$

$$I_{\sigma_\pm}(\omega) = |\hat{\epsilon}_{\pm}.\vec{\mathcal{E}}_l|^2 = \frac{I_o}{2}\exp\left[-4\pi kl.\mathrm{Im}(\chi_\pm)\right] , \tag{4.10d}$$

where, $I_o = |\mathcal{E}|^2$ is the input intensity of laser field.

4.1.3 Recent experiment

Labeyrie *et al.* performed an experiment on cold ^{85}Rb atoms which are subjected to an external magnetic field (so as to make the system anisotropic). A weak laser field with different Lorentzian line-widths have been sent through the medium along the direction of the applied magnetic field. Next they investigated its output intensity measured at different polarization directions by changing the optical density α. They have reported very large MOR angle ($\sim 150^0$) in this experiment. Optical density of the order of $10 - 20$ has been achieved. The authors have shown that the MOR angle depends *nonlinearly* on the optical density for larger densities. This departure has been ascribed to the the nonmonochromatic nature of the input field. If one increases the line-width of the electric field, then this nonlinearity arises even for smaller values of α. Clearly, as the standard theory of MOR does not explain this behavior, a more quantitative analysis is warranted. Specifically, in this chapter, we show how the *spectral impurity* of the input field affects the polarization of the output field.

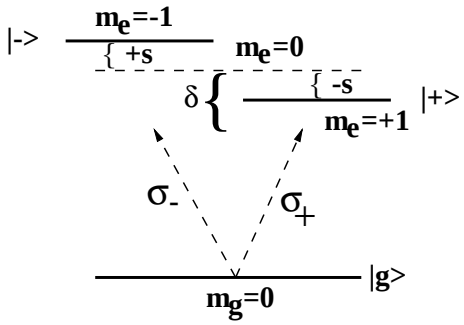

Figure 4.1: Level diagram for a three-level configuration. The excited levels $|\pm\rangle$ ($m_e = \pm 1$) are Zeeman shifted from the level $m_e = 0$ by an amount s. The detuning δ is defined between the levels $m_e = 0$ and $m_g = 0$.

For simplicity, we assume that the line-shape of the input is Lorentzian in nature:

$$S(\omega) \equiv I_o \frac{\gamma_c/\pi}{\gamma_c^2 + (\omega - \omega_l)^2} , \tag{4.11}$$

where, ω_l is the central frequency of the laser field and $2\gamma_c$ is the full width at half maximum. Note that all the measured quantities defined by Eq. (4.10) are functions of the frequency of the exciting field. If the exciting field is spectrally impure, then the Stokes parameters $\langle S_\alpha \rangle$ are to be obtained by averaging over the spectrum $S(\omega)$ of the laser field. Thus, I's in Eq. (4.8) are to be obtained from

$$\langle I_{\hat{n}} \rangle = \frac{1}{I_o} \int_{-\infty}^{\infty} d\omega I_{\hat{n}}(\omega) S(\omega) . \tag{4.12}$$

We next use these equations to uncover the effect of optical density and non-monochromaticity of the exciting field on MOR angle.

4.2 A simplified atomic model

We first consider a three-level atom in V configuration (see Fig. 4.1). The levels $|\pm\rangle$ ($J_e = 1, m_e = \pm 1$) are coupled to the ground state $|g\rangle$ ($J_g = 0, m_g = 0$) by two circular components $\sigma_\pm$ of $\hat{x}$-polarized electric field [Eq. (3.3)]. The excited level degeneracy has been removed by an uniform magnetic field $\vec{B}$ applied in the direction of propagation of the applied electric field. The levels $|e_\pm\rangle$ are shifted about line-center by an amount of $\mp\mu_B B/\hbar$ (μ_B=Bohr magneton). The field $\vec{E}$ is

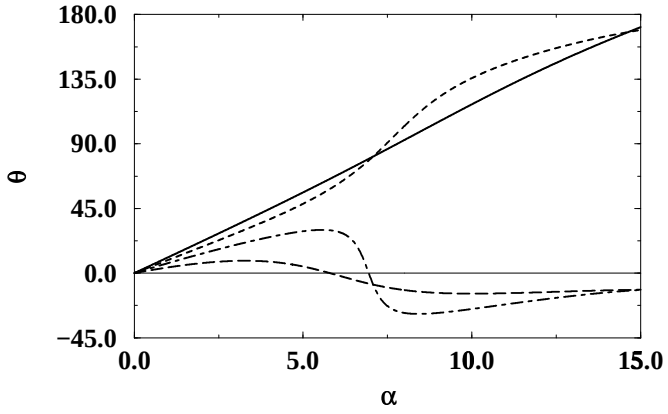

Figure 4.2: Variation of MOR angle θ with optical density α for $s = 2\gamma$ and different laser line-widths $\gamma_c = 0.1\gamma$ (solid line), $\gamma_c = 0.5\gamma$ (dashed line), $\gamma_c = \gamma$ (dot-dashed line), and $\gamma_c = 2\gamma$ (long-dashed line). We have chosen $\lambda = 422.67$ nm corresponding to ^{40}Ca $1S_0 \leftrightarrow 1P_1$ transitions. Note the nonlinear dependence of θ on α for larger γ_c.

detuned from the line center by an amount $\delta = \omega_{+g}(B = 0) - \omega$, $\omega_{+g}(B = 0)$ being the atomic transition frequency in absence of the magnetic field.

The susceptibilities of the $\sigma_\pm$ components inside the medium can be written as

$$\chi_\pm = \frac{N|\vec{d}|^2}{\hbar\gamma}\rho_\pm; \quad \rho_\pm = \frac{i\gamma}{\gamma + i(\delta \mp s)} , \tag{4.13}$$

where, $2\gamma = 4|\vec{d}|^2\omega^3/3\hbar c^3$ is the spontaneous decay rate of the levels $|\pm\rangle$, $|\vec{d}|$ is the magnitude of the dipole moment vector for the transitions $|\pm\rangle \leftrightarrow |g\rangle$, N is the atomic number density, and $s = \mu_B B/\hbar$ is the Zeeman splitting of the excited levels. Using these $\chi_\pm$, we can now write the field amplitude from Eq. (3.5) as

$$\vec{\mathcal{E}}_l = \left[\hat{\epsilon}_+\mathcal{E}_+ e^{i\frac{\alpha}{2}\rho_+} + \hat{\epsilon}_-\mathcal{E}_- e^{i\frac{\alpha}{2}\rho_-}\right] , \tag{4.14}$$

where, $\alpha = 4\pi klN|\vec{d}|^2/\hbar\gamma = (3\lambda^2/2\pi)Nl$ is the optical density of the medium.

4.2.1 Numerical results

In what follows, we will assume that $\omega_l = \omega_{+g}(B = 0)$, i.e., the applied field is in resonance with the $m_e = 0$ level at its central frequency. We calculate $\langle I_{\hat{n}}\rangle$'s using Eqs. (4.11) and (4.12) numerically for different values of γ_c and s. We show the results in Fig. 4.2. We clearly see that for $\gamma_c \ll s$, the rotation angle θ is linearly

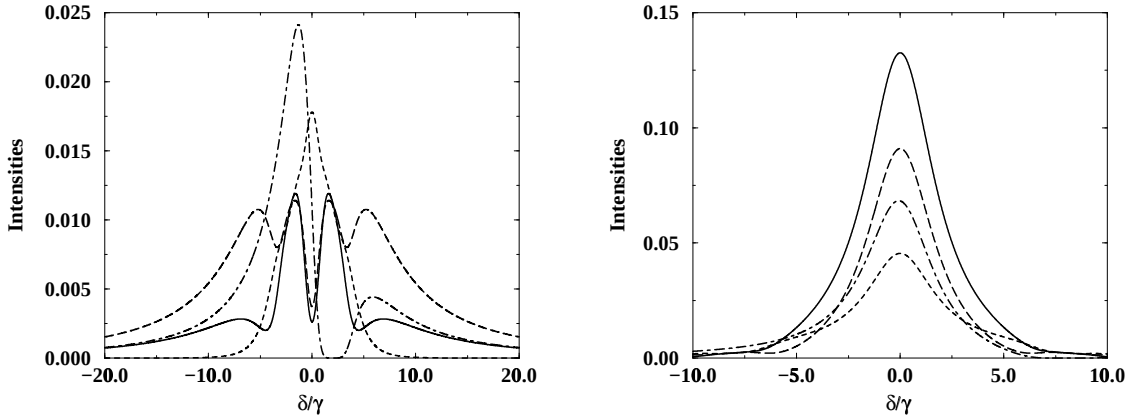

Figure 4.3: Variation of the output intensities I_{+45° (solid line), $I_{||}$ (dashed line), $I_{\perp}$ (long-dashed line), and I_{σ_+} (dot-dashed line) multiplied by the Lorentzian line-shape profile $S(\omega)$ for (a) $\gamma_c = 0.5\gamma$ and (b) $\gamma_c = 2\gamma$. We have chosen $\alpha = 10$, $s = 2\gamma$, and the input intensity to be normalized. Note that for lager γ_c, the contribution of the off-resonant components to the output become larger.

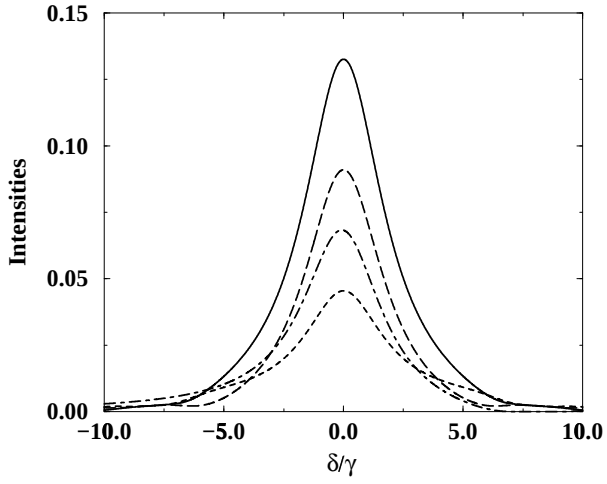

Figure 4.4: Variation of the output intensities (with the same legends) for $s = 8\gamma$ and $\gamma_c = 2\gamma$. The other parameters are the same as in Fig. 4.3.

proportional to α. But for $\gamma_c \gtrsim s$, this variation deviates from linearity in large α domain. This behavior can be explained in terms of the off-resonant components which dominate for the large γ_c and large α.

4.2.2 Analysis

In order to understand the numerical results, we first consider the limit of small optical densities whence

$$S_1 = \frac{1}{2}[2 + \alpha \mathrm{Re}\{i(\rho_+ + \rho_-)\}] \,, \tag{4.15a}$$

$$S_2 = \frac{\alpha}{2}\mathrm{Re}(\rho_- - \rho_+) \,. \tag{4.15b}$$

Thus, the departure of the rotation angle from the linearity has to do with the averages of the exponentials appearing in I's [Eq. (4.10)]. If one were to make the approximation of replacing all χ's in Eq. (4.10) by their averages, i.e.,

$$\langle \exp\left[2\pi i k l \chi_\pm\right] \rangle \equiv \exp[2\pi i k l \langle \chi_\pm \rangle] \,, \tag{4.16}$$

then the Stokes parameters $\langle S_1 \rangle$ and $\langle S_2 \rangle$ would be

$$\langle S_1 \rangle = e^{-\frac{\alpha}{2}(\langle \rho_2^+ \rangle + \langle \rho_2^- \rangle)} \cos\left[\frac{\alpha}{2}(\langle \rho_1^+ \rangle - \langle \rho_1^- \rangle)\right] \,, \tag{4.17a}$$

$$\langle S_2 \rangle = -e^{-\frac{\alpha}{2}(\langle \rho_2^+ \rangle + \langle \rho_2^- \rangle)} \sin\left[\frac{\alpha}{2}(\langle \rho_1^+ \rangle - \langle \rho_1^- \rangle)\right] \,, \tag{4.17b}$$

where, $\langle \rho_\pm \rangle = \langle \rho_1^\pm \rangle + i\langle \rho_2^\pm \rangle$ and thus

$$\langle \theta \rangle = \frac{\alpha}{4}(\langle \rho_1^- \rangle - \langle \rho_1^+ \rangle) = \frac{1}{2} \cdot \frac{\alpha \gamma s}{(\gamma + \gamma_c)^2 + s^2} \,. \tag{4.18}$$

Clearly, the absorption does not contribute to the rotation angle. We have again obtained the linear dependence of θ on α, provided the approximation (4.16) is valid. Thus, any departure in linearity of θ with respect to α indicates the breakdown the approximation (4.16). The numerical results of Fig. 4.2 clearly show the breakdown of the mean field description obtained by replacing χ's by their average values.

From the Eq. (4.18), we readily see that in the low α-domain, by increasing s (or γ_c) while keeping γ_c (or s) constant, the slope of θ with α decreases. This is clear from the numerical results of Fig. 4.2. Also, for larger values of γ_c, variation

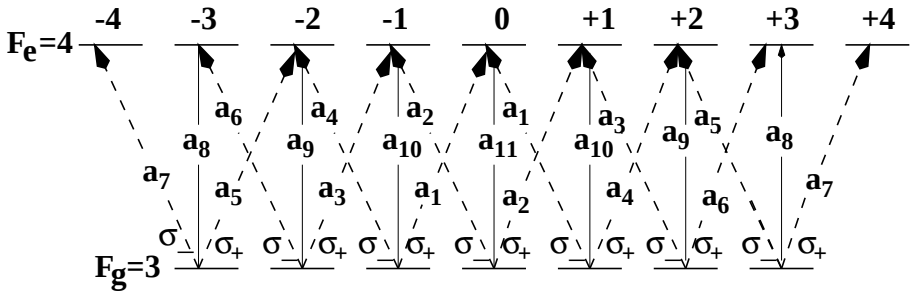

Figure 4.5: Level diagram for the $F_e = 4 \leftrightarrow F_g = 3$ transition. The numbers at the top of the figure indicate the magnetic quantum numbers of the sublevels. The relevant Clebsch-Gordan coefficients for the corresponding transitions are given by $a_1 = -1/\sqrt{42}, a_2 = -\sqrt{5}/3\sqrt{14}, a_3 = -1/2\sqrt{21}, a_4 = -\sqrt{5}/2\sqrt{21}, a_5 = -1/6\sqrt{7}, a_6 = -1/2\sqrt{3}, a_7 = -1/3, a_8 = -1/6, a_9 = -1/\sqrt{21}, a_{10} = -\sqrt{15}/6\sqrt{7}, a_{11} = 2/3\sqrt{7}$. The Zeeman splitting of the various sublevels are not shown.

of θ with α is deviated from linearity. We should emphasize that linear variation of θ with α is attributed to the monochromatic laser field. If the electric field is spectrally impure, then the off-resonant components also contribute to θ, through the relations (4.8), (4.9), and (4.12). Thus, θ starts varying with α linearly in low α limit, then saturates, and finally decreases to zero to change the direction of rotation, for larger γ_c (see Fig. 4.2). But for smaller γ_c, the linear behavior is retained even for larger α, as the off-resonant components are not dominant in this parameter zone. We show in Fig. 4.3 how the intensities of the off-resonant components vary with δ for different γ_c. Clearly, for larger γ_c, the intensities at the output become larger for the frequencies $\delta \neq 0$, which means the off-resonant components contribute to the MOR angle θ to a large extent through the relations (4.8), (4.8b), (4.8c), and (4.9b). However as shown in the Fig. 4.4, for a given γ_c, if one increases the magnetic field s, then the contribution of the on-resonant components prevails and thus the linearity between θ and α would retain.

Next we consider the variation of the degree of polarization P and the ellipticity e with α. We have noticed that P decreases from unity for increasing α. This means that the output field no longer remains fully polarized, rather it becomes partially polarized.

Again, from the Eqs. (4.8d), (4.10d), and (4.13), it is clear that an integration over the entire range of detuning δ would yield $\langle S_3 \rangle = 0$, as the integrand is an odd

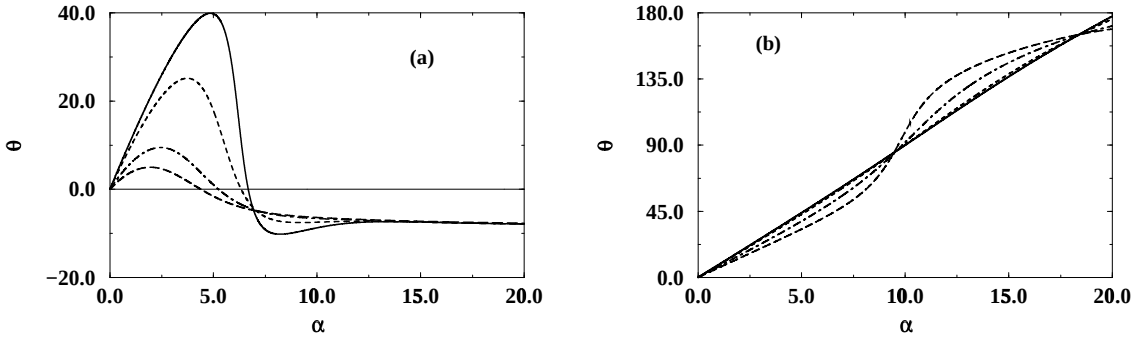

Figure 4.6: Variation of magneto-optical rotation angle θ with α for magnetic field (a) 2 Gauss ($\equiv 2\pi \times 2.8$ MHz) and (b) 8 Gauss ($\equiv 2\pi \times 11.2$ MHz) for laser line-widths $2\gamma_c = 2\pi \times 0.5$ MHz (solid line), $2\gamma_c = 2\pi \times 1$ MHz (dashed line), $2\gamma_c = 2\pi \times 3$ MHz (dot-dashed line), and $2\gamma_c = 2\pi \times 5$ MHz (long-dashed line). The dot-dashed curves correspond to the width of the laser used in the experiment [154]. Note that the line-width of the D_2 line is $2\pi \times 5.88$ MHz.

function of ω. Thus the ellipticity e becomes zero. This means that the polarized part of the output field remains linear.

From the above discussion, it is clear that the output field gets rotated as a manifestation of cumulative effect of optical density, magnetic field, and laser line-width. Also it becomes partially polarized with no ellipticity.

4.3 Quantitative modeling of experimental results of Labeyrie *et al.* for MOR in spectrally impure fields

We now extend our understanding of resonant MOR as described in the previous section to explain the experimental data of Labeyrie *et al.*. In their experiment, a cold atomic cloud of Rb^{85} is subjected to a static magnetic field. The laser probe beam passing through the medium in the direction of the magnetic field is tuned to the D_2 line of the atoms ($2S_{1/2} \leftrightarrow 2P_{3/2}$; λ=780.2 nm). They have measured the intensities of outputs with different polarizations, as function of laser detuning and also at different values of optical density. They have found a nonlinear dependence of the MOR angle θ on optical density. They found for larger magnetic field that the linear behavior persists.

To explain these observations in light of our previous discussions, we consider

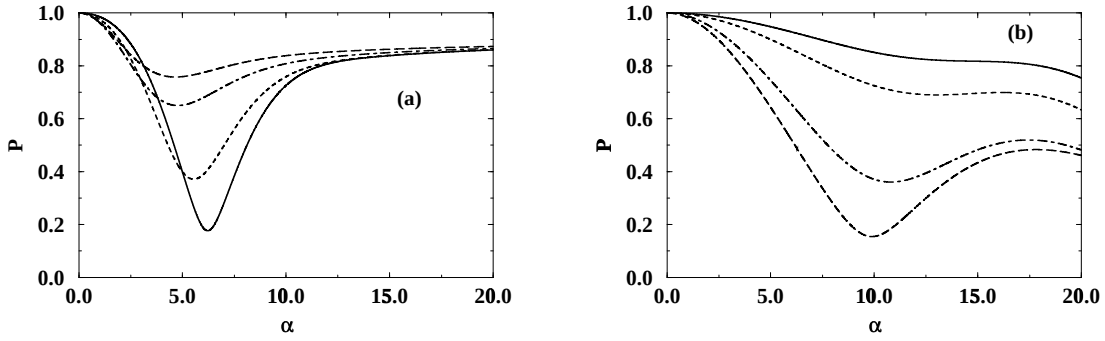

Figure 4.7: Variation of degree of polarization P with α is shown for magnetic field (a) 2 Gauss and (b) 8 Gauss, for laser line-widths $2\gamma_c = 2\pi \times 0.5$ MHz (solid line), $2\gamma_c = 2\pi \times 1$ MHz (dashed line), $2\gamma_c = 2\pi \times 3$ MHz (dot-dashed line), and $2\gamma_c = 2\pi \times 5$ MHz (long-dashed line). The dot-dashed curves correspond to the width of the laser used in the experiment [154].

the relevant energy levels of Rb^{85} as used in the experiment (see Fig. 4.5). The $\hat{x}$-polarized electric field (3.3) is applied to cold Rb^{85} medium near resonantly. The medium is subjected to uniform magnetic field $\vec{B}$ applied in the z-direction, i.e., along the direction of propagation of (3.3).

4.3.1 Calculation of $\chi_\pm$ and optical density

The circular components $\sigma_\pm$ of the input electric field (3.3) interact with the transitions $m_e \leftrightarrow m_g = m_e - 1$ and $m_e \leftrightarrow m_g = m_e + 1$, respectively. We assume that the electric field is weak enough so that it is sufficient to use the linear response of the system to the laser field. We neglect the ground-state coherences. As we are considering the cold atoms, we neglect the collisional relaxations and Doppler broadening of the sublevels. We also assume that the atomic population is equally distributed over all the ground sublevels.

Using all these assumptions, we can write the susceptibilities $\chi_\pm$ for the $\sigma_\pm$ components as the sum of the susceptibilities of all the relevant $m_e \leftrightarrow m_g$ transitions in the following way:

$$\chi_\pm \equiv \sum_{m_e,m_g} \frac{1}{7} \frac{N|\vec{d}_{m_e,m_g}.\hat{\epsilon}_\pm|^2}{\hbar} . \frac{i}{\Gamma_{m_e,m_g} + i(\delta + s_{m_e,m_g})} , \tag{4.19}$$

where, $s_{m_e,m_g} = (g_g m_g - g_e m_e)s$ is the relative amount of Zeeman shift of the excited

sublevel m_e with respect to the Zeeman shifted ground sublevel m_g, $g_g = 1/3$ and $g_e = 1/2$ are the Landé-g factors of the ground and excited levels, respectively. The factor $1/7$ comes into the expression (4.19) as we have assumed equal population distribution in all the $(2F_g + 1) = 7$ ground sublevels. The coherence relaxation rate Γ_{m_e,m_g} in Eq. (4.19) is given by

$$\Gamma_{m_e,m_g} = \frac{1}{2}\sum_k \gamma_{k,m_e} \ , \tag{4.20}$$

where, $\gamma_{i,j}$ is the spontaneous relaxation rate from the sublevel j to i. Here we have assumed that there is no spontaneous relaxation from the ground sublevels. The terms $\vec{d}_{m_e,m_g}$ and Γ_{m_e,m_g}'s can be calculated from the relevant Clebsch-Gordan coefficients (see Fig. 4.5) [177]. The Einstein's A coefficient for the D_2 line is known to be

$$A = \frac{4\omega^3}{3\hbar c^3}\frac{|(J=\frac{3}{2} \parallel D \parallel J'=\frac{1}{2})|^2}{4} = \frac{4\omega^3}{3\hbar c^3}\frac{|(\frac{3}{2},\frac{5}{2},4 \parallel D \parallel \frac{1}{2},\frac{5}{2},3)|^2}{9} \ , \tag{4.21}$$

where, $(\ \ \parallel D \parallel \ \ )$ represents the reduced matrix element of the dipole moment vector $\vec{d}_{m_e,m_g}$ (see Appendix E). The three symbols $3/2$, $5/2$, and 4 correspond to J, I, and F values respectively of the upper levels. Thus all Γ_{m_e,m_g}'s in (4.19) are found to be equal to $(4\omega^3/3\hbar c^3)|(\frac{3}{2},\frac{5}{2},4 \parallel D \parallel \frac{1}{2},\frac{5}{2},3)|^2/2$.

We calculate the optical density α of the medium, when the input light field is resonant with $m_e = 0 \leftrightarrow m_g = 0$ transition ($\delta = 0$) in the absence of any magnetic field ($B = 0$). For this, we first obtain the total output intensity from Eq. (4.8a) averaged by a very narrow laser line-shape, i.e., in the limit $\gamma_c \to 0$. Using Eq. (4.19), we thus find that the transmittivity of the medium becomes

$$T = \frac{1}{I_o}\langle S_0\rangle_{\gamma_c\to 0} = \frac{1}{I_o}S_0|_{\delta=0} = \exp(-\alpha) \ , \tag{4.22}$$

where, $\alpha = (3/7).(3\lambda^2/2\pi)Nl$. It should be borne in mind that it is different from the definition in Sec. 4.2.

4.3.2 Discussions

Using the above expressions of $\chi_\pm$ [Eq. (4.19)] and Eq. (4.12), we calculate the averaged intensities $\langle I_{\hat{n}}\rangle$ in different polarization directions. The Stokes parameters

S_α, degree of polarization P, and the MOR angle θ are calculated using the relations (4.9). In Fig. 4.6, we show how θ varies with the optical density α for different values of γ_c and B. Clearly, for $\gamma_c \ll s$, the rotation angle θ varies linearly with α. But for larger γ_c ($\gtrsim s$), the variation of θ with α deviates from linearity in large α. This is because the off-resonant components contribute to the output intensity. Also, note that for a given value of γ_c, if s is increased, the linearity is maintained even in the large α-domain. This is because for larger s, the off-resonant components do not contribute much to the output intensity. The resonant frequency component is always dominant in the optical density range considered. We also note that, as γ_c increases, the linear slope of θ with α decreases in the small α domain.

In Fig. 4.7, we show the variation of degree of polarization P with α for various values of the B and γ_c. These results reveal that with increase in α, the degree of polarization deviates from unity, i.e., the output electric field not only rotates in polarization, but also it becomes *partially* polarized. However, the ellipticity of the output field still remains zero as we have argued in Sec. 4.2.

Chapter 5

Electromagnetically induced transparency, gain without inversion, and magneto-optical rotation in $J = 1/2 \leftrightarrow J = 1/2$ transition

We have discussed in Chapter 1 that EIT occurs in a driven atom in Λ configuration. This refers to probe-transparency associated with zero probe coherence. We show that an *extra control field* in such a driven medium (so that the configuration becomes a four-level one) can lead to transparency associated with *non-zero* probe coherence and thereby decreases the refractive index of the medium to zero, and even negative. Also, in a driven Λ system, there arises Autler-Townes doublet [47] in the absorption spectrum. An extra control field can make such a system a gain medium, and thus can lead to lasing without inversion in bare basis. Moreover, such a medium enhances the MOR angle, when subjected to the control field.

5.1 Model configuration

We consider the $J = 1/2 \leftrightarrow J = 1/2$ transition in alkali atoms, as shown in Fig. 5.1. This kind of configuration has been used to show gain arising due to cross-talk of the pump and probe fields [178]. We apply a dc magnetic field to remove the degeneracy of the excited and the ground states. In general, the Zeeman separation $2B$ of the excited magnetic sublevels $m_e = \pm 1/2 (\equiv |e_{\mp}\rangle)$ is not the same

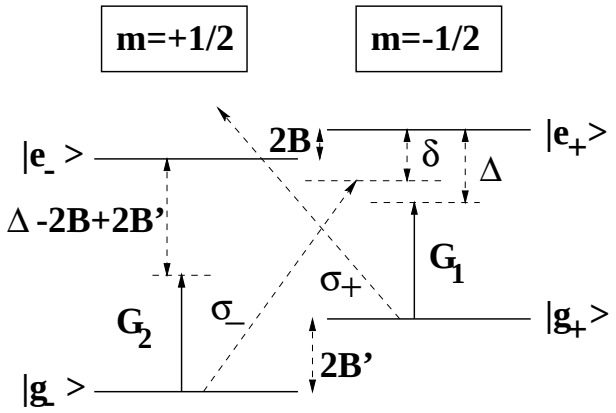

Figure 5.1: Relevant configuration of a four-level atom. The degeneracy of the excited sublevels $|e_\pm\rangle$ and the ground sublevels $|g_\pm\rangle$ have been removed by applying a dc magnetic field, so as to make the system anisotropic. The corresponding Zeeman separations are $2B$ and $2B'$, respectively. The $\sigma_\pm$ components (with Rabi frequencies $2g_\pm$) of the $\hat{x}$-polarized input field interact with the $|e_\mp\rangle \leftrightarrow |g_\pm\rangle$ transitions. $2G_1$ and $2G_2$ are the pump Rabi frequencies. Here, ω_1 and ω_2 are the angular frequencies of the probe and pump fields, respectively, δ and Δ are the pump and probe detunings as shown in the figure.

as the Zeeman separation $2B'$ of the ground manifolds ($\equiv |g_\mp\rangle$), due to difference in Landé g-factors in these manifolds. For example in ^{39}K atom $B' = 3B$, where $B = \mu_B g_e M/\hbar$ (μ_B is the Bohr magneton), $g_e = 2/3$ and $g_g = 2$ are the Landé g-factors of the excited and the ground sublevels.

We allow an $\hat{x}$ polarized weak field $\vec{E}_p = \hat{x}\mathcal{E}_p e^{ikz - i\omega_1 t} + \text{c.c.}$ to probe the properties of the atom, where $k = \omega_1/c$ is the wave number of the field and ω_1 is the corresponding angular frequency. The $\sigma_\pm$ component of this probe field interacts with $|e_\mp\rangle \leftrightarrow |g_\pm\rangle$ transitions. The respective Rabi frequencies are $2g_\pm = 2(\vec{d}_{e_\mp g_\pm}.\hat{x}\mathcal{E}_p)/\hbar$.

Next we apply a π-polarized strong field

$$\vec{E}_c = \vec{\mathcal{E}}_c e^{-i\omega_2 t} + \text{c.c.}\,, \tag{5.1}$$

which interacts with the $|e_\pm\rangle \leftrightarrow |g_\pm\rangle$ transitions. The corresponding Rabi frequencies are $2G_{1,2} = 2\vec{d}_{e_\pm g_\pm}.\vec{\mathcal{E}}_c/\hbar$. Here $\vec{d}_{ij}$ is the electric dipole moment between the levels $|i\rangle$ and $|j\rangle$.

The interaction Hamiltonian of this system in dipole approximation is

$$\begin{aligned} H &= \hbar\left[(\omega_{e_-g_-}|e_-\rangle\langle e_-| + \omega_{e_+g_-}|e_+\rangle\langle e_+| + \omega_{g_+g_-}|g_+\rangle\langle g_+|)\right. \\ &\quad -(\vec{d}_{e_-g_+}|e_-\rangle\langle g_+| + \vec{d}_{e_+g_-}|e_+\rangle\langle g_-| + \text{h.c.}).(\hat{x}\mathcal{E}_p e^{-i\omega_1 t} + \text{c.c.}) \\ &\quad \left.-(\vec{d}_{e_+g_+}|e_+\rangle\langle g_+| + \vec{d}_{e_-g_-}|e_-\rangle\langle g_-| + \text{h.c.}).(\hat{x}\vec{\mathcal{E}}_c e^{-i\omega_2 t} + \text{c.c.})\right] . \end{aligned} \tag{5.2}$$

Here the zero of energy is defined at the level $|g_-\rangle$ and $\hbar\omega_{\alpha\beta}$ is the energy difference between the levels $|\alpha\rangle$ and $|\beta\rangle$.

We consider the natural decay terms in our analysis and hence invoke the density matrix formalism to find the following equations for different density matrix elements:

$$\begin{aligned}
\dot{\tilde{\rho}}_{e_+g_-} &= -\left[i(\Delta + 2B') + \Gamma_{e_+g_-}\right]\tilde{\rho}_{e_+g_-} + i\left[g_- e^{-i\omega_{12}t}(\tilde{\rho}_{g_-g_-} - \tilde{\rho}_{e_+e_+})\right. \\
&\qquad \left. + G_1\tilde{\rho}_{g_+g_-} - G_2\tilde{\rho}_{e_+e_-}\right] \\
\dot{\tilde{\rho}}_{e_-g_+} &= -\left[i(\Delta - 2B) + \Gamma_{e_-g_+}\right]\tilde{\rho}_{e_-g_+} + i\left[g_+ e^{-i\omega_{12}t}(\tilde{\rho}_{g_+g_+} - \tilde{\rho}_{e_-e_-})\right. \\
&\qquad \left. + G_2\tilde{\rho}_{g_-g_+} - G_1\tilde{\rho}_{e_-e_+}\right] \\
\dot{\tilde{\rho}}_{e_+g_+} &= -\left[i\Delta + \Gamma_{e_+g_+}\right]\tilde{\rho}_{e_+g_+} + i\left[g_- e^{-i\omega_{12}t}\tilde{\rho}_{g_-g_+} - g_+ e^{-i\omega_{12}t}\tilde{\rho}_{e_+e_-}\right. \\
&\qquad \left. + G_1(\tilde{\rho}_{g_+g_+} - \tilde{\rho}_{e_+e_+})\right] \\
\dot{\tilde{\rho}}_{e_-g_-} &= -\left[i(\Delta - 2B + 2B') + \Gamma_{e_-g_-}\right]\tilde{\rho}_{e_-g_-} + i\left[g_+ e^{-i\omega_{12}t}\tilde{\rho}_{g_+g_-} - g_- e^{-i\omega_{12}t}\tilde{\rho}_{e_-e_+}\right. \\
&\qquad \left. + G_2(\tilde{\rho}_{g_-g_-} - \tilde{\rho}_{e_-e_-})\right] \\
\dot{\tilde{\rho}}_{g_+g_-} &= -(2iB' + \Gamma_{g_+g_-})\tilde{\rho}_{g_+g_-} + \left[g_+^* e^{i\omega_{12}t}\tilde{\rho}_{e_-g_-} - g_- e^{-i\omega_{12}t}\tilde{\rho}_{g_+e_+} + G_1^*\tilde{\rho}_{e_+g_-} - G_2\tilde{\rho}_{g_+e_-}\right] \\
\dot{\tilde{\rho}}_{e_-e_+} &= (2iB - \Gamma_{e_-e_+})\tilde{\rho}_{e_-e_+} + i\left[g_+ e^{-i\omega_{12}t}\tilde{\rho}_{g_+e_+} - g_-^* e^{i\omega_{12}t}\tilde{\rho}_{e_-g_-} + G_2\tilde{\rho}_{g_-e_+} - G_1^*\tilde{\rho}_{e_-g_+}\right] \\
\dot{\tilde{\rho}}_{g_-g_-} &= \gamma_{g_-e_-}\tilde{\rho}_{e_-e_-} + \gamma_{g_-e_+}\tilde{\rho}_{e_+e_+} + i\left[g_-^* e^{i\omega_{12}t}\tilde{\rho}_{e_+g_-} + G_2^*\tilde{\rho}_{e_-g_-} - \text{h.c.}\right] \\
\dot{\tilde{\rho}}_{e_-e_-} &= -(\gamma_{g_-e_-} + \gamma_{g_+e_-})\tilde{\rho}_{e_-e_-} + i\left[g_+ e^{-i\omega_{12}t}\tilde{\rho}_{g_+e_-} + G_2\tilde{\rho}_{g_-e_-} - \text{h.c.}\right] \\
\dot{\tilde{\rho}}_{e_+e_+} &= -(\gamma_{g_-e_+} + \gamma_{g_+e_+})\tilde{\rho}_{e_+e_+} + i\left[g_- e^{-i\omega_{12}t}\tilde{\rho}_{g_-e_+} + G_1\tilde{\rho}_{g_+e_+} - \text{h.c.}\right]
\end{aligned} \tag{5.3}$$

where, $\Delta = \omega_{e_+g_+} - \omega_2$ is the pump detuning from the transition $|e_+\rangle \leftrightarrow |g_+\rangle$, $\omega_{12} = \omega_1 - \omega_2 = \Delta - \delta + 2B'$ is the probe-pump detuning, δ is the probe detuning, $\gamma_{\alpha\beta}$ is the spontaneous emission rate from the level $|\beta\rangle$ to $|\alpha\rangle$, $\Gamma_{\alpha\beta}$ is the dephasing rate of the coherence between the levels $|\alpha\rangle$ and $|\beta\rangle$. where γ_{coll} accounts for the collisional broadening.

To obtain the above equations, we applied the RWA to neglect the highly oscillating terms. In the original frame of reference, the matrix elements are given by

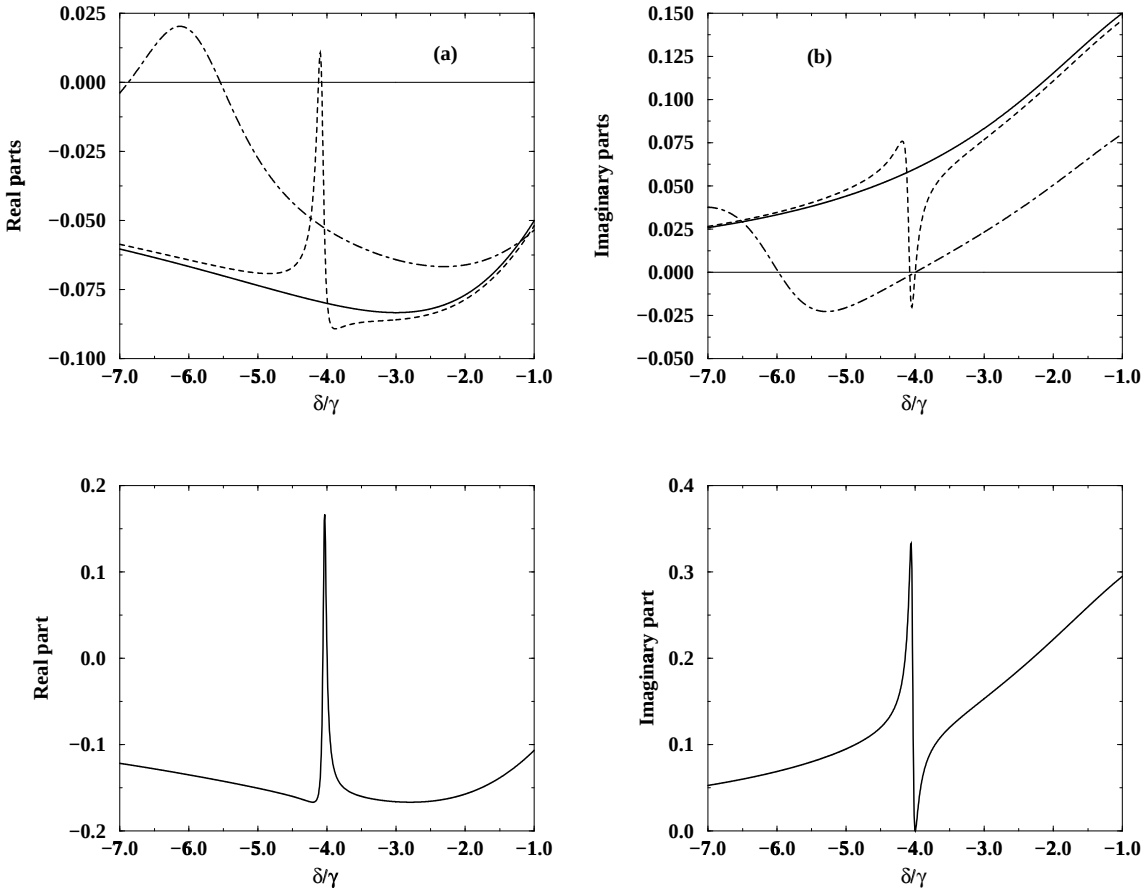

Figure 5.2: The variation of (a) real and (b) imaginary parts of χ_- in units of $N|\vec{d}_{e_+g_-}|^2/\hbar\gamma$ with probe detuning δ for $G = 0$ (solid line), $G = 0.5\gamma$ (dashed line), and $G = 2.5\gamma$ (dot-dashed line). Variation of the (c) real and (d) imaginary parts of the same with δ for $G_1 = 0.5\gamma$ and $G_2 = 0$ have been shown also. The parameters chosen here are $\Delta = B - B'$, $B = 2\gamma$, $B' = 3B$, $\gamma_{g_\pm e_\pm} = 2\gamma$, $\gamma_{g_\pm e_\mp} = 4\gamma$, and $\gamma_{\text{coll}} = 0$. The parameter γ is defined as $\gamma = A/12$, taking all the decays from $|e_\pm\rangle$ to $|g_\pm\rangle$ levels into account, $A = 2\pi \times 6.079$ MHz being the corresponding Einstein's A-coefficient in ^{39}K.

$\rho_{e_+g_-} = \tilde{\rho}_{e_+g_-}e^{-i\omega_2 t}$, $\rho_{e_-g_+} = \tilde{\rho}_{e_-g_+}e^{-i\omega_2 t}$, $\rho_{e_+g_+} = \tilde{\rho}_{e_+g_+}e^{-i\omega_2 t}$, and $\rho_{e_-g_-} = \tilde{\rho}_{e_-g_-}e^{-i\omega_2 t}$, whereas the other elements remain unchanged.

The steady state solutions of the above equations (5.3) can be found by expanding the density matrix elements in terms of the harmonics of ω_{12} as

$$\begin{aligned}\tilde{\rho}_{\alpha\beta} &= \tilde{\rho}^{(0)}_{\alpha\beta} + g_- e^{-i\omega_{12}t}\tilde{\rho}^{\prime(-1)}_{\alpha\beta} + g_-^* e^{i\omega_{12}t}\tilde{\rho}^{\prime\prime(-1)}_{\alpha\beta} \\ &\quad + g_+ e^{-i\omega_{12}t}\tilde{\rho}^{\prime(+1)}_{\alpha\beta} + g_+^* e^{i\omega_{12}t}\tilde{\rho}^{\prime\prime(+1)}_{\alpha\beta}. \end{aligned} \tag{5.4}$$

Thus, we obtain a set of equations of $\tilde{\rho}^{(r)}_{\alpha\beta}$ which can be solved algebraically. We found the following zeroth order population terms:

$$\tilde{\rho}^{(0)}_{e_\pm e_\pm} = \frac{x}{Q}, \tag{5.5a}$$

$$\tilde{\rho}^{(0)}_{g_-g_-} = \frac{1}{Q}(\gamma_{g_-e_-} + \gamma_{g_+e_-} + x), \tag{5.5b}$$

$$\tilde{\rho}^{(0)}_{g_+g_+} = \frac{1}{Q}\left\{\frac{x}{y}(\gamma_{g_-e_+} + \gamma_{g_+e_+}) + x\right\}, \tag{5.5c}$$

where

$$\begin{aligned} x &= \frac{2|G_2|^2\Gamma_{e_-g_-}}{|d|^2};\ y = \frac{2|G_1|^2\Gamma_{e_+g_+}}{|c|^2}, \\ Q &= \frac{x}{y}(\gamma_{g_-e_+} + \gamma_{g_+e_+}) + (\gamma_{g_-e_-} + \gamma_{g_+e_-}) + 4x, \\ c &= -i\Delta + \Gamma_{e_+g_+}, \\ d &= -i(\Delta - 2B + 2B') + \Gamma_{e_-g_-}. \end{aligned} \tag{5.6}$$

Here, we have assumed $\gamma_{g_+e_-} = \gamma_{g_-e_+}$, without loss of generalization.

Therefore, the relevant zeroth order coherence terms turn out to be

$$\tilde{\rho}^{(0)}_{g_+e_+} = -\frac{iG_1^*}{cQ}\frac{x}{y}(\gamma_{g_-e_+} + \gamma_{g_+e_+}), \tag{5.7}$$

$$\tilde{\rho}^{(0)}_{g_-e_-} = -\frac{iG_2^*}{dQ}(\gamma_{g_-e_-} + \gamma_{g_+e_-}). \tag{5.8}$$

Thus the probe coherence terms for $\sigma_\mp$ components can be written as

$$\begin{aligned}\tilde{\rho}^{\prime(-1)}_{e_+g_-} &= \frac{1}{M_1}\Big[G_1(|G_1|^2 - |G_2|^2 + a_+p_+)\tilde{\rho}^{(0)}_{g_+e_+} - G_2(|G_1|^2 - |G_2|^2 - b_+p_+)\tilde{\rho}^{(0)}_{g_-e_-} \\ &\quad + i(a_+b_+p_+ + |G_1|^2 b_+ + |G_2|^2 a_+)(\tilde{\rho}^{(0)}_{g_-g_-} - \tilde{\rho}^{(0)}_{e_+e_+})\Big], \end{aligned} \tag{5.9}$$

$$\begin{aligned}\tilde{\rho}^{\prime(+1)}_{e_-g_+} &= \frac{1}{M_2}\Big[G_1(|G_1|^2 - |G_2|^2 + b_-q_-)\tilde{\rho}^{(0)}_{g_+e_+} - G_2(|G_1|^2 - |G_2|^2 - a_-q_-)\tilde{\rho}^{(0)}_{g_-e_-} \\ &\quad + i(a_-b_-q_- + |G_1|^2 a_- + |G_2|^2 b_-)(\tilde{\rho}^{(0)}_{g_+g_+} - \tilde{\rho}^{(0)}_{e_-e_-})\Big] \end{aligned} \tag{5.10}$$

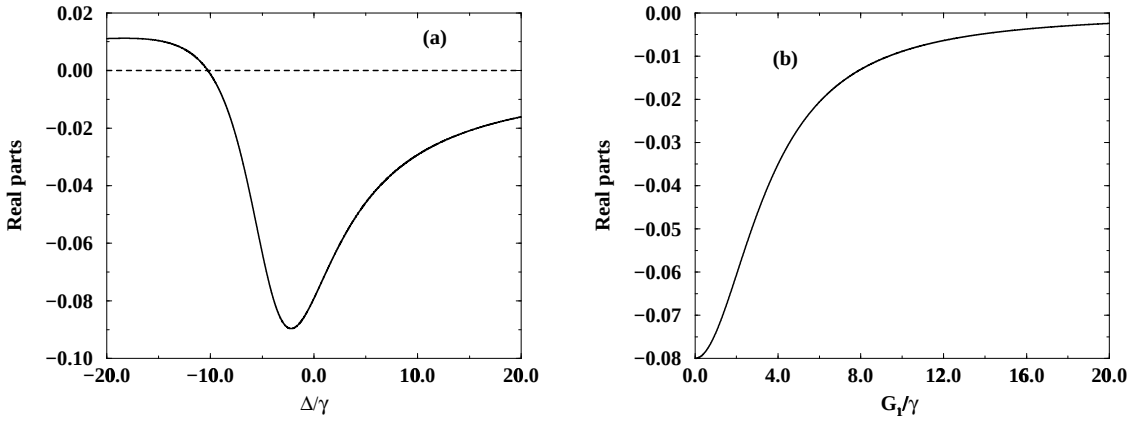

Figure 5.3: Variation of real part of χ_- in unit of $N|\vec{d}_{e_+g_-}|^2/\hbar\gamma$ with respect to (a) Δ and (b) G at the EIT point $\delta = \Delta = B - B'$. The parameter chosen in (a) is $G = 0.5\gamma$ and in (b) is $\Delta = B - B'$. The other parameters are the same as in Fig. 5.2.

where,

$$\begin{aligned} M_1 &= q_+(a_+b_+p_+ + |G_1|^2 b_+ + |G_2|^2 a_+) \\ &\quad +(|G_1|^2 - |G_2|^2)^2 + |G_1|^2 a_+ p_+ + |G_2|^2 b_+ p_+, \\ M_2 &= p_-(a_-b_-q_- + |G_1|^2 a_- + |G_2|^2 b_-) \\ &\quad +(|G_1|^2 - |G_2|^2)^2 + |G_1|^2 b_- q_- + |G_2|^2 a_- q_- \end{aligned}$$

and

$$\begin{aligned} a_\pm &= -i\omega_{12} \pm 2iB + \Gamma_{e_-e_+}, \\ b_\pm &= -i\omega_{12} \pm 2iB' + \Gamma_{g_+g_-}, \\ p_\pm &= -i\omega_{12} \mp i(\Delta - 2B) + \Gamma_{e_-g_+}, \\ q_\pm &= -i\omega_{12} \pm i(\Delta + 2B') + \Gamma_{e_+g_-}. \end{aligned}$$

5.2 Absorption and dispersion profile of $\sigma_\pm$ components

We first analyze the configuration in Fig. 5.1. It is clear from this figure that if both G_1 and G_2 are made zero, the configuration for $\sigma_\pm$ components become like

a two-level system. The

$$\tilde{\rho}'^{(+1)}_{e_-g_+} = \frac{i}{2[i(\delta - 2B - 2B') + \Gamma_{e_-g_+}]} \; , \; \tilde{\rho}'^{(-1)}_{e_+g_-} = \frac{i}{2(i\delta + \Gamma_{e_+g_-})} \; . \tag{5.11}$$

The absorption profile of the σ_- components has a peak at its resonance. We show the corresponding absorption and dispersion profiles in Figs. 5.2(a) and (b).

Now let us introduce the control fields. Note that if $G_2 = 0$, then the system would attain the configuration of a Λ system for the σ_- component with the non-zero pump G_1. Then the corresponding coherence of the σ_- component becomes

$$\tilde{\rho}^{(-1)}_{e_+g_-} = \frac{i\{i(\delta - \Delta) + \Gamma_{g_+g_-}\}}{\{i(\delta - \Delta) + \Gamma_{g_+g_-}\}(i\delta + \Gamma_{e_+g_-}) + |G_1|^2} \; . \tag{5.12}$$

However, because we apply a π-polarized pump, it must interact with both the $|e_\pm\rangle \leftrightarrow |g_\pm\rangle$ transitions. Thus G_2 must be non-zero and we assume that $G_2 = G_1 = G$. Thus all the new features in the susceptibility of σ_-, we describe in the rest of this chapter, can be interpreted as the effect of an extra control field (namely, G_2) in a driven Λ-system. We show the absorption and dispersion profiles of σ_- component for $G_2 = G_1 = G \neq 0$ as well as for $G_2 = 0$ in Figs. 5.2 for non-zero pump detuning $\Delta = B - B'$. The similar profiles of σ_+ component could also be considered. However in terms of physical origin, the profiles of $\sigma_\pm$ components are complementary to each other. Thus it suffices to consider the either component.

In the dispersion profile in Fig. 5.2(a), one clearly sees that, at two-photon resonance (i.e., at $\delta = \Delta$), the real part of the susceptibility χ_- [$\equiv (N|\vec{d}_{e_+g_-}|^2/\hbar\gamma)\tilde{\rho}'^{(-1)}_{e_+g_-}$ which provides the dispersion] of the σ_- component is non-zero and negative. This is unlike the case in a Λ-system, where, at two-photon resonance, Re(χ_-) is zero [see Fig. 5.2(c)]. Thus, an extra control field creates negative Re(χ_-) region in a Λ-system. On the other hand, in the absorption profile in Fig. 5.2(b), gain arises in the medium at certain region of the probe detuning δ. If G_2 would be zero, then, there would be no possibility of gain in the medium [see Fig. 5.2(d)]. However, at the EIT point $\delta = \Delta$, transparency (i.e., zero absorption) persists irrespective of the value of G_2.

In the next section, we analyze these new features, like non-zero and negative susceptibility and arising of gain in the medium, in terms of the effect of the extra control field G_2.

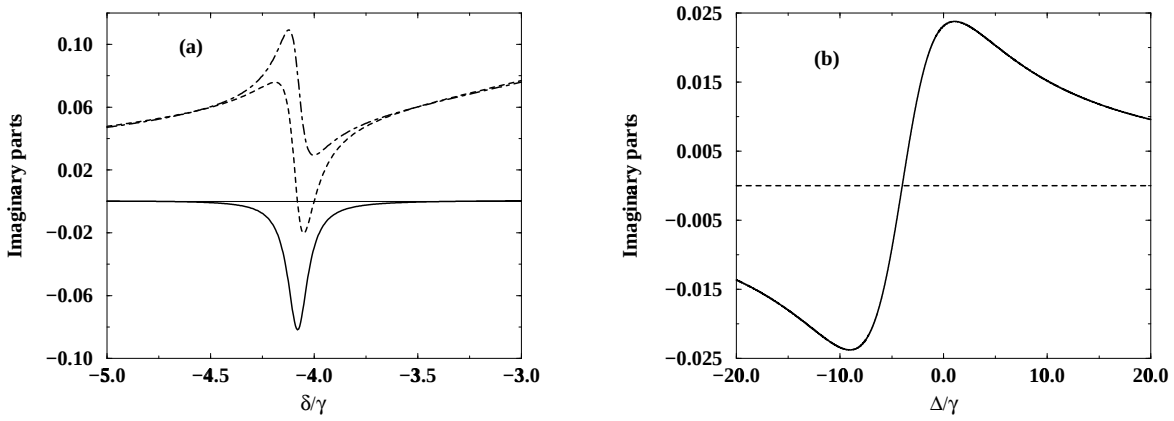

Figure 5.4: (a) Variation of the imaginary parts of the first term in Eq. (5.14) (solid line), the second term (dot-dashed line), and of $\tilde{\rho}^{\prime(-1)}_{e_+g_-}$ (dashed line) with probe detuning δ. We have chosen $G = 0.5\gamma$ and the other parameters are the same as in Fig. 5.2. (b) Variation of imaginary part of χ_- in unit of $N|\vec{d}_{e_+g_-}|^2/\hbar\gamma$ with Δ. The parameters chosen here are the same as in Fig. 5.3(a).

5.3 Discussions

5.3.1 Origin of non-zero susceptibility

We start with the expression (5.9) for $\tilde{\rho}^{\prime(-1)}_{e_+g_-}$. If G_2 is made zero, it is found that,

$$\tilde{\rho}^{\prime(-1)}_{e_+g_-} = \frac{ib_+}{b_+q_+ + |G_1|^2}(\tilde{\rho}^{(0)}_{g_-g_-} - \tilde{\rho}^{(0)}_{e_+e_+}) \ . \tag{5.13}$$

Thus, the population difference between the relevant levels contributes to the probe coherence. Note that at the EIT ($\delta = \Delta$), $b_+ = 0$[1] and then $\tilde{\rho}^{(1)}_{e_+g_-}$ vanishes. But, if we make $G_2 \neq 0$ and $G_1 = G_2 = G$, then one can find

$$\tilde{\rho}^{\prime(-1)}_{e_+g_-} = \frac{1}{M_1}\left[Ga_+p_+\tilde{\rho}^{(0)}_{g_+e_+} + Gb_+p_+\tilde{\rho}^{(0)}_{g_-e_-} + i(a_+b_+p_+ + G^2a_+ + G^2b_+)(\tilde{\rho}^{(0)}_{g_-g_-} - \tilde{\rho}^{(0)}_{e_+e_+})\right] \ . \tag{5.14}$$

Clearly, the coherence $\tilde{\rho}^{(0)}_{g_+e_+}$, which is non-zero due to the spontaneous decay from $|e_-\rangle$ to $|g_+\rangle$, also contributes to the probe susceptibility. We next show that it is the effect of this coherence, which gives rise to all the new features being discussed in this paper.

[1]This is because we are assuming there is no spontaneous emission from the ground states $|g_\pm\rangle$.

Further at the EIT point ($\delta = \Delta$), $b_+ = 0$ and thus, contribution from $\tilde{\rho}^{(0)}_{g_-e_-}$ to the probe coherence vanishes. Then, we can write,

$$\tilde{\rho}'^{(-1)}_{e_+g_-} = \frac{i}{2q_+}\left(1 - \frac{q_+}{c}\right)\frac{6}{Q}\,, \tag{5.15}$$

where, $q_+ = p_+ = c^* = 3 + i(B - B')$, and $Q > 0$. Here the first term inside the bracket is due to the contribution of $\tilde{\rho}^{(0)}_{g_-g_-} - \tilde{\rho}^{(0)}_{e_+e_+}$ and the second term is due to the coherence $\tilde{\rho}^{(0)}_{g_+e_+}$. We clearly see from the above expression, that the real parts of these two terms cancel each other, and it is essentially the imaginary parts which contribute to the probe susceptibility. We find that

$$\tilde{\rho}'^{(-1)}_{e_+g_-} = \frac{-(B' - B)/2}{9 + (B' - B)^2 + 2G^2} \tag{5.16}$$

which is negative as $B' > B$ in the present case. Thus nonzero susceptibility in the configuration of Fig. 5.1 manifests itself as an effect of the zeroth order coherence in the $|e_+\rangle \leftrightarrow |g_+\rangle$ transition (which, in turn, is an effect of the extra control field G_2). Further we should comment here that the negativity of the susceptibility comes into the picture due to larger Landé g factor of the ground state manifold. One has to choose the atomic configuration accordingly. Without any magnetic field applied to the system, i.e., in an isotropic medium one could not obtain any special features in the dispersion profile, indeed.

In Fig. 5.3(a), we show how the parameter Re(χ_-) varies with pump detuning Δ at the EIT point. Thus even for resonant pump ($\Delta = 0$), the susceptibility is negative. In Fig. 5.3(b), we show that, the extra control field can be a good control parameter for the susceptibility. The susceptibility remains negative for the entire range of $G_1 = G_2 \neq 0$ at the EIT point. However for $G_2 = 0$ and $G_1 \neq 0$, the Re(χ_-) would become zero at two-photon resonance which is an usual case in a Λ-system.

5.3.2 Origin of gain

It is well understood that, for $G_2 = 0$, the present configuration becomes like a Λ-system. Thus the probe absorption spectrum shows Autler-Townes doublet. Moreover, there does not arise any gain in the medium. At the EIT point $\delta = \Delta$, the absorption becomes zero.

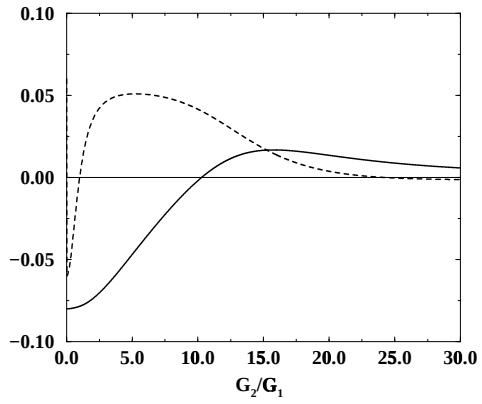

Figure 5.5: Variation of real part (solid line) and imaginary part (dashed line) of χ_- in unit of $N|\vec{d}_{e_+g_-}|^2/\hbar\gamma$ with respect to G_2/G_1, where $G_1 = 0.5\gamma$. We have chosen the other parameters as in Fig. 5.3(b).

However, the case of $G_1 = G_2 \neq 0$ is different. We already have noted that the probe coherence is contributed by two terms : $\tilde{\rho}^{(0)}_{g_+e_+}$ and $\tilde{\rho}^{(0)}_{g_-g_-} - \tilde{\rho}^{(0)}_{e_+e_+}$. We show the individual contribution of these two terms in the absorption spectra in Fig. 5.4(a). From this figure one can see that in certain region of probe frequency ($\delta < B - B'$), the negative contribution of $\tilde{\rho}^{(0)}_{g_+e_+}$ is larger in magnitude than the positive contribution of $\tilde{\rho}^{(0)}_{g_-g_-} - \tilde{\rho}^{(0)}_{e_+e_+}$. Thus the gain arises in the medium. This novel feature can be attributed to the extra control field G_2, which gives rise to the coherence $\tilde{\rho}^{(0)}_{g_+e_+}$. This coherence is the key source of gain. If G_2 would be zero, then, $\tilde{\rho}^{(0)}_{g_+e_+}$ would vanish and there would be no possibility of gain in the medium. Note that at two-photon resonance, $\delta = \Delta$, the contributions from both the terms to the absorption profile cancel each other. Thus one obtains a transparency at this point. We should mention here that the contribution of $\tilde{\rho}^{(0)}_{g_-e_-}$ to the gain is negligible for all δ.

In Fig. 5.4(b), we show, how the imaginary part of χ_- varies with Δ at $\delta = 2B'$. Clearly at $\Delta = B - B'$, the EIT situation arises. For $\Delta < (B - B')$, one achieves gain whereas, for $\Delta > (B - B')$, there is no possibility of gain.

Form the above discussions, we identify certain parameter zone, namely $\delta = \Delta = B - B'$ and $G \gtrsim 0$, where one can obtain large negative susceptibility, associ-

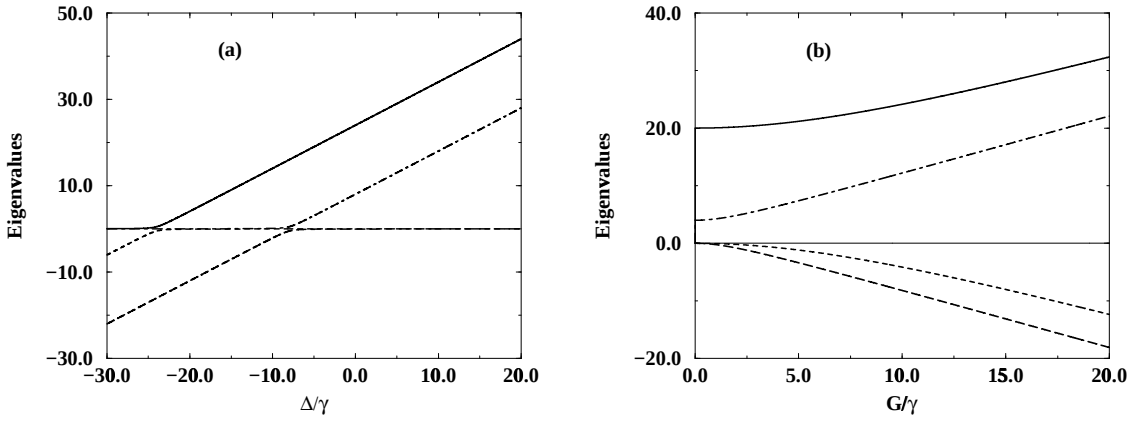

Figure 5.6: Variation of eigenvalues λ_1^+ (solid line), λ_1^- (dashed line), λ_2^+ (dot-dashed line), and λ_2^- (long-dashed line) with respect to (a) Δ and (b) G. The parameters in (a) and (b) are the same as in Figs. 5.3(a) and (b), respectively.

ated with no absorption. Then the refractive index can be written as

$$\eta = 1 + 2\pi \mathrm{Re}(\chi_-) = 1 + \frac{3N\lambda^3}{2\pi^2}\mathrm{Re}(\tilde{\rho}^{\prime(-1)}_{e_+g_-}) \,, \tag{5.17}$$

which, in principle, can be made much less than unity by suitably choosing the number density N of the medium and the transition wavelength λ.

5.3.3 Effect of different values of control field

We further discuss the situation, when G_2 and G_1 are different. We plot the imaginary and real parts of χ_- at the EIT point with respect to the ratio G_2/G_1 in Fig. 5.5. Clearly for $G_2/G_1 = 1$, the non-zero susceptibility appears associated with zero absorption. In fact, this is the optimal condition for attaining this situation.

5.4 Dressed state analysis

In this section, we analyze the gain in the medium in terms of the dressed states of the system. From the expansion of $\tilde{\rho}^{(0)}_{g_\pm g_\pm}$ and $\tilde{\rho}^{(0)}_{e_\pm e_\pm}$ [Eq. (5.5)], one sees that the zeroth order populations in both the $|g_\pm\rangle$ states are larger than those in the levels $|e_\pm\rangle$ due to presence of the non-zero decay rates $\gamma_{\alpha\beta}$'s. Thus there is no population inversion in the bare basis. We arrive at a situation, namely, gain

without inversion. We show, however, that population inversion really occurs in dressed state basis and thereby the gain arises.

5.4.1 Calculations of dressed states

We start with the Hamiltonian (5.2). The state $|\psi\rangle$ of the system obeys the following Schrödinger equation:

$$i\hbar\frac{\partial|\psi\rangle}{\partial t} = H|\psi\rangle \ . \tag{5.18}$$

We now apply an unitary transformation $|\psi\rangle \rightarrow |\phi\rangle = U|\psi\rangle$, where

$$U = \exp[i\omega_2 t(|e_+\rangle\langle e_+| + |e_-\rangle\langle e_-|)]. \tag{5.19}$$

Then the effective Hamiltonian H' for $|\phi\rangle$ can be written as

$$\begin{aligned}\frac{H'}{\hbar} &= -\omega_2|e_+\rangle\langle e_+| - \omega_2|e_-\rangle\langle e_-| + UHU^{-1} \\ &= (\Delta + 2B')|e_+\rangle\langle e_+| + (\Delta - 2B + 2B')|e_-\rangle\langle e_-| + 2B'|g_+\rangle\langle g_+| \\ &\quad - \left[(g_-|e_+\rangle\langle g_-| + g_+|e_-\rangle\langle g_+|)e^{-i\omega_{12}t} + (G_1|e_+\rangle\langle g_+| + G_2|e_-\rangle\langle g_-|) + \text{h.c.}\right]\end{aligned} \tag{5.20}$$

Without any probe field terms, the above Hamiltonian reads as

$$\begin{aligned}\frac{H''}{\hbar} &= (\Delta + 2B')|e_+\rangle\langle e_+| + (\Delta - 2B + 2B')|e_-\rangle\langle e_-| \\ &+ 2B'|g_+\rangle\langle g_+| - [G_1|e_+\rangle\langle g_+| + G_2|e_-\rangle\langle g_-| + \text{h.c.}] \ .\end{aligned} \tag{5.21}$$

The dressed states (dressed by the pump fields) are the eigenstates of this Hamiltonian.

Rewriting the Hamiltonian in the following matrix form in $(|e_+\rangle, |g_+\rangle, |e_-\rangle, |g_-\rangle)$ basis

$$\begin{pmatrix} \Delta + 2B' & -G_1 & 0 & 0 \\ -G_1^* & 2B' & 0 & 0 \\ 0 & 0 & \Delta - 2B + 2B' & -G_2 \\ 0 & 0 & -G_2^* & 0 \end{pmatrix} , \tag{5.22}$$

the corresponding eigenvalues can be calculated as

$$\lambda_i^+ = \frac{1}{2}[(\Delta + 4B') \pm \sqrt{(\Delta + 4B')^2 + 4|G_1|^2}] , \tag{5.23}$$

$$\lambda_i^- = \frac{1}{2}[(\Delta - 2B + 2B') \pm \sqrt{(\Delta - 2B + 2B')^2 + 4|G_2|^2}] , \tag{5.24}$$

where $i \in 1, 2$. The eigenvalues λ_i^+ correspond to the dressed states comprised of the bare states $|e_+\rangle$ and $|g_+\rangle$, whereas the eigenvalues λ_i^- correspond to those comprised of the states $|e_-\rangle$ and $|g_-\rangle$. These eigenvalues have been plotted with Δ and $G_1 = G_2 = G$ in Figs. 5.6.

The dressed states can be calculated as

$$|+\rangle_1 = \frac{(\Delta + 2B' - \lambda_1^+)|e_+\rangle + G_1|g_+\rangle}{\sqrt{(\Delta + 2B' - \lambda_1^+)^2 + |G_1|^2}} , \tag{5.25}$$

$$|+\rangle_2 = \frac{G_1^*|e_+\rangle + (2B' - \lambda_2^+)|g_+\rangle}{\sqrt{|G_1|^2 + (2B' - \lambda_2^+)^2}} , \tag{5.26}$$

$$|-\rangle_1 = \frac{(\Delta - 2B + 2B' - \lambda_1^-)|e_-\rangle + G_2|g_-\rangle}{\sqrt{(\Delta - 2B + 2B' - \lambda_1^-)^2 + |G_2|^2}} \tag{5.27}$$

$$|-\rangle_2 = \frac{G_2^*|e_-\rangle - \lambda_2^-|g_-\rangle}{\sqrt{|G_2|^2 + \lambda_2^{-2}}} . \tag{5.28}$$

We show these eigenstates explicitly in the Fig. 5.7.

5.4.2 Explanation of gain

The population in any dressed state $|s\rangle$ in steady state is given by

$$\rho_{ss} = \langle s|\tilde{\rho}^{(0)}|s\rangle, \tag{5.29}$$

in absence of any probe field. We plot the total population in the dressed states $|+\rangle_i$ ($i \in 1, 2$) in ($|e_+\rangle$, $|g_+\rangle$) manifold and that in the dressed states $|-\rangle_i$ ($i \in 1, 2$) in ($|e_-\rangle$, $|g_-\rangle$) manifold with respect to Δ in Fig. 5.8. One clearly sees that the population inversion dressed basis (total population in $|+\rangle_i$ states exceeds that in $|-\rangle_i$ states) occurs for $\Delta < (B - B')$, which gives rise to gain in this region. and this result is quite consistent with the Fig. 5.4(b). When $\Delta = B - B'$, the population

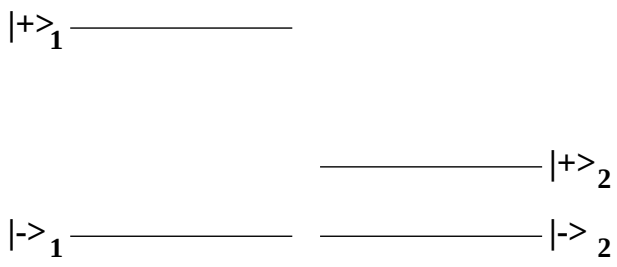

Figure 5.7: Schematic diagram for the dressed states for the parameter zone used in the present model.

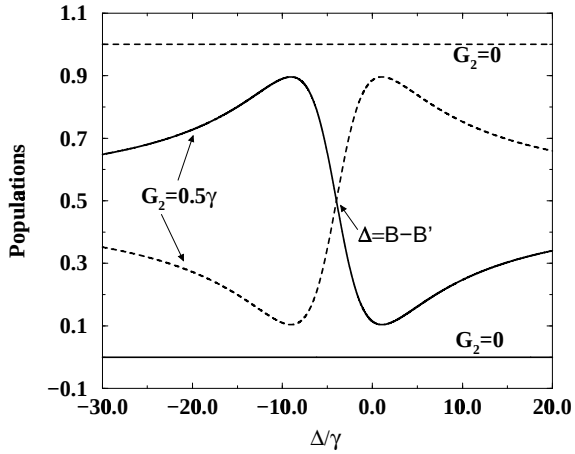

Figure 5.8: Variation of total population in the states $|+\rangle_i$ (solid line) and $|-\rangle_i$ (dashed line) with Δ. The other parameters are the same as in Fig. 5.3(a).

in the $(|e_+\rangle,\ |g_+\rangle)$ manifold and in the $(|e_-\rangle,\ |g_-\rangle)$ manifold are the same. Thus no gain or no absorption arises. In other words, there arises a transparency in the medium, which can be easily identified with EIT. Moreover, for $\Delta > B - B'$ the medium becomes absorptive, because, there is no inversion in dressed basis in this region. Note that for no control field ($G = 0$) there is no possibility of gain as the the dressed states $|+\rangle_i$ are never populated; all the population reside in the states $|-\rangle_i$ irrespective of the values of Δ. Thus population inversion does not occur at all.

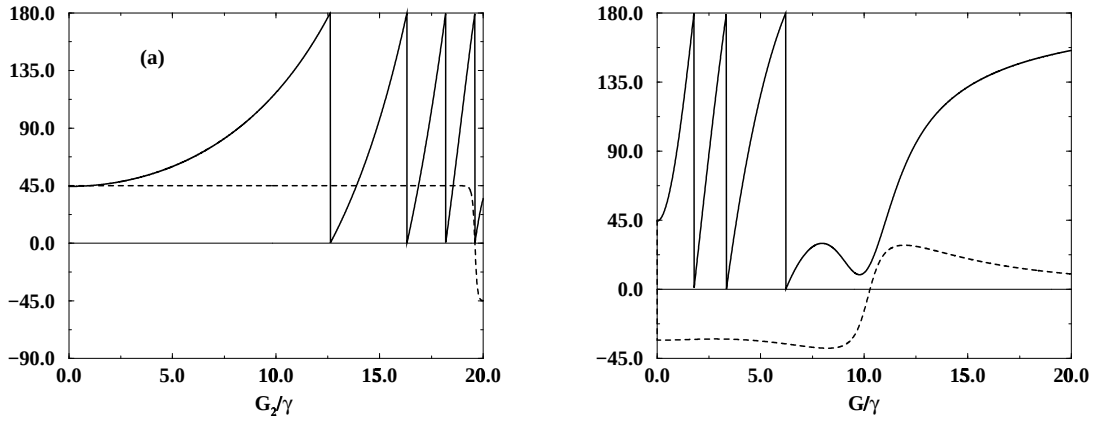

Figure 5.9: Variation of MOR angle θ (in degrees) and ellipticity angle ϕ (in degrees) with (a) G_2 (when $G_1 = 0$) and (b) $G_1 = G_2 = G$ in the output of an atomic medium with length $L = 1$ cm. We have used $N = 7.5 \times 10^{10}$ cm^{-3} and $\lambda = 769.89$ nm, as for D_1 transition of the ^{39}K. All the other parameters are the same as in Fig. 5.3(b).

5.5 Coherent control of MOR : Large MOR

In this section we investigate the magneto-optical rotation (MOR) of the input $\hat{x}$-polarized field $\vec{E}_p$ propagating through the medium under consideration. The MOR angle θ can be defined in terms of difference in the susceptibilities $\chi_\pm$ of the $\sigma_\pm$ components, only if their absorptions inside the medium are negligibly small. But, as we have discussed in chapter 4, if the absorption is significant enough, one has to adopt the Stoke's formalism to fully characterize the polarization state of the output field.

We use the relevant equations (4.10), (4.8), and (4.9) to calculate the MOR angle θ, ellipticity angle ϕ, and the degree P of polarization of the output field.

When both the pumps are not present, then the $\sigma_\pm$ components interact with corresponding two-level configuration and the respective probe coherences are given by (5.11).

We now consider three cases: (i) When only the pump G_1 is applied and $G_2 = 0$, then the σ_- component interacts with an effective three-level Λ configuration and its coherence is given by Eq. (5.12). On the other hand, the σ_+ component interacts with an effective two-level configuration and its first-order coherence is given by Eq. (5.11). (ii) When only the pump G_2 is applied and $G_1 = 0$, then the

probe coherence of the $\sigma_{\mp}$ components are given by Eq. (5.11) and

$$\tilde{\rho}^{\prime(+1)}_{e_-g_+} = \frac{i\{i(\delta - \Delta - 4B') + \Gamma_{g_+g_-}\}}{2[\{i(\delta - \Delta - 4B') + \Gamma_{g_+g_-}\}\{i(\delta - 2B - 2B') + \Gamma_{e_-g_+}\} + |G_2|^2]} \,. \tag{5.30}$$

We calculate the variation of angles θ and ϕ with G_1 and G_2 at $\delta = \Delta$, respectively. We noticed that these angles remain constant at $\theta \sim 117^o$ and $\phi \sim -33^o$ for all G_1. This is because, the susceptibilities become independent of G_1 at two-photon resonance $\delta = \Delta$, when $G_2 = 0$. On the other hand, when $G_1 = 0$, the variation of these angles, calculated at $\delta = \Delta$ using the formulae (5.30) with G_2 are shown in Fig. 5.9(a). Note that the angles can be altered with G_2 and can be much large ($\sim 180^o$) for $G_2 \gtrsim 12.5\gamma$. In case (iii), we consider that both the pumps G_1 and G_2 are present and they are equal to G. In Fig. 5.9(b), we show the variation of the angle θ and ϕ with respect to control field Rabi frequency G ($= G_1 = G_2$). It is clear from this figure that the MOR angle can be enhanced to an angle as large as $\sim 180^o$ by applying an extra control field $G_2 = G_1$. Interestingly, large MOR angle can also be procduced as in case (ii), but for large G_2. If one switches both the pumps on, then even for small $G \sim 2\gamma$, one can achieve large MOR. Note further that for certain range of G, the variation of θ remains linear with G. However, the output field most often does not remain linearly polarized. The non-zero ellipticity angle ϕ reflects the fact that large absorption of the field components occurs inside the medium. Also, at a definite value of G ($\gtrsim 10$), the ellipticity angle ϕ becomes zero. This is because, at this point, the absorptions of both the $\sigma_{\pm}$ components become zero. We also have investigated the behavior of the degree of polarization P of the output field, which remains unity for the entire range of G. This means that the output field always remains fully polarized.

Chapter 6

Coherent Control of the Fidelity of Quantum Cloning

So far we have discussed how dispersion and absorption of a probe field inside an anisotropic medium can be controlled by a strong coherent field. In chapter 4, we have described some remarkable effects arising due to the monochromaticity of the probe field. Indeed all the previous discussions in this thesis are based on a semiclassical treatment for the interaction of atoms with fields. As we have mentioned earlier, the field can be considered quantum-mechanical which helps in understanding and exploring many new phenomena which could be impossible to observe in a semiclassical treatment. This chapter devotes to a fully quantum-mechanical treatment of this interaction and a new application of coherent control.

6.1 No-cloning theorem

In a seminal paper, Wootters and Zurek [180] have shown that an arbitrary quantum state cannot be cloned, i.e., one cannot prepare a true replica of the state keeping the initial state intact. They have followed the following argument.

Let us consider a perfect cloning device can clone an incoming photon which are in either vertical or horizontal polarization basis, i.e.,

$$|A_0\rangle|\updownarrow\rangle \longrightarrow |A_{\rm vert}\rangle|\updownarrow\updownarrow\rangle\ , \quad |A_0\rangle|\leftrightarrow\rangle \longrightarrow |A_{\rm hor}\rangle|\leftrightarrow\leftrightarrow\rangle\ , \tag{6.1}$$

We ask the question whether the above cloning device can clone an arbitrary polarization state $|s\rangle = \alpha|\updownarrow\rangle + \beta|\leftrightarrow\rangle$ properly. The cloning device will result in the following:

$$|A_0\rangle|s\rangle \longrightarrow \alpha|A_{\rm vert}\rangle|\updownarrow\updownarrow\rangle + \beta|A_{\rm hor}|\leftrightarrow\leftrightarrow\rangle \ . \tag{6.2}$$

If the states of the cloning device at the end of the process are identical, then the photon state can be written as

$$\alpha|\updownarrow\updownarrow\rangle + \beta|\leftrightarrow\leftrightarrow\rangle \ . \tag{6.3}$$

On the other hand, the perfect cloning requires that the output should be

$$|ss\rangle \equiv \ \alpha^2|\updownarrow\updownarrow\rangle + \beta^2|\leftrightarrow\leftrightarrow\rangle + \alpha\beta(|\updownarrow\leftrightarrow\rangle + |\leftrightarrow\updownarrow\rangle) \ , \tag{6.4}$$

which clearly is not the same as (6.3), which one gets. Clearly, perfect cloning is not performed. In fact, it is in the heart of quantum mechanics. The linearity of the superposition principle itself prevents perfect cloning. In fact, this linearity has many important implications. For example, Dieks [181] and Bussey [182] independently have shown that it is not possible to have faster-than-light communication, thanks to linearity of the quantum mechanics. In fact, no-cloning principle and no-signalling constraint are complementary to each other [183]. It has been proved that only any set of mutually orthogonal quantum states (not their superposition) can be cloned perfectly by a cloning device [184].

Milonni and Hardies were first to propose a physical process regarding quantum cloning [185]. They have shown that it is the unavoidable presence of spontaneous emission, which prevents perfect cloning of photonic states by stimulated emission (Note that the probability of spontaneous emission and stimulated emission when there is one photon are the same ; see [3].). Making use of two two-level atoms with orthogonal transition dipole moments, Mandel [186] proved that one can make the output of the photon amplifier independent of the input polarization.

6.1.1 How better one can clone an arbitrary state ?

Because it is not possible to perfectly clone any arbitrary state, one may ask to what extent the cloning can be done. It is already shown that the cloning process

destroys the original state also. Thus one can rather compromise by assuming that the cloning device should at least clone all the possible states (including the orthogonal ones) *equally well*. This is referred to as optimal cloning. A decade after the conjecture in [180], Buzek and Hillery have shown that the fidelity[1] (defined by the square of the overlap amplitude of the input and the output states) for $1 \rightarrow 2$ optimal cloning should not exceed $5/6$ [189]. This is universal for all input qubits and is compatible with no-signalling constraint too. A series of investigation of quantum cloning followed this paper. The optimal cloning has been generalized [190, 191] for the case of $N \rightarrow M$ $(M \geq N)$ cloner. The upper bound for the fidelity of a $N \rightarrow M$ cloner has been established [192]. Results are also available for the optimal cloning of arbitrary pure and mixed states in d-dimensions $(d \geq 2)$ [191, 193]. Besides, cloning of entangled states [194] and of Gaussian-distributed quantum variables [195] has been considered. It has also been shown that it is impossible to perfectly clone any arbitrary mixed state also [196]. Besides optimal cloning, state-dependent cloning (different fidelity for different initial states) has been investigated too [197].

6.2 Quantum cloning based on stimulated emission in a V-system

6.2.1 Quantization of electric field

In the rest part of this chapter, we focus on the quantum cloning of polarization state of the photon inside a cavity. To explain this issue, we first explain how the em field can be quantized in a cavity. Next we describe its interaction with atoms.

Inside a cavity resonator, a limited number of oscillation modes are possible which depends upon the cavity length and volume of the cavity. The electric and magnetic fields in the Maxwell's equations can be expanded in terms of normal

[1] We should mention that the concept of fidelity for information transfer was first introduced by Shannon [187] in classical sense and was reformulated later in contexts of quantum coding [188] and cloning [189].

modes of the cavity of length L in CGS unit as

$$\begin{aligned} E_x(z,t) &= \sum_j A_j q_j(t) \sin(k_j z) \ , \\ H_y(z,t) &= \sum_j A_j \left(\frac{\dot{q}_j}{c k_j} \right) \cos(k_j z) \ , \end{aligned} \tag{6.5}$$

where q_j is the normal mode amplitude, $k_j = j\pi/L$ ($j \in 1, 2, 3, \ldots$), $\omega_j = ck_j = j\pi c/L$ is the cavity mode frequency, V is the cavity volume, m_j is a constant with dimension of mass, and A_j is a constant determined by ω_j, m_j, and V. In the above we have assumed that the electric field is linearly polarized in x-direction and propagating in the z-direction. One can write a classical Hamiltonian for the field as

$$\mathcal{H} = \frac{1}{8\pi} \int_V d\tau (E_x^2 + H_y^2) \ , \tag{6.6}$$

where the integration is carried over the volume of the cavity. After substituting the mode-expansions of electric and magnetic field, we obtain

$$\mathcal{H} = \frac{1}{2} \sum_j \left(m_j \omega_j^2 q_j^2 + \frac{p_j^2}{m_j} \right) \ , \tag{6.7}$$

where $p_j = m_j \dot{q}_j$ is the canonical momentum of the jth mode and we have identified the constant $A_j = (8\pi m_j \omega_j^2 / V)^{1/2}$. The above equation expresses Hamiltonian of the radiation field as a sum of independent oscillator energies. Each mode of the field is thereby dynamically equivalent to a mechanical harmonic oscillator.

Quantization of field refers to identify the q_j and p_j as operators and to make use of a canonical transformations as

$$\begin{aligned} a_j e^{-i\omega_j t} &= \frac{1}{\sqrt{2 m_j \hbar \omega_j}} (m_j \omega_j q_j + i p_j) \ , \\ a_j^\dagger e^{i\omega_j t} &= \frac{1}{\sqrt{2 m_j \hbar \omega_j}} (m_j \omega_j q_j - i p_j) \ . \end{aligned} \tag{6.8}$$

Thus the quantized Hamiltonian reads as

$$\mathcal{H} = \hbar \sum_j \omega_j \left(a_j^\dagger a_j + \frac{1}{2} \right) \ . \tag{6.9}$$

In terms of two new operators, the quantized electric and magnetic fields inside the cavity become

$$\begin{aligned} E_x(z,t) &= \sum_j \mathcal{E}_j (a_j e^{-i\omega_j t} + a_j^\dagger e^{i\omega_j t}) \sin(k_j z) \ , \\ H_y(z,t) &= \sum_j -i\mathcal{E}_j (a_j e^{-i\omega_j t} - a_j^\dagger e^{i\omega_j t}) \cos(k_j z) \ , \end{aligned} \tag{6.10}$$

where $\mathcal{E}_j = A_j(\hbar/2m_j\omega_j)^{1/2}$ is a constant.

Two important points are in order. The quantized forms of the electric and magnetic fields in a free space (which satisfies the periodic boundary conditions) are as follows.

$$\vec{E}(\vec{r},t) = \sum_k \hat{\epsilon}_{\vec{k}} \mathcal{E}_{\vec{k}} a_{\vec{k}} e^{-i\omega_k t + i\vec{k}.\vec{r}} + \text{h.c.} \ , \tag{6.11}$$

$$\vec{H}(\vec{r},t) = \sum_k \frac{\vec{k} \times \hat{\epsilon}_{\vec{k}}}{\omega_k} \mathcal{E}_{\vec{k}} a_{\vec{k}} e^{-i\omega_k t + i\vec{k}.\vec{r}} + \text{h.c.} \ , \tag{6.12}$$

where $\mathcal{E}_{\vec{k}}$ is a constant determined by ω_j and V. Secondly, we should mention some of the properties of the newly introduced operators $a_{\vec{k}}$ and $a_{\vec{k}}^\dagger$. These are called annihilation operators and creation operators, respectively, because they annihilate a photon or create an extra photon inside the cavity. In number state basis $|n_{\vec{k}}\rangle$ of the cavity field with n photons in $\vec{k}$-mode, we can write

$$a_{\vec{k}}|n\rangle_{\vec{k}} = \sqrt{n_{\vec{k}}}|n-1\rangle_{\vec{k}} \ , \quad a_{\vec{k}}^\dagger|n\rangle_{\vec{k}} = \sqrt{n_{\vec{k}}+1}|n+1\rangle_{\vec{k}} \tag{6.13}$$

6.2.2 Optimal photon cloner with a V-configuration

Recently Simon *et al.* [198, 199] have proposed a new scheme for quantum cloning of a photonic qubit. They considered a cloning device consisting of an ensemble of atoms trapped inside a cavity. The relevant atomic transitions correspond to the V-system. These are three-level systems with two degenerate excited states $|e_1\rangle$ and $|e_2\rangle$ and a common ground level $|g\rangle$. The ground level is coupled to the excited states by two orthogonal field modes a_1 and a_2, respectively.

The unperturbed Hamiltonian of this system can be written as

$$H_0 = \hbar(\omega_{e1}|e_1\rangle\langle e_1| + \omega_{e2}|e_2\rangle\langle e_2|) + \hbar(\omega_1 a_1^\dagger a_1 + \omega_2 a_2^\dagger a_2) \ , \tag{6.14}$$

where ω_{ei} is the energy of the level $|e_i\rangle$ ($i \in 1,2$), with respect to the energy of the ground level $|g\rangle$ (i.e., the energy of the level $|g\rangle$ is assumed to be zero of the energy), ω_i ($i \in 1,2$) is the frequency of the the orthogonal modes a_i.

We assume the interaction of the field modes with the atoms in dipole approximation. The electric field in this approximation should be considered in its quantized form [see Eq. (6.10)]. Thus the dipole interaction part of the total Hamiltonian can be written as

$$\begin{aligned} H_1 &= \hbar g \sum_{k=1}^{N} (\sigma_{+1}^k a_1 e^{-i\omega_1 t} + \sigma_{+2}^k a_2 e^{-i\omega_2 t}) + \text{h.c.} \\ &+ (\sigma_{+1}^k a_1^\dagger e^{i\omega_1 t} + \sigma_{+2}^k a_2^\dagger e^{i\omega_2 t}) + \text{h.c.}, \end{aligned} \tag{6.15}$$

where g is the coupling constant between the atoms and the cavity modes with dimension of angular frequency and, $\sigma_{+1(2)}^k$'s [$= (|e_{1(2)}\rangle\langle g|)_k$] are the raising operators between the corresponding states of the k-th atom. Here g is assumed to be equal for all the atoms. This means that all the atoms are in equivalent positions relative to the cavity mode. This condition can be achieved by trapping the atoms inside the cavity, so that the field interacting with the atom is the same for all atoms. This kind of trapping of atoms has been reported recently in [200].

Now in the interaction picture, the effective Hamiltonian under RWA can be written as

$$H_I = \hbar g \sum_{k=1}^{N} (\sigma_{+1}^k a_1 + \sigma_{+2}^k a_2) + \text{ H. c.}, \tag{6.16}$$

Here we have assumed that the field modes are in resonance with the atomic transitions. Note that while using RWA, we have discarded the terms like $|\sigma_{+1(2)}^k a_{1(2)}^\dagger$, which are in fact energy nonconserving terms (see [179], chapter 6). These terms are associated with the excitation of the atom as well as creation of a single photon, which is intuitively impossible in the present situation.

Let each atom be prepared initially in a mixed excited state

$$\rho = \frac{1}{2}(|e_1\rangle\langle e_1| + |e_2\rangle\langle e_2|) \ . \tag{6.17}$$

This is possible by spontaneous emission from a higher energy level. We assume that the photonic qubit is in a state $a_1^\dagger|0,0\rangle \equiv |1,0\rangle$. Here $|n,\mu\rangle$ refers to the photonic state in which n photons are in a_1 mode and μ photons are in a_2 mode. The

time-development operator $U = e^{-iH_I t}$ will provide the time-evolution of the entire (atom+photon) system and this is used to study quantum cloning.

The quality of cloning is characterized in terms of fidelity [187], which can be defined [198] in the following way:

$$F = \sum_{k=0}^{N+1} \sum_{l=0}^{N} p(k,l) \left(\frac{k}{k+l} \right). \tag{6.18}$$

Here $p(k,l)$ represents the probability of finding k photons in the initial mode and l photons in the orthogonal mode a_2 in the evolved state. It should be noted that for an ensemble of N atoms, the maximum value of k will be $N+1$, which corresponds to all the atoms decaying to the ground state through the emission of the a_1-photon. Thus F is a kind of an average of the relative frequency of photons in initial mode a_1 in the final state.

As shown by Simon *et al.*, the fidelity is optimal for short interaction times and for $N = 6$. It decreases for later times. They have explained this behavior in terms of stimulated and spontaneous emissions on the transitions $|e_1\rangle \rightarrow |g\rangle$ and $|e_2\rangle \rightarrow |g\rangle$, respectively. We should precisely mention that if there is an extra photon in a_1-mode, it can be considered as a clone of the initial qubit. Note that the probability to get a clone is reduced if there is an extra photon in the other (a_2) mode, which is due to spontaneous emission.

6.2.3 Question of universality of cloning by a V-system

It is mentioned in Ref. [199] that the above scheme is universal, i.e., the V-system cloner can clone even any arbitrary photonic qubit, say, $(\alpha a_1^\dagger + \beta a_2^\dagger)|0,0\rangle$ with the same non-unity fidelity. Simon *et al.* argued that this is because the initial mixed state and the Hamiltonian are invariant under a unitary transformation. In what follows, we demonstrate explicitly this universality by changing the basis to a general qubit state.

Consider a single atom in V-configuration, initially prepared in an incoherent superposition of the two excited states. We will work with wavefuntions and hence we use an initial state

$$|s\rangle = \frac{1}{\sqrt{2}} \left(|e_1\rangle + e^{i\theta} |e_2\rangle \right). \tag{6.19}$$

and average the final results over all possible values of the parameter θ. Let the photon be in a superposition state

$$b_1^\dagger|0,0\rangle \equiv \left(\alpha a_1^\dagger + \beta a_2^\dagger\right)|0,0\rangle \equiv \alpha|1,0\rangle + \beta|0,1\rangle \tag{6.20}$$

as well, where α and β are the complex numbers satisfying $|\alpha|^2+|\beta|^2 = 1$. Note that an average over θ will give an initial state of the atom, which is a mixed state. We consider the photon as a qubit [188], which can be in any linear superposition of the two orthogonal states. Let us define the basis state $b_2^\dagger|0,0\rangle$, which is orthogonal to (6.20). The new operators b_1 and b_2 must satisfy the commutation relations

$$[b_1, b_2] = [b_1, b_2^\dagger] = 0. \tag{6.21}$$

Using Eqs. (6.20) and (6.21), we get

$$b_2^\dagger \equiv -\beta^* a_1^\dagger + \alpha^* a_2^\dagger. \tag{6.22}$$

The time-evolution of the entire system is determined by the Schrödinger equation

$$i\hbar\frac{d}{dt}|\Psi(t)\rangle = H_I|\Psi(t)\rangle, \tag{6.23}$$

where H_I is given by Eq. (6.16) for $N = 1$. We expand $|\Psi(t)\rangle$ in terms of the relevant basis states. Starting with the initial conditions [Eqs. (6.19) and (6.20)], these relevant states were found to be

$$|e_1\rangle|1,0\rangle\ ;\ |e_2\rangle|1,0\rangle\ ;\ |g\rangle|2,0\rangle\ ;\ |g\rangle|1,1\rangle\ ;\ |g\rangle|0,2\rangle\ ;\ |e_1\rangle|0,1\rangle\ ;\ |e_2\rangle|0,1\rangle. \tag{6.24}$$

The only non-zero expansion amplitudes C_α^{mn} at time $t = 0$ are

$$C_{e_1}^{10}(0) = \frac{\alpha}{\sqrt{2}}\ ;\ C_{e_1}^{01}(0) = \frac{\beta}{\sqrt{2}}\ ;\ C_{e_2}^{10}(0) = \frac{\alpha}{\sqrt{2}}e^{i\theta}\ ;\ C_{e_2}^{01}(0) = \frac{\beta}{\sqrt{2}}e^{i\theta}, \tag{6.25}$$

where the subscript (superscript) denotes the atom (photons) in the state α (m, n). Then all the expansion amplitudes can be evaluated in closed form with the fol-

lowing results:

$$\begin{aligned}
C_{e_1}^{10}(t) &= \frac{\alpha}{\sqrt{2}}\cos\left(\sqrt{2}gt\right), \\
C_{g}^{20}(t) &= -i\frac{\alpha}{\sqrt{2}}\sin\left(\sqrt{2}gt\right), \\
C_{e_2}^{10}(t) &= \frac{1}{2\sqrt{2}}\left[\left(\alpha e^{i\theta}-\beta\right)+\left(\beta+\alpha e^{i\theta}\right)\cos\left(\sqrt{2}gt\right)\right], \\
C_{e_1}^{01}(t) &= \frac{1}{2\sqrt{2}}\left[\left(\beta-\alpha e^{i\theta}\right)+\left(\beta+\alpha e^{i\theta}\right)\cos\left(\sqrt{2}gt\right)\right], \\
C_{g}^{11}(t) &= -\frac{i}{2}\left(\beta+\alpha e^{i\theta}\right)\sin\left(\sqrt{2}gt\right), \\
C_{g}^{02}(t) &= -i\frac{\beta}{\sqrt{2}}e^{i\theta}\sin\left(\sqrt{2}gt\right), \\
C_{e_2}^{01}(t) &= \frac{\beta}{\sqrt{2}}e^{i\theta}\cos\left(\sqrt{2}gt\right).
\end{aligned} \tag{6.26}$$

The reduced density matrix of the field is defined by

$$\rho_F = \mathrm{Tr}_A(|\Psi(t)\rangle\langle\Psi(t)|)\ , \tag{6.27}$$

where the trace has been taken in the atomic basis. Thereby the field is prepared in a mixed state defined by ρ_F. Using Eq. (6.27), the probability $\tilde{p}(k,l)$ that k photons will be in b_1-mode and l photons in b_2-mode can be written in terms of b-operators as

$$\tilde{p}(k,l) = \langle 0,0|\frac{b_1^k\, b_2^l}{\sqrt{k!\,l!}}\,\rho_F\,\frac{b_1^{\dagger k}\, b_2^{\dagger l}}{\sqrt{k!\,l!}}|0,0\rangle. \tag{6.28}$$

Further in order to get the initial atomic state used by Simon *et al.*, we average $\tilde{p}(k,l)$ over all values of θ. A lengthy derivation yields the following:

$$\tilde{p}_a(2,0) = \frac{1}{2}\sin^2\left(\sqrt{2}gt\right), \tag{6.29a}$$

$$\tilde{p}_a(1,1) = \frac{1}{4}\sin^2\left(\sqrt{2}gt\right), \tag{6.29b}$$

$$\tilde{p}_a(0,1) = \frac{1}{8}\cos^2\left(\sqrt{2}gt\right)-\frac{1}{4}\cos\left(\sqrt{2}gt\right)+\frac{1}{8}, \tag{6.29c}$$

$$\tilde{p}_a(1,0) = \frac{5}{8}\cos^2\left(\sqrt{2}gt\right)+\frac{1}{4}\cos\left(\sqrt{2}gt\right)+\frac{1}{8}, \tag{6.29d}$$

where $\tilde{p}_a(k,l)$ is the θ-averaged value of $\tilde{p}(k,l)$. The Eqs. (14) lead to the following expression for the fidelity:

$$F = \tilde{p}_a(1,0)+\tilde{p}_a(2,0)+\frac{1}{2}\tilde{p}_a(1,1) = \frac{3}{4}+\frac{1}{4}\cos\left(\sqrt{2}gt\right). \tag{6.30}$$

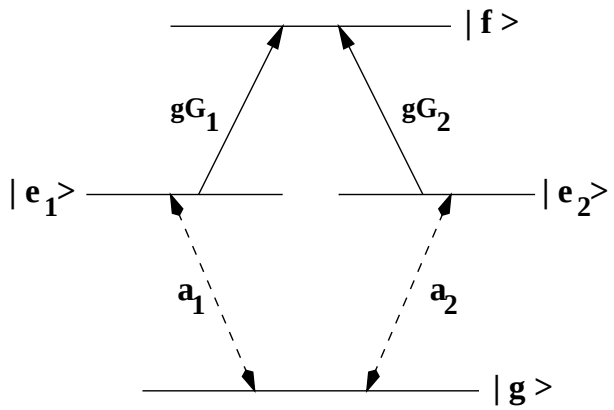

Figure 6.1: An atomic level configuration to improve the fidelity of quantum cloning. Here the classical fields with Rabi frequency $2gG_i$ $(i = 1, 2)$ couple the levels $|e_1\rangle$ and $|e_2\rangle$ with the metastable state $|f\rangle$. The atom is inside a cavity, which allows only two field-modes a_1 and a_2.

Clearly the fidelity does not depend upon α and β. This reflects the fact that the V-scheme is universal as a cloner, which can clone even a general superposition of two orthogonal modes of the field, albeit imperfectly. A similar result has been reported recently using an atomic system in Λ configuration [201].

We should emphasize here that while calculating the fidelity, we have considered the probabilities of the event like spontaneous emission of a single or two photons in b_2-mode. Different definitions of fidelity also exist in the literature, which does not consider these events into account [199].

6.3 A method to improve the fidelity of the V-scheme for arbitrary state of the input photon

From the discussion in the previous section, it is clear that the fidelity of cloning is degraded by the emission of a photon of the "wrong" type (in a mode which is not the initial one). This is possible irrespective of whether there is any photon in a_1 mode or not. Thus we obtain the non-zero values of the probabilities like $p(1,1)$ and $p(0,1)$. The fidelity oscillates sinusoidally between 0 and 1 with times [see Eq. (6.30)]. To improve this fidelity (so that it becomes close to unity for longer times), one should reduce the probability $p(1,1)$ and $p(0,1)$ of emitting photon in

the mode a_2. This emission is caused by the atomic population in $|e_2\rangle$ level. One possible way of doing this is to *cycle* this population away, so that this unwanted spontaneous decay does not occur very often. We show that it can be done by applying a classical pump field, which causes the population in the state $|e_2\rangle$ to pulsate between a metastable state $|f\rangle$ and $|e_2\rangle$. However any biasing by the external field is likely to take away the system from universality. By making the bias dependent on the state, any state can be cloned better than the optimal limit, or even perfectly at some times.

6.3.1 Model configuration

We consider a four-level atomic configuration as shown in Fig. 6.1. The excited states $|e_1\rangle$ and $|e_2\rangle$ are coupled to the common ground level $|g\rangle$ through the two orthogonal modes a_1 and a_2 of the quantized electromagnetic field, respectively as in the model in [198]. The coupling constant between each of these excited states and $|g\rangle$ is g. We consider the action of classical fields coupling the state $|e_i\rangle$ $(i = 1, 2)$ with the metastable state $|f\rangle$. The corresponding Rabi frequency is $2gG_i$, where G_i is a multiplying factor and is related to the number of photons in the classical field. We assume all the fields to be resonant with the corresponding atomic transitions.

We start with a single atom prepared in the state $|s\rangle$ [Eq. (6.19)]. The initial photonic qubit is in b_1-mode. We will work in the interaction picture. Then using the rotating wave approximation to eliminate the fast-oscillating energy non-conserving terms, we obtain the effective Hamiltonian as

$$H_I = \hbar g \left[\sigma_{+1} a_1 + \sigma_{+2} a_2 + \sum_{i=1,2} G_i |e_i\rangle\langle f| \right] + \text{H.c.}, \tag{6.31}$$

where $\sigma_{+1(2)} = |e_{1(2)}\rangle\langle g|$ are the raising operators of the atom as defined in the previous section.

6.3.2 Analysis

In order to understand how all the states can be cloned by choosing state-dependent bias, we rewrite (6.31) in terms of the b_1 and b_2-modes and redefined atomic states

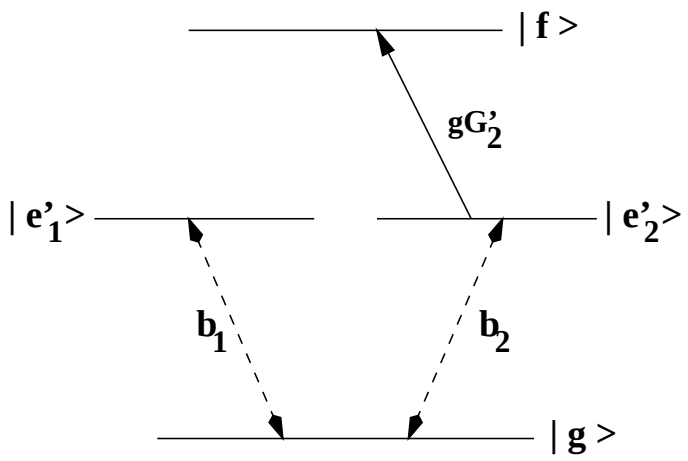

Figure 6.2: Equivalent level diagram for $G_1' = 0$. The new field operators b_i's and the levels $|e_i'\rangle$'s have been defined in the text.

$|e_1'\rangle$ and $|e_2'\rangle$ as

$$H_I = \hbar g \left[|e_1'\rangle\langle g|b_1 + |e_2'\rangle\langle g|b_2 + G_1'|e_1'\rangle\langle f| + G_2'|e_2'\rangle\langle f|\right] + \text{H.c.}, \tag{6.32}$$

where

$$|e_1'\rangle = \alpha|e_1\rangle + \beta|e_2\rangle \; ; \; |e_2'\rangle = \alpha^*|e_2\rangle - \beta^*|e_1\rangle \; ; \; G_1' = \alpha^* G_1 + \beta^* G_2 \; ; \; G_2' = -\beta G_1 + \alpha G_2. \tag{6.33}$$

Clearly if we choose $G_1' = 0$, i.e.,

$$G_1/G_2 = -(\beta^*/\alpha^*), \tag{6.34}$$

then the Hamiltonian in the new basis is like a single bias field acting on the atomic transition. We show this equivalent configuration in Fig. 6.2. This analysis implies that we can deal with arbitrary input states of the qubit by just choosing the bias field appropriately [Eq. (6.34)]. Note also the important property

$$|e_1\rangle\langle e_1| + |e_2\rangle\langle e_2| = |e_1'\rangle\langle e_1'| + |e_2'\rangle\langle e_2'|, \tag{6.35}$$

so that the initial incoherent superposition remains an incoherent superposition in the primed basis.

We next calculate the effect of the bias field on the fidelity of the system by setting $G_1' = 0$ in Eq. (6.32). Let the eigenstates of $b_1^\dagger b_1$ and $b_2^\dagger b_2$ be denoted by

$\widetilde{|n,m\rangle}$. Thus

$$\widetilde{|n,m\rangle} \equiv \frac{b_1^{\dagger k} b_2^{\dagger l}}{\sqrt{k!\,l!}}|0,0\rangle\ , \tag{6.36}$$

where $|0,0\rangle$ represents the vacuum in the (a_1, a_2) basis. From (6.32) we find that the following states participate in time evolution:

$$|e_1'\rangle\widetilde{|1,0\rangle}\ ;\ |e_2'\rangle\widetilde{|1,0\rangle}\ ;\ |f\rangle\widetilde{|1,0\rangle}\ ;\ |g\rangle\widetilde{|1,1\rangle}\ ;\ |g\rangle\widetilde{|2,0\rangle}\ ;\ |e_1'\rangle\widetilde{|0,1\rangle}. \tag{6.37}$$

Note that the state $|e_1'\rangle\widetilde{|0,1\rangle}$ is produced by the two-step process $|e_2'\rangle\widetilde{|1,0\rangle} \rightarrow |g\rangle\widetilde{|1,1\rangle} \rightarrow |e_1'\rangle\widetilde{|0,1\rangle}$. We expand $|\Psi(t)\rangle$ in terms of these basis states and we obtain the following first order differential equations for the corresponding expansion amplitudes $\tilde{C}$'s, using the Schrödinger equation:

$$\begin{aligned}
\dot{\tilde{C}}^{10}_{e_1'}(t) &= -\sqrt{2}ig\tilde{C}^{20}_{g}(t),\\
\dot{\tilde{C}}^{20}_{g}(t) &= -\sqrt{2}ig\tilde{C}^{10}_{e_1'}(t),\\
\dot{\tilde{C}}^{10}_{e_2'}(t) &= -ig\tilde{C}^{11}_{g}(t) - igG_2'\tilde{C}^{10}_{f}(t),\\
\dot{\tilde{C}}^{10}_{f}(t) &= -igG_2'\tilde{C}^{10}_{e_2'}(t),\\
\dot{\tilde{C}}^{11}_{g}(t) &= -ig\tilde{C}^{01}_{e_1'}(t) - ig\tilde{C}^{10}_{e_2'}(t),\\
\dot{\tilde{C}}^{01}_{e_1'}(t) &= -ig\tilde{C}^{11}_{g}(t).
\end{aligned} \tag{6.38}$$

We assume that the atom is initially in a state $|e_1\rangle = (|e_1'\rangle + e^{i\theta}|e_2'\rangle)/\sqrt{2}$, i.e.,

$$\tilde{C}^{10}_{e_1'}(0) = \frac{1}{\sqrt{2}} \quad ; \quad \tilde{C}^{10}_{e_2'}(0) = \frac{1}{\sqrt{2}}e^{i\theta}, \tag{6.39}$$

Thus we obtain the following solutions of the above equations:

$$\begin{aligned}
\tilde{C}^{11}_{g}(t) &= A\sin\left(\frac{\Omega_1}{\sqrt{2}}gt\right) + B\sin\left(\frac{\Omega_2}{\sqrt{2}}gt\right),\\
\tilde{C}^{10}_{f}(t) &= \frac{1}{2G_2'}\left[(\Omega_1^2-4)A\sin\left(\frac{\Omega_1}{\sqrt{2}}gt\right) + (\Omega_2^2-4)B\sin\left(\frac{\Omega_2}{\sqrt{2}}gt\right)\right],\\
\tilde{C}^{10}_{e_2'}(t) &= \frac{i}{2\sqrt{2}G'^2{}_2}\left[\Omega_1(\Omega_1^2-4)A\cos\left(\frac{\Omega_1}{\sqrt{2}}gt\right) + \Omega_2(\Omega_2^2-4)B\cos\left(\frac{\Omega_2}{\sqrt{2}}gt\right)\right],\\
\tilde{C}^{01}_{e_1'}(t) &= -\frac{i}{2\sqrt{2}G'^2{}_2}\left[\Omega_1(\Omega_1^2-2G'^2{}_2-4)A\cos\left(\frac{\Omega_1}{\sqrt{2}}gt\right) + \Omega_2(\Omega_2^2-2G'^2{}_2-4)B\cos\left(\frac{\Omega_2}{\sqrt{2}}gt\right)\right],\\
\tilde{C}^{10}_{e_1'}(t) &= \frac{1}{\sqrt{2}}\cos\left(\sqrt{2}gt\right),\\
\tilde{C}^{20}_{g}(t) &= -\frac{i}{\sqrt{2}}\sin\left(\sqrt{2}gt\right),
\end{aligned} \tag{6.40}$$

where

$$\Omega_1 = \left(G'^2{}_2 + 2 + \sqrt{G'^4{}_2 + 4}\right)^{\frac{1}{2}} \quad , \quad \Omega_2 = \left(G'^2{}_2 + 2 - \sqrt{G'^4{}_2 + 4}\right)^{\frac{1}{2}},$$

$$\begin{aligned} A &= \frac{1}{2} i e^{i\theta} \frac{(\Omega_2^2 - 2G'^2{}_2 - 4)}{\Omega_1 \sqrt{G'^4{}_2 + 4}}, \\ B &= -\frac{1}{2} i e^{i\theta} \frac{(\Omega_1^2 - 2G'^2{}_2 - 4)}{\Omega_2 \sqrt{G'^4{}_2 + 4}}. \end{aligned} \tag{6.41}$$

Using the relation (6.27), we get the reduced density matrix of the field. The diagonal element of this density matrix in field basis $|\widetilde{k,l}\rangle$ gives the probability $\tilde{p}(k,l)$ that k photons are in b_1-mode and l photons are in b_2-mode and these are given by

$$\begin{aligned} \tilde{p}(2,0) &= |\tilde{C}_g^{20}(t)|^2 = \frac{1}{2}\sin^2\left(\sqrt{2}gt\right), \\ \tilde{p}(1,1) &= |\tilde{C}_g^{11}(t)|^2, \\ \tilde{p}(1,0) &= |\tilde{C}_f^{10}(t)|^2 + |\tilde{C}_{e_2'}^{10}(t)|^2 + |\tilde{C}_{e_1'}^{10}(t)|^2, \\ \tilde{p}(0,1) &= |\tilde{C}_{e_1'}^{01}(t)|^2. \end{aligned} \tag{6.42}$$

Hence the fidelity F takes the following form:

$$F = 1 - \left[\tilde{p}_a(0,1) + \frac{1}{2}\tilde{p}_a(1,1)\right]. \tag{6.43}$$

6.3.3 Numerical results

We have plotted this as a function of time for $G_2' = 0, 3$ in Fig. 6.3. It is found that as G_2' increases, the fidelity becomes unity more often. Whenever both $\tilde{p}_a(1,1)$ and $\tilde{p}_a(0,1)$ become zero, $F(t)$ becomes unity. In fact, by introducing the classical pump field, we cycle the atomic population in the state $|e_2'\rangle$ to the state $|f\rangle$ and back. This inhibits the spontaneous decay of the atom in the state $|e_2'\rangle$ to the ground state $|g\rangle$ irrespective of whether there is any photon or not in "right" (initial) mode. There are two time-scales of oscillation of $F(t)$. The faster small-amplitude oscillation is attributed to that of $[\tilde{p}_a(0,1) + (1/2)\tilde{p}_a(1,1)]$. This oscillation can be increased by G_2' so that the atom effectively goes to the state $|f\rangle$ very frequently. This means that $F(t)$ becomes close to unity more frequently. The effect of spontaneous emission from the state $|f\rangle$ is ignored assuming that the time

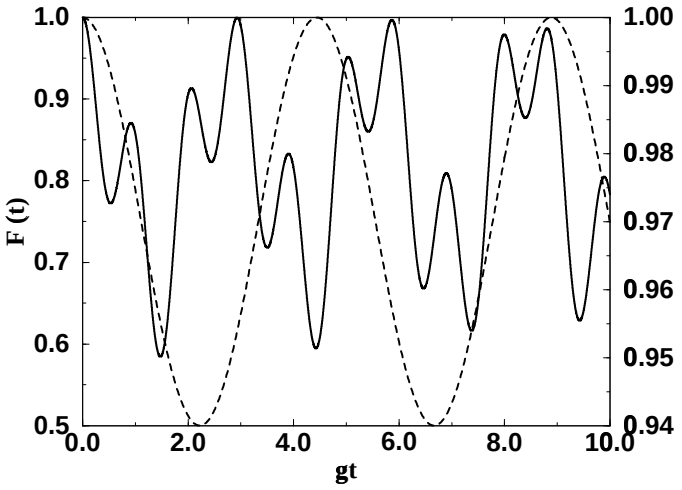

Figure 6.3: These figures show the time-dependence of the fidelity of a four-level atomic cloner comprising a single atom for no cycling field ($G_1' = G_2' = 0$; dashed curve : tick levels are on left side) and in presence of external fields ($G_1' = 0$, $G_2' = 3$; solid curve : tick levels are on right side). It is obvious that the bias field improves the fidelity of cloning considerably. We assumed that the atom is initially in the state $|e_1\rangle$.

scale for this decay is much larger than that for Rabi oscillation between $|e_2'\rangle$ and $|f\rangle$-levels.

In Fig. 6.4 we display the mean number of "right" and of all photons. These are given by

$$N_{\rm right} = {\rm Tr}_F(b_1^\dagger b_2^\dagger \rho_F) \ , \quad N_{\rm all} = {\rm Tr}_F[(b_1^\dagger b_1 + b_2^\dagger b_2)\rho_F] \ . \tag{6.44}$$

In the present case, we can calculate

$$N_{\rm right} = 2p(2,0) + p(1,0) + p(1,1) \ , \quad N_{\rm all} = 2p(2,0) + p(1,0) + 2p(1,1) + p(0,1) \ . \tag{6.45}$$

This figure also supports the improvement in cloning by the use of a cycling or bias field.

6.4 Fidelity of cloning with two atoms

In this section, we consider a cloning machine consisting of two atoms and we demonstrate improvement in the fidelity for a larger domain of times if we adopt the use of the cycling or bias field. We consider the case of two V-atoms. The

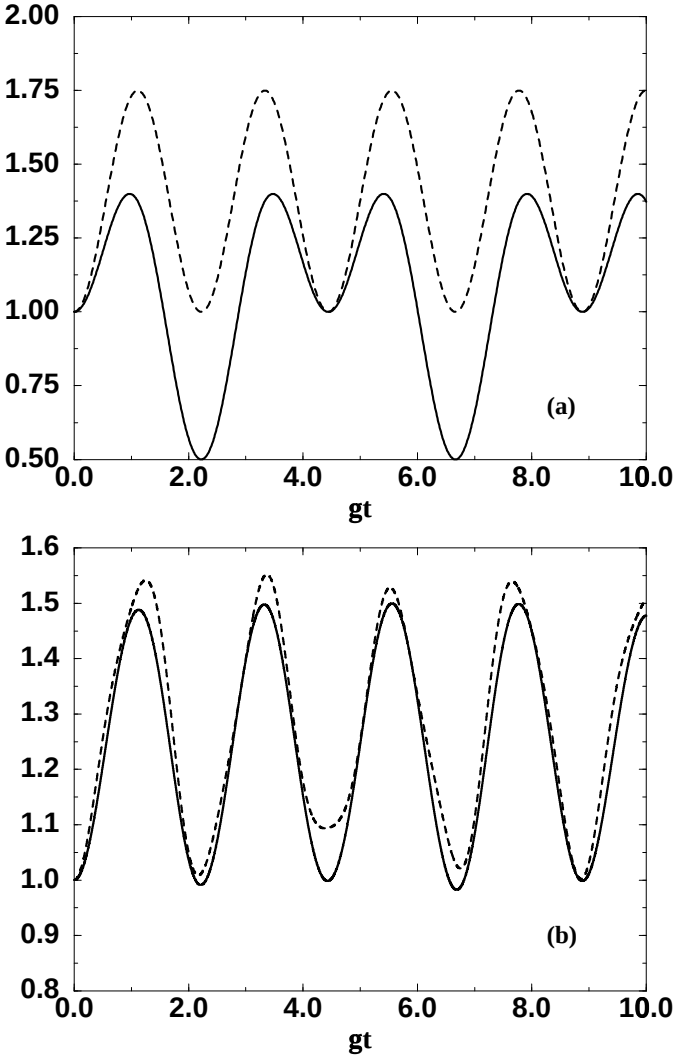

Figure 6.4: These figures display the time-dependence of average number of photons in "right" mode, i.e., in b_1-mode ($N_{\rm right}$; solid curve) and of all photons ($N_{\rm all}$; dashed curve) in a single atom cloner under the conditions $G_1' = G_2' = 0$ [Fig. (a)] and $G_1' = 0$, $G_2' = 3$ [Fig. (b)]. It is seen that for non-zero G_2', $N_{\rm right}$ and $N_{\rm all}$ approach each other. We have seen that for $G_2' = 8$, i.e., for faster cycling of the population, they are nearly equal for almost all times.

interaction Hamiltonian is obtained by summing (6.32) and a similar Hamiltonian involving the interaction of the another atom B with the fields. The initial state of the atomic system is

$$\rho_{\rm AB} = \prod_{\mu={\rm A},B} \left(|e_1\rangle_\mu \, {}_\mu\langle e_1| + |e_2\rangle_\mu \, {}_\mu\langle e_2| \right), \tag{6.46}$$

i.e., both the atoms are in mixed excited state. We further assume single photon in the mode b_1. We work under the condition (6.34) so that the Hamiltonian reduces to

$$H_I = \hbar g \sum_{\mu={\rm A},B} \left(|e_1'\rangle_\mu \, {}_\mu\langle g|b_1 + |e_2'\rangle_\mu \, {}_\mu\langle g|b_2 + G_2'|e_2'\rangle_\mu \, {}_\mu\langle f| \right) + {\rm H.c.}. \tag{6.47}$$

In order to use the wavefunction picture we use the initial condition for the atom as

$$\rho = |\Psi_A\rangle\langle\Psi_B| \; ; \qquad |\Psi_\mu\rangle = \frac{1}{\sqrt{2}} \left(|e_1'\rangle_\mu + e^{i\theta_\mu} |e_2'\rangle_\mu \right), \tag{6.48}$$

and average the final results over $\theta_{\rm A}$ and $\theta_{\rm B}$. For the two-atom case with bias field we have to use a large number of relevant basis states – the size of the Hilbert space increases very rapidly with increase in the number of atoms.

The equations for the amplitudes are solved numerically using fifth-order Runge-Kutta method. From the numerical solutions we calculate the fidelity F. It is clear from the Fig. 6.5 that the cycling field makes the fidelity much higher for a very large range of times. Note that the fidelity of the two-atom cloner can be expressed as

$$F(t) = 1 - \left[\frac{1}{3}\tilde{p}_a(2,1) + \frac{2}{3}\tilde{p}_a(1,2) + \frac{1}{2}\tilde{p}_a(1,1) + \tilde{p}_a(0,1) + \tilde{p}_a(0,2) \right]. \tag{6.49}$$

Obviously, it becomes unity only if the probabilities of spontaneous emission in b_2-mode (both in presence and in absence of photons in b_1-mode) are zero. Then all the photons present in the cavity would be in b_1-mode. However due to complex nature of time-dependence of $\tilde{p}_a(k,l)$'s, one does not find any periodicity in the variation of $F(t)$. To calculate the average number of "right" photons and of all photons in the evolved state of the two-atom cloner, one has to find the reduced density matrix of the field only. This can be obtained by tracing the total density

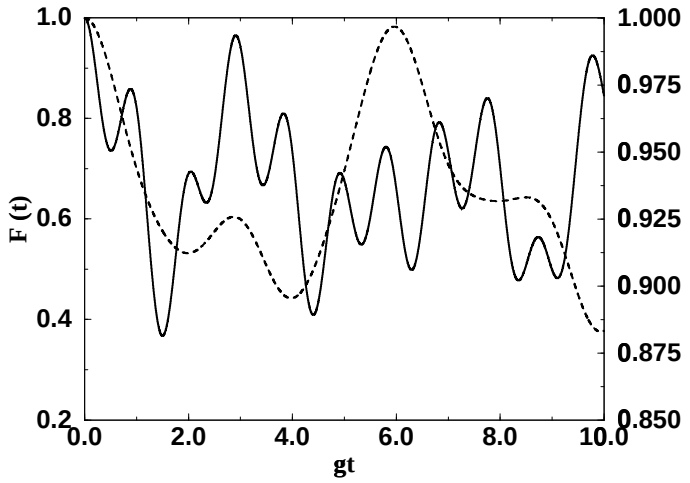

Figure 6.5: The fidelity of a two-atom cloner is plotted as a function of time for no cycling field ($G_1' = G_2' = 0$; dashed curve : tick levels are on left side) and in presence of the bias field ($G_1' = 0$, $G_2' = 3$; solid curve : tick levels are on right side). Clearly the fidelity of cloning is improved by cycling of atomic population through a metastable state using a classical bias field.

matrix of the atom+field system over the atomic basis. These average numbers have been plotted as functions of time in the Fig. 6.6(b). A comparison of Figs. 6.6(a) and 6.6(b) shows tremendous improvement in cloning due to the cycling field.

6.5 Average fidelity of cloning for a fixed biasing field

In the previous sections we had discussed the possibility of improvement in fidelity by changing the bias field as one changes the input state of the qubit. The question arises what is the fidelity of cloning for a fixed bias field. In such a case we have to work with the average of fidelity over all the input states of the qubit. To be precise let us consider the input state of the qubit as given by Eq. (6.20). We calculate the probability $\tilde{p}(k,l)$ as defined by (6.28). We next average this probability over all values of $\alpha = \cos(\chi/2)$ and $\beta = \sin(\chi/2)e^{i\varphi}$, where $0 \leq \chi \leq \pi$, $0 \leq \varphi \leq 2\pi$. Averaging over α and β are equivalent to average over all values of χ and φ. Using average probabilities $\overline{p}(k,l)$ we obtain the average fidelity for all the states of the input qubit. The calculations are lengthy and we present results in the Fig. 6.7a.

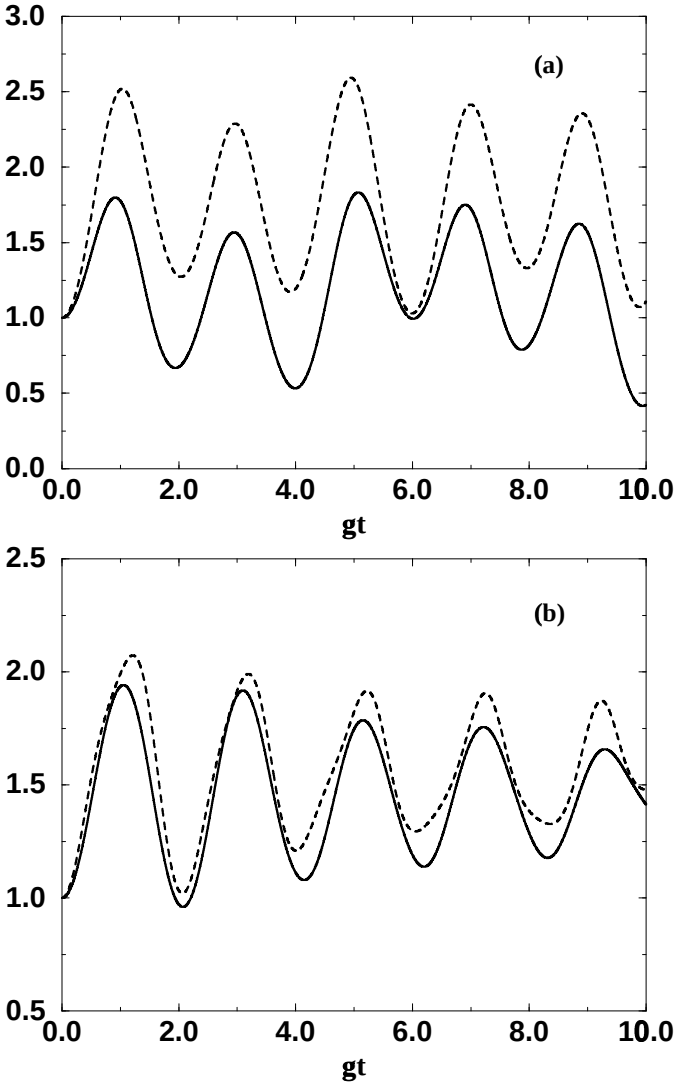

Figure 6.6: The time-variation of average number of the photons in the b_1-mode (N_{right} ; solid curve) and all photons (N_{all} ; dashed curve) in a two-atom cloner have been displayed for $G_1' = G_2' = 0$ [Fig. (a)] and $G_1' = 0$, $G_2' = 3$ [Fig. (b)]. This shows that N_{right} and N_{all} become closer for larger value of G_2'.

Note that for no bias, the fidelity is periodic in time whereas in presence of the bias field it is quasiperiodic. We conclude from this figure that there is considerable *improvement* in fidelity upto times of order $gt \sim 2$. This is also reflected by the behavior of the mean photon number in the "right" mode (Fig. 6.7b).

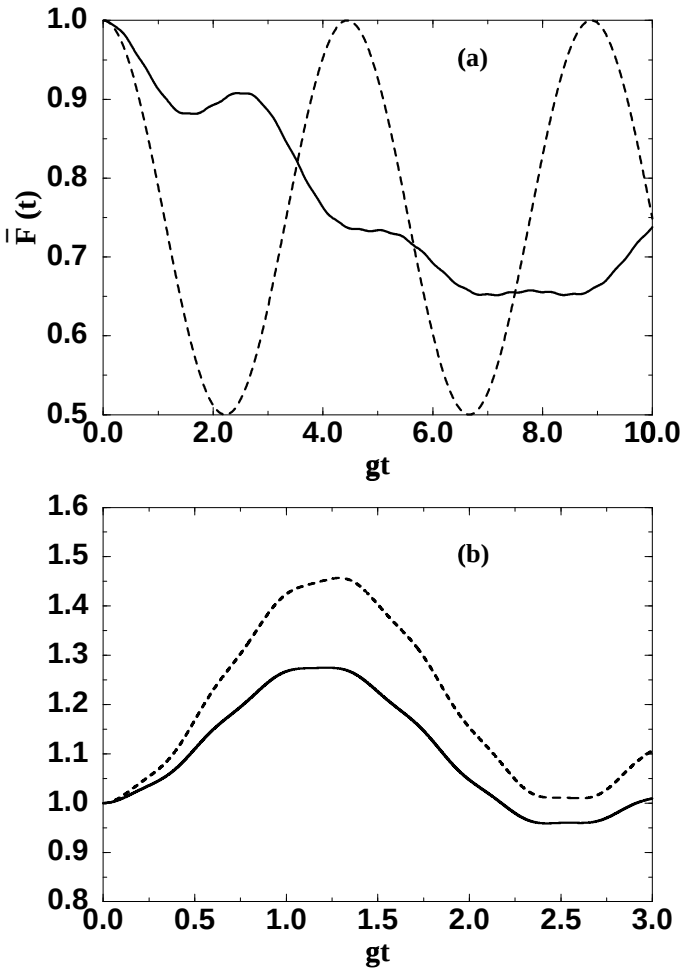

Figure 6.7: (a) The fidelity of a single atom cloner averaged over all states of the input qubit is plotted as a function of time for the cases $G_1' = G_2' = 0$ (dashed curve) and $G_1' = 0$, $G_2' = 8$ (solid curve). (b) The time-variation of number of "right" photons (solid curve) and all photons (dashed curve), averaged over all states of the input qubit are shown for some external field parameters $G_1' = 0$, $G_2' = 8$.

Conclusions and Future Outlook

In conclusion, this thesis reports the several coherent control effects in an anisotropic medium. Manipulation of atomic coherence by external cw fields leads to many interesting phenomena. These have been elucidated by analytical and numerical results based on the parameters which are experimentally achievable. In the following, the main results of each chapter and possibility of further study on it are discussed in brief.

In chapter 2, it is shown that it is possible to temporally separate the two orthogonal polarization components of a weak linearly polarized pulse by using coherent control. This is possible in a situation where the group velocities of the components are different and have negligible absorption, as well. A four-level atomic system is studied in details in this context. It is shown that by applying a strong coherent field, one can achieve a EIT condition so as to split the input pulse in time domain. Numerical demonstration of pulse splitting phenomenon is described in context of propagation of Gaussian pulse through the medium. An analytical estimate of the the broadening of the pulse at the output is given which is in good agreement with the numerical results.

In chapter 3, dependence of the output intensity on the direction of the applied magnetic field is described in context of propagation of unpolarized light through an anisotropic medium. The idea was to create a EIT condition at the resonance of either polarization component using a coherent field, whereas the other component remains detuned from the corresponding transition. Thus, for the magnetic field applied parallel to the direction of propagation, absorption of both the components are negligible. On the other hand, for the magnetic field applied in the direction opposite to that of the field, one of the polarization components gets absorbed at its resonance, whereas the other one remains unabsorbed due to

off-resonance. Thus the intensity gets reduced substantially at the output. Thus a situation arises, where the intensity at the output depends upon the direction of the magnetic field. This idea is demonstrated using atomic models. Effect of Doppler distribution of atomic velocities has been explored. One can find a situation where, the transmittivity of the medium can be changed much more drastically, so that an opaque medium becomes transparent and vice versa upon reversal of direction of the magnetic field. Effect of collisional broadening and large magnetic field on MFRA can also be explored.

In chapter 4, we set out to explain the experimental results of Labeyrie *et al.* on the optical density dependence of the MOR angle. We have provided a possible model for this. We have shown that MOR angle of a linearly polarized field with nonzero spectral width does not depend linearly on the optical density of the anisotropic medium in large optical density domain. This can be understood in terms of contribution of the off-resonant components of the input field to the output intensity. This has been shown that for small optical density, the absorption does not substantially affect the MOR angle, and thus this angle exhibits linear dependence on the optical density. This occurs because the mean field approximation remains valid for small optical density. The results of this chapter is in good agreement with the experimental findingsof Labeyrie *et al.*. The effect of large magnetic field to achieve large MOR angle can be investigated as a possible extension. It is expected that the polarization of the input field can be reversed (which is equivalent to a MOR angle $\sim 180^o$).

In chapter 5, possibility of non-zero susceptibility at two-photon resonance and of gain at certain probe frequencies has been explored. It can be understood in terms of the effect of atomic coherence that is induced by an external control field. The dressed state analysis shows that the gain arises due to population inversion in the dressed state basis. Further, it is shown that the control field can control the MOR angle inside such a medium.

In chapter 6, we have shown that the fidelity of photon cloning can be improved much beyond the optimal limit by suitably choosing classical cycling fields. The Rabi frequencies of the fields depend upon the initial superposition of the input polarization state. The dynamics of fidelity of a quantum cloner based on single

atom and two atoms is analyzed. However, the atomic cloning machine deviates from the universality due to usage of external coherent fields.

Recently, EIT is used in the context of implementation of logic gates in quantum computation. One can use the idea of coherent control to improve the speed of these gates so that decoherence effect would become much less. Further, it would be interesting if one can find a coherent system, which can produce polarized light from an unpolarized light with more than 50% efficiency.

Appendix: A

Basic procedure for semiclassical treatment for atom-field interaction

Here we provide a brief outline how to calculate the probe susceptibility for any driven multilevel system. We write down the unperturbed Hamiltonian H_0 as

$$H_0 = \hbar \sum_i \omega_i |i\rangle\langle i| \ . \tag{A.1}$$

We assume that the perturbation arises from the interaction of the atomic dipole operator $\vec{d}$ with the interacting classical field $\vec{E}$. This interaction part is thus given by $H_1 = -\vec{d}.\vec{E}$, where $\vec{d} \equiv \sum_{i \neq j} \vec{d}_{ij} |i\rangle\langle j|$ and $\vec{E} = \vec{\mathcal{E}} e^{-i\omega t} + \vec{\mathcal{E}}^{\star} e^{i\omega t}$. Here we have assumed that there is no dipole transition between the levels of the same parity. The Rabi frequency in this interaction can be defined as $2\Omega \equiv 2\vec{d}_{ij}.\vec{\mathcal{E}}/\hbar$.

We start with the Liouville equation for the density matrix equations:

$$\dot{\rho} = -\frac{i}{\hbar}[H, \rho] + \mathcal{L}\rho \ , \tag{A.2}$$

where the dot represents the time-derivative and $H = H_0 + H_1$ is the total Hamiltonian. We have added the second term phenomenologically on the right hand side of the above equation, which represent the incoherent processes like decays due to spontaneous emission, collisional process etc. The explicit forms of this term are as follows: In the equation for diagonal density matrix element ρ_{ii}, one adds $-\sum_j \gamma_{ji}\rho_{ii} + \sum_j \gamma_{ij}\rho_{jj}$, where the first term stands for all the decays from the relevant level $|i\rangle$ to a manifold $\{|j\rangle\}$ of other levels, where the decay is allowed and the second term stands for the all possible decays to the level $|i\rangle$ from the other levels. Here γ's represent the decay rate and have dimension of angular frequency. On the other hand, in the equation for the off-diagonal matrix elements ρ_{ij}, one adds the term $-\Gamma_{ij}\rho_{ij}$, where $\Gamma_{ij} = \frac{1}{2}\sum_k (\gamma_{ki} + \gamma_{kj}) + \gamma_{\rm coll}$. Here $\gamma_{\rm coll}$ refers to the collisional decay rate.

Next we change $\rho_{ij} \to \tilde{\rho}_{ij}$ in a rotating reference frame so that all the explicit time-dependence on the right hand side of the above equations will be removed making use of RWA. As we have mentioned that in presence of decay channels, the system comes to a steady state in the time-scale much larger than the atomic decay time. Thus, we work under steady state condition $\dot{\rho}_{ij} = 0$. Thus we obtain a set of algebraic equations, which can be solved perturbatively. We expand the density matrix elements $\tilde{\rho}_{ij}$ in terms of the weak probe field as

$$\tilde{\rho}_{ij} = \tilde{\rho}_{ij}^{(0)} + \frac{\Omega}{\gamma}\tilde{\rho}_{ij}^{(1)} \ , \tag{A.3}$$

where Ω is the half of the Rabi frequency of the probe field. We then equate the coefficients of Ω^n $(n \in 0, 1, 2, \ldots)$ and solve algebraically for $\tilde{\rho}_{ij}^{(n)}$.

We have already discussed in subsection 1.2.1, how the first order susceptibility of the medium is related to the off-diagonal density matrix element between the levels which are coupled by the probe field. This matrix element is often called as probe coherence. In fact, if we assume that $\rho_{ij}^{(0)} = 0$, then the relation (1.51) becomes

$$\chi_{\alpha\beta}^{(1)}(\omega) = N\frac{\rho_{ij}^{(1)}|d_{ij}^{(\alpha)}|^2}{\hbar\gamma_{ji}} \ , \tag{A.4}$$

where N is the number density of atomic medium. Thus the phase change Φ and the absorption coefficient αL as defined in (1.17) can be rewritten as

$$\alpha L = 4\pi\frac{\omega_{ij}L}{c}\frac{N|d_{ij}^{(\alpha)}|^2}{\hbar\gamma_{ji}}\mathrm{Im}[\rho_{ij}^{(1)}] \ , \tag{A.5}$$

$$\Phi = 2\pi\frac{\omega_{ij}L}{c}\frac{N|d_{ij}^{(\alpha)}|^2}{\hbar\gamma_{ji}}\mathrm{Re}[\rho_{ij}^{(1)}] \ , \tag{A.6}$$

where L is the length of the medium.

Now we introduce the Einstein's A-coefficient which is given by[2]

$$A = 2\gamma_{ji} = \frac{4}{3}\frac{|d_{ij}^{(\alpha)}|^2\omega_{ij}^3}{\hbar c^3} \ , \tag{A.7}$$

[2]If there are two or more transitions involved, then one has to find the ratios of the corresponding dipole matrix elements using Clebsch-Gordan coefficients. Then A-coefficient is to be defined in terms of sum of all the decay rates, i.e., $A = 2\gamma[1 + \sum(\text{ratio of dipole matrix elements})^2]$.

where ω_{ij} is the atomic transition frequency. Then substituting $|d_{ij}^{(\alpha)}|^2/\hbar\gamma_{ji} = 3c^3/2\omega_{ij}^3$, we obtain

$$\chi_{\alpha\beta}^{(1)}(\omega) = \frac{3Nc^3}{2\omega_{ij}^3}\rho_{ij}^{(1)} \ . \tag{A.8}$$

We can rewrite αL and Φ accordingly as

$$\begin{aligned} \alpha &= \alpha_0 L \mathrm{Im}[\rho_{ij}^{(1)}], \quad \alpha_0 L = \frac{3NL\lambda_{ij}^2}{2\pi} \ , \\ \Phi &= \frac{3}{4\pi} NL\lambda_{ij}^2 \mathrm{Re}[\rho_{ij}^{(1)}] \ , \end{aligned} \tag{A.9}$$

where $\lambda_{ij} = 2\pi c/\omega_{ij}$. Clearly the coefficients of the real or imaginary parts of $\rho_{ij}^{(1)}$ are easily calculable if one knows the number density N of the atomic vapor medium, transition wavelength λ_{ij}, and length L of the medium.

Derivation of group velocity:

We start with the plane wave solution (1.5), and assume that the frequency ω is a function of k, i.e., $\omega = \omega(k)$. Since dispersive property does not depend upon the direction of propagation, $\omega(k)$ can be considered as an even function. We assume that $\omega(k)$ is real. In most of the practical situations, even a monochromatic light is not truly monochromatic. A finite spread of frequencies or wavelengths exists. Origin of this spread may be due to finite duration of the pulse or some incoherent broadening in the source. Since the Maxwell's equations are linear, so a linear superpositions of the plane wave solutions at different frequencies is also a solution. We consider such a superposition

$$E(z,t) = \frac{1}{\sqrt{2\pi}} \int_{-\infty}^{\infty} \mathcal{E}(k) e^{ikz - i\omega(k)t} dk \ , \tag{A.10}$$

where $\mathcal{E}(k)$ describes the properties of the linear superpositions of the different waves and is given by

$$\mathcal{E}(k) = \frac{1}{\sqrt{2\pi}} \int_{-\infty}^{\infty} E(z,0) e^{-ikz} dz \ . \tag{A.11}$$

We assume now that the pulse, we are considering, is not too broad in the wave-number spectrum. Further the medium, in which the pulse is propagating, is

such that ω has a weak dependence on k. Then we can expand

$$\omega(k) = \omega_0 + \left.\frac{d\omega}{dk}\right|_{k_0} (k - k_0) + \cdots , \tag{A.12}$$

where we have assumed that $\mathcal{E}(k)$ is fairly sharply peaked around $k = k_0$. Then the pulse at some time t is given by

$$E(z,t) = E\left(z - \left.\frac{d\omega}{dk}\right|_{k_0} t, 0\right) \exp\left[i\left\{k_0\left(\frac{d\omega}{dk}\right)_{k_0} - \omega_0\right\} t\right] . \tag{A.13}$$

This shows that apart from an overall phase factor, the pulse travels along undistorted in shape with a *group velocity*

$$v_g = \left.\frac{d\omega}{dk}\right|_{k_0} . \tag{A.14}$$

For light waves, $\omega(k) = ck/\eta(k)$. For most optical wavelengths, $\eta(k)$ is greater than unity in almost all substances. Then

$$v_g = \frac{c}{n_g} = \frac{c}{\eta(\omega) + \omega\frac{d\eta}{d\omega}} , \tag{A.15}$$

where $\eta = 1 + 2\pi \mathrm{Re}[\chi(\omega)]$ is the linear refractive index, and n_g is the group index. Normally, one is much interested to calculate the group velocities at resonance. Thus the group index n_g is given by

$$\begin{aligned} n_g &= \left[\eta(\omega) + \omega\frac{\partial\eta(\omega)}{\partial\omega}\right]_{\omega=\omega_{ij}} \\ &= 1 + 2\pi \mathrm{Re}\chi^{(1)}_{\alpha\beta}(\omega_{ij}) + 2\pi\omega_{ij}\left.\frac{\partial}{\partial\omega}(\mathrm{Re}\chi^{(1)}_{\alpha\beta})\right|_{\omega=\omega_{ij}} \\ &= 1 + \frac{3}{2}\frac{N\lambda_{ij}^3}{(2\pi)^2}\left.\mathrm{Re}[\rho^{(1)}_{ij}]\right|_{\omega=\omega_{ij}} + \frac{3Nc\lambda_{ij}^2}{2\pi}\left.\frac{\partial}{\partial\omega}\mathrm{Re}\rho^{(1)}_{ij}\right|_{\omega=\omega_{ij}} . \end{aligned} \tag{A.16}$$

Appendix: B

Coherent control in Λ systems : Basic equations

We consider the level diagram in Fig. B.1. We assume that the transition between the levels $|b\rangle$ and $|c\rangle$ is dipole-forbidden. The pump (probe) is acting with the transition $|a\rangle \leftrightarrow |b\rangle$ ($|a\rangle \leftrightarrow |c\rangle$). Spontaneous decay can occur from the level $|a\rangle$ to the other two levels. The pump and probe fields are given by

$$\vec{E}_i = \vec{\mathcal{E}}_i e^{-i\omega_i t} + \vec{\mathcal{E}}_i^* e^{i\omega_i t} \quad (i \in 1, 2). \tag{B.1}$$

The Hamiltonian in the dipole approximation can be written as

$$H = \hbar(\omega_a|a\rangle\langle a| + \omega_b|b\rangle\langle b| + \omega_c|c\rangle\langle c|) - \hbar(\vec{d}_{ab}|a\rangle\langle b| + \vec{d}_{ac}|a\rangle\langle c| + \text{c.c}).(\vec{E}_1 + \vec{E}_2). \tag{B.2}$$

We use the Liouville equation and consider all the decays possible in the system. Then the density matrix equations under RWA in the rotated frame

$$\tilde{\rho}_{ab} = \rho_{ab}e^{i\omega_1 t}, \quad \tilde{\rho}_{ac} = \rho_{ac}e^{i\omega_2 t}, \quad \text{and} \quad \tilde{\rho}_{cb} = \rho_{cb}e^{-i(\omega_1 - \omega_2)t}. \tag{B.3}$$

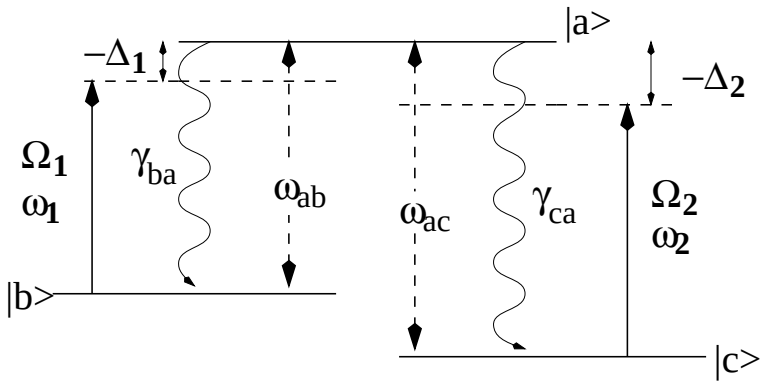

Figure B.1: Level configuration of a Lambda system

can be written as

$$\begin{aligned}
\dot{\tilde{\rho}}_{bb} &= i(\tilde{\rho}_{ab}\Omega_1^* - c.c) + \gamma_{ba}\tilde{\rho}_{aa}, \\
\dot{\tilde{\rho}}_{cc} &= i(\tilde{\rho}_{ac}\Omega_2^* - c.c) + \gamma_{ca}\tilde{\rho}_{aa}, \\
\dot{\tilde{\rho}}_{ab} &= (i\Delta_1 - \Gamma_{ab})\tilde{\rho}_{ab} - i\Omega_1(\tilde{\rho}_{aa} - \tilde{\rho}_{bb}) + i\Omega_2\tilde{\rho}_{cb}, \\
\dot{\tilde{\rho}}_{ac} &= (i\Delta_2 - \Gamma_{ac})\tilde{\rho}_{ac} - i\Omega_2(\tilde{\rho}_{aa} - \tilde{\rho}_{cc}) + i\Omega_1\tilde{\rho}_{bc}, \\
\dot{\tilde{\rho}}_{bc} &= \{i(\Delta_2 - \Delta_1) - \Gamma_{bc}\}\tilde{\rho}_{bc} + i\Omega_1^*\tilde{\rho}_{ac} - i\Omega_2\tilde{\rho}_{ba} \ , \qquad \text{(B.4)}
\end{aligned}$$

where we have used $\Delta_1 = \omega_1 - \omega_{ab}$, $\Delta_2 = \omega_2 - \omega_{ac}$, $\Gamma_{ab} = \Gamma_{ac} = \frac{1}{2}(\gamma_{ba} + \gamma_{ca}) + \gamma_{\rm coll}$, $\Gamma_{bc} = \gamma_{\rm coll}$. Here $\Omega_1 = \vec{d}_{ab}.\vec{E}_1/\hbar$ and $\Omega_2 = \vec{d}_{ac}.\vec{E}_2/\hbar$ represent half of the pump and probe Rabi frequencies. These equations can be solved in the steady state, i.e., in the long time limit ($t \gg 1/\gamma$), when the time-dependence of the $\tilde{\rho}_{\alpha\beta}$ can be neglected. We assume that atomic population initially resides in the ground level $|c\rangle$.

We consider $\Omega_1 \gg \Omega_2$ and expand

$$\tilde{\rho}_{\alpha\beta} = \tilde{\rho}_{\alpha\beta}^{(0)} + \frac{\Omega_2}{\gamma}\tilde{\rho}_{\alpha\beta}^{(1)} \qquad \text{(B.5)}$$

upto first order of the probe Rabi frequency. Comparing the coefficients of Ω_2^n ($n \in 0, 1$), we obtain the following solution for the probe coherence:

$$\tilde{\rho}_{ac} = \frac{\Omega_2}{\gamma}\tilde{\rho}_{ac}^{(1)} = \frac{\Omega_2}{\gamma}\frac{i\gamma[i(\Delta_1 - \Delta_2) + \Gamma_{bc}]}{[(\Gamma_{ac} - i\Delta_2)\{\Gamma_{bc} + i(\Delta_1 - \Delta_2)\}] + |\Omega_1|^2}, \qquad \text{(B.6)}$$

under the condition that the atoms initially reside in the level $|c\rangle$. Note that the imaginary part of $\tilde{\rho}_{ac}$ under two-photon resonance can be written as

$$\mathrm{Im}(\tilde{\rho}_{ac}) = \frac{\Gamma_{bc}(\Gamma_{ac}\Gamma_{bc} + |\Omega_1|^2)}{\{\Gamma_{ac}\Gamma_{bc} + |\Omega_1|^2\}^2 + \Delta_2^2\Gamma_{bc}^2} \ , \qquad \text{(B.7)}$$

which becomes zero if there is no collisional relaxation, i.e., if $\gamma_{\rm coll} = 0$ (i.e., $\Gamma_{bc} = 0$). This situation corresponds to EIT, which will be described later.

Dressed State analysis

Using the transformation

$$|\Psi\rangle = \exp\left[-i\omega_2 t|a\rangle\langle a| - i(\omega_1 - \omega_2)t|b\rangle\langle b|\right]|\phi\rangle \qquad \text{(B.8)}$$

so that the Schrödinger equation $|\dot{\Psi}\rangle = -iH/\hbar|\Psi\rangle$ becomes $|\dot{\phi}\rangle = -iH_{\text{eff}}/\hbar|\phi\rangle$, we obtain the following effective Hamiltonian under RWA:

$$\begin{aligned}\frac{1}{\hbar}H_{\text{eff}} &= -\Delta_2|a\rangle\langle a| + (\Delta_1 - \Delta_2)|b\rangle\langle b| - |\Omega_1||b\rangle\langle a| - |\Omega_1||a\rangle\langle b| \\ &\quad -|\Omega_2||a\rangle\langle c| - |\Omega_2||c\rangle\langle a| \end{aligned} \tag{B.9}$$

The eigenstates of this Hamiltonian are the dressed states of the Lambda system and can be expanded as

$$|k\rangle = \alpha_k|a\rangle + \beta_k|b\rangle + \gamma_k|c\rangle \; ; \quad k = \pm, 0. \tag{B.10}$$

The coefficients are as follows:

$$\begin{pmatrix} \alpha_k \\ \beta_k \\ \gamma_k \end{pmatrix} = \frac{1}{\sqrt{(|\Omega_2|^2 + \omega_k^2)(\Delta_1 - \Delta_2 - \omega_k)^2 + |\Omega_1|^2\omega_k^2}} \begin{pmatrix} \omega_k(\Delta_1 - \Delta_2 - \omega_k) \\ |\Omega_1|\omega_k \\ -|\Omega_2|(\Delta_1 - \Delta_2 - \omega_k) \end{pmatrix}. \tag{B.11}$$

The corresponding eigenvalues are

$$\omega_k = -\frac{1}{3}A \pm \frac{2}{3}\sqrt{A^2 - 3B}\cos\left[\frac{1}{3}\cos^{-1}\left\{\mp\frac{27C + 2A^3 - 9AB}{2(A^2 - 3B)^{3/2}}\right\}\right] \tag{B.12}$$

with

$$A = -(\Delta_1 - 2\Delta_2),\; B = -\Delta_2(\Delta_1 - \Delta_2) - |\Omega_1|^2 - |\Omega_2|^2,\; C = |\Omega_2|^2(\Delta_1 - \Delta_2)\; . \tag{B.13}$$

In case of two-photon resonance $\Delta_1 = \Delta_2 = \Delta$, the eigenstates become

$$\begin{pmatrix} \alpha_+ \\ \beta_+ \\ \gamma_+ \end{pmatrix} = \frac{1}{\sqrt{\omega_+^2 + |\Omega_1|^2 + |\Omega_2|^2}} \begin{pmatrix} -\omega_+ \\ |\Omega_1| \\ |\Omega_2| \end{pmatrix}; \qquad \omega_+ = \frac{1}{2}\left[\Delta - \sqrt{\Delta^2 + 4(|\Omega_1|^2 + |\Omega_2|^2)}\right]$$

$$\begin{pmatrix} \alpha_0 \\ \beta_0 \\ \gamma_0 \end{pmatrix} = \frac{1}{\sqrt{|\Omega_1|^2 + |\Omega_2|^2}} \begin{pmatrix} 0 \\ -|\Omega_2| \\ |\Omega_1| \end{pmatrix}; \qquad \omega_0 = 0$$

$$\begin{pmatrix} \alpha_- \\ \beta_- \\ \gamma_- \end{pmatrix} = \frac{1}{\sqrt{\omega_-^2 + |\Omega_1|^2 + |\Omega_2|^2}} \begin{pmatrix} -\omega_- \\ |\Omega_1| \\ |\Omega_2| \end{pmatrix}; \qquad \omega_- = \frac{1}{2}\left[\Delta + \sqrt{\Delta^2 + 4(|\Omega_1|^2 + |\Omega_2|^2)}\right]$$

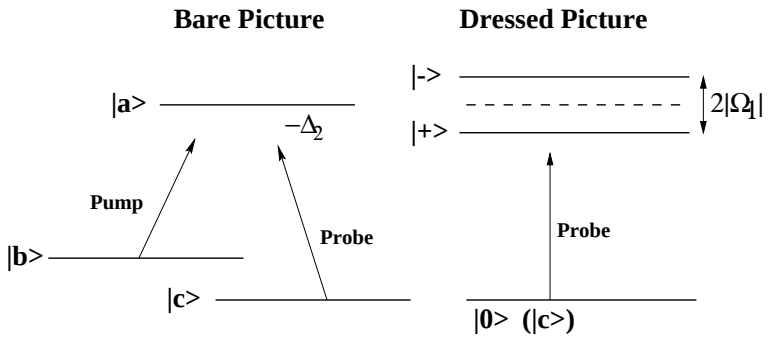

Figure B.2: Dressed state picture of Lambda system for resonant pump field.

Utility of the dressed state analysis : EIT

In a Λ system, under the condition $\Delta_1 = \Delta_2 = \Delta$, a zero occurs in the absorption spectra, referring to a transparency point for the probe field. This is called electromagnetically induced transparency (EIT). Also there are two Autler-Townes peaks positioned at ω_+ and ω_-. If we consider $\Omega_2 = 0$ then the positions of these peaks become

$$\begin{aligned} \omega_+ &= \frac{1}{2}[\Delta - \sqrt{\Delta^2 + 4|\Omega 1|^2}], \\ \omega_- &= \frac{1}{2}[\Delta + \sqrt{\Delta^2 + 4|\Omega_1|^2}]. \end{aligned} \tag{B.14}$$

The dressed states (dressed by the pump field only, assuming $\Omega_1 = 0$) for $\Delta_1 = 0$ (resonant pump) can be written as

$$|+\rangle = \frac{1}{\sqrt{2}}(-|a\rangle + |b\rangle) \ , \ |0\rangle = |c\rangle \ , \ |-\rangle = \frac{1}{\sqrt{2}}(|a\rangle + |b\rangle) \ . \tag{B.15}$$

These states have been shown in Fig. B.2. The frequency separation of these states is $2|\Omega_1|$. The two absorption peaks are at $\Delta_2 = \pm|\Omega_1|$ corresponding to the $|c\rangle \leftrightarrow |-\rangle$ and $|c\rangle \leftrightarrow |+\rangle$ transitions, respectively.

Consider now the expression for $\tilde{\rho}_{ac}$. The imaginary part of it is zero if $\Gamma_{bc} = 0$ and the real part of it is zero if $\Delta_1 = \Delta_2$ (two-photon resonance). These are the characteristics of EIT. *Lambda systems* are very useful to obtain EIT, because *the decay rate of the ground levels is very much small*. This leads to large coherence

time of the ground state coherence.

Positions and widths of absorption peaks

To calculate the exact positions and widths of the EIT peaks without any approximations, we write $\tilde{\rho}_{ac}$ as the sum of two Lorentzians

$$\tilde{\rho}_{ac} \equiv \frac{F(\Delta_+)}{(\Delta_+ - \Delta_-)(\Delta_2 - \Delta_+)} + \frac{F(\Delta_-)}{(\Delta_- - \Delta_+)(\Delta_2 - \Delta_-)} , \tag{B.16}$$

where

$$\begin{aligned} F(\Delta_\pm) &= -\frac{1}{2}(\Delta_1 \mp M) + \frac{i}{2}(\Gamma_{ac} - \Gamma_{bc}) \\ M &= \sqrt{4|\Omega_1|^2 - (\Gamma_{bc} - \Gamma_{ac} + i\Delta_1)^2} . \end{aligned} \tag{B.17}$$

Here, $\Delta_\pm$ are the two poles of the denominator of $\tilde{\rho}_{ac}$ and are given by

$$\Delta_\pm = \frac{\Delta_1}{2} - \frac{i}{2}(\Gamma_{ac} + \Gamma_{bc}) \pm \frac{1}{2}M . \tag{B.18}$$

Real part of this would give us the positions and the imaginary part gives the widths of the absorption peaks. If we consider the pump field to be one-photon resonant, i.e., $\Delta_1 = 0$, then

$$\Delta_\pm = \pm\sqrt{4|\Omega_1|^2 - (\Gamma_{bc} - \Gamma_{ac})^2)} - \frac{i}{2}(\Gamma_{ac} + \Gamma_{bc}) . \tag{B.19}$$

Thus, the position of the absorption peaks are given by the first term above and the width of the peaks becomes $(\Gamma_{ac} + \Gamma_{bc})/2$. Note that for $\Delta_1 = 0$, the positions of the absorption peaks are not exactly $\pm|\Omega_1|$, rather it has some Γ-dependence.

Further, if we assume that Im(χ) has very small variation at resonance, then we can expand

$$\mathrm{Im}(\chi) = \mathrm{Im}\chi(\delta = 0) + \delta^2 \frac{\partial^2}{\partial \delta^2}\mathrm{Im}(\chi)|_{\delta=0} + \cdots \tag{B.20}$$

At EIT, the first term of the above expression vanishes and thus the absorption coefficient can be written as

$$\alpha l = 4\pi k l \delta^2 \frac{\partial^2}{\partial \delta^2}\mathrm{Im}(\chi)|_{\delta=0} . \tag{B.21}$$

Thus the width σ of the EIT window can be expressed as $\sigma^2 = \delta^2/2\alpha l$ such that

$$\sigma^2 = \frac{1}{8\pi k l \frac{\partial^2}{\partial \delta^2}\mathrm{Im}(\chi)|_{\delta=0}} = \frac{2|\Omega_1|^4}{3Nkl\lambda^3\Gamma_{ac}^2} , \tag{B.22}$$

for $\Delta_1 = 0$. Clearly, EIT window narrows down with increase in number density N. This width increases with Rabi frequency $|\Omega_1|$ of the control field.

Appendix: C

Coherent control of Ξ systems : Basic equations

We consider the level diagram in Fig. C.1. We assume that the transition between the levels $|a\rangle$ and $|c\rangle$ is dipole-forbidden. The pump (probe) field is acting with the transition $|a\rangle \leftrightarrow |b\rangle$ ($|b\rangle \leftrightarrow \langle c\rangle$). These fields are given by

$$\vec{E}_i = \vec{\mathcal{E}}_i e^{-i\omega_i t} + \vec{\mathcal{E}}_i^* e^{i\omega_i t} \quad (i \in 1,2) \tag{C.1}$$

The Hamiltonian of the system in the dipole approximation can be written as:

$$H_0 = \hbar(\omega_a|a\rangle\langle a| + \omega_b|b\rangle\langle b| + \omega_c|c\rangle\langle c|) - \hbar(\vec{d}_{ab}|a\rangle\langle b| + \vec{d}_{bc}|b\rangle\langle c| + \text{c.c.}).(\vec{E}_1 + \vec{E}_2)\ . \tag{C.2}$$

The density matrix equations can be obtained using the Liouville equation considering all the possible decay channels into account and using the RWA in the rotating frame

$$\tilde{\rho}_{ab} = \rho_{ab}e^{i\omega_1 t}, \quad \tilde{\rho}_{bc} = \rho_{bc}e^{i\omega_2 t}, \quad \text{and} \quad \tilde{\rho}_{ac} = \rho_{ac}e^{i(\omega_1+\omega_2)t}\ . \tag{C.3}$$

We thus obtain the following equations:

$$\begin{aligned}
\dot{\tilde{\rho}}_{aa} &= i(\Omega_1\tilde{\rho}_{ba} - \Omega_1^*\tilde{\rho}_{ab}) - \gamma_{ba}\tilde{\rho}_{aa}, \\
\dot{\tilde{\rho}}_{cc} &= (i\Omega_2\tilde{\rho}_{bc} - i\Omega_2^*\tilde{\rho}_{cb}) + \gamma_{cb}\tilde{\rho}_{bb}, \\
\dot{\tilde{\rho}}_{bb} &= -(\dot{\tilde{\rho}}_{aa} + \dot{\tilde{\rho}}_{cc}), \\
\dot{\tilde{\rho}}_{ab} &= i\Delta_1\tilde{\rho}_{ab} - \Gamma_{ab}\tilde{\rho}_{ab} - i\Omega_1(\tilde{\rho}_{aa} - \tilde{\rho}_{bb}) - i\Omega_2^*\tilde{\rho}_{ac}, \\
\dot{\tilde{\rho}}_{bc} &= i\Delta_2\tilde{\rho}_{bc} - \Gamma_{bc}\tilde{\rho}_{bc} - i\Omega_2(\tilde{\rho}_{bb} - \tilde{\rho}_{cc}) + i\Omega_1^*\tilde{\rho}_{ac}, \\
\dot{\tilde{\rho}}_{ac} &= i(\Delta_1 + \Delta_2)\tilde{\rho}_{ac} - \Gamma_{ac}\tilde{\rho}_{ac} + i\Omega_1^*\tilde{\rho}_{bc} - i\Omega_2\tilde{\rho}_{ab},
\end{aligned} \tag{C.4}$$

where we have used, $\Delta_1 = \omega_1 - \omega_{ab}$, $\Delta_2 = \omega_2 - \omega_{bc}$, $\Gamma_{ac} = \frac{1}{2}\gamma_{ba} + \gamma_{\text{coll}}$, $\Gamma_{bc} = \frac{1}{2}\gamma_{cb} + \gamma_{\text{coll}}$, $\Gamma_{ab} = \frac{1}{2}(\gamma_{ba} + \gamma_{cb}) + \gamma_{\text{coll}}$. Here $\Omega_1 = \vec{d}_{ab}.\vec{E}_1/\hbar$ and $\Omega_2 = \vec{d}_{bc}.\vec{E}_2/\hbar$ are half of the pump and probe Rabi frequencies, respectively.

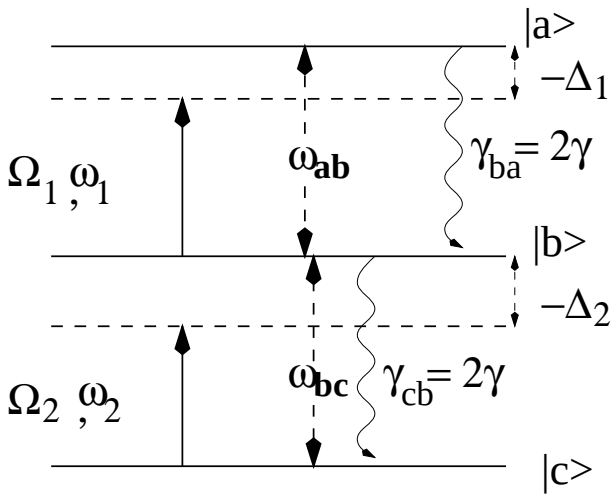

Figure C.1: Level diagram for Ladder System

In steady state $\dot{\tilde{\rho}}_{\alpha\beta}$ is made zero. Also in our consideration $\Omega_2 \ll \Omega_1$. So we will expand $\tilde{\rho}_{\alpha\beta}$ in terms of Ω_2 as:

$$\tilde{\rho}_{\alpha\beta} = \tilde{\rho}^{(0)}_{\alpha\beta} + \frac{\Omega_2}{\gamma}\tilde{\rho}^{(1)}_{\alpha\beta} \ . \tag{C.5}$$

Using the above, we have the following perturbative solution for the probe coherence: Thus,

$$\tilde{\rho}_{bc} = \frac{\Omega_2}{\gamma}\tilde{\rho}^{(1)}_{bc} = \frac{\Omega_2}{\gamma}\frac{i\gamma\{\Gamma_{ac} - i(\Delta_1 + \Delta_2)\}}{\{\Gamma_{ac} - i(\Delta_1 + \Delta_2)\}\{\Gamma_{bc} - i\Delta_2\} + |\Omega_1|^2} \ . \tag{C.6}$$

Position and widths of the absorption peaks

We consider the expression for $\tilde{\rho}_{bc}$ above. The poles of this complex function can be found by solving the denominator for Δ_2. The solution for Δ_2 gives

$$\Delta_2 = \frac{1}{2}\left[-\{\Delta_1 + i(\Gamma_{bc} + \Gamma_{ac})\} \pm \sqrt{\{\Delta_1 + i(\Gamma_{bc} + \Gamma_{ac})\}^2 + 4(\Gamma_{ac}\Gamma_{bc} - i\Delta_1\Gamma_{bc}|\Omega_1|^2)}\right] \ . \tag{C.7}$$

For $\Delta_1 = 0$ and $\Gamma_{ac} = \Gamma_{bc} = \Gamma$, this yields $\Delta_2 = \pm|\Omega_1| - i\Gamma$. Clearly, there will be two absorption peaks at $\Delta_2 = \pm|\Omega_1|$ with width Γ[3].

[3]For $|\Omega_1| = 0$, one retrieves the two-level result $\Delta_2 = -i\Gamma_{bc}$, which refers to a single peak at $\Delta_2 = 0$ with width Γ_{bc}. Because, we are not solving the present problem with all orders of Ω_2, so we are not getting the power-dependence of the width of the absorption peak in two-level limit [see Eq. 1.54].

Further, we note that at two-photon resonance (i.e., $\Delta_1 + \Delta_2 = 0$),

$$\mathrm{Im}(\tilde{\rho}_{bc}) = \frac{\Gamma_{ac}(\Gamma_{ac} + \Gamma_{bc} + |\Omega_1|^2)}{(\Gamma_{ac}\Gamma_{bc} + |\Omega_1|^2)^2 + \Delta_2^2\Gamma_{ac}^2} \tag{C.8}$$

Note that the imaginary part can never be zero, as $\Gamma_{ac} \neq 0$. However, at two-photon resonance,

$$\mathrm{Re}(\tilde{\rho}_{bc}) = \frac{-\Delta_2\Gamma_{ac}^2}{(\Gamma_{ac}\Gamma_{bc} + |\Omega_1|^2)^2 + \Delta_2^2\Gamma_{ac}^2} \tag{C.9}$$

can be zero only if $\Delta_2 = 0$.

Dressed State Analysis

Using the transformation

$$|\Psi\rangle = \exp\left[-i\omega_2 t|b\rangle\langle b| - i(\omega_1 + \omega_2)t|a\rangle\langle a|\right]|\phi\rangle$$

and RWA, we obtain the following effective Hamiltonian H_{eff} with no explicit time-dependence:

$$\begin{aligned}\frac{1}{\hbar}H_{\mathrm{eff}} \quad = \quad & -\Delta_2|b\rangle\langle b| - (\Delta_1 + \Delta_2)|a\rangle\langle a| - |\Omega_2||b\rangle\langle c| - |\Omega_2||c\rangle\langle b| \\ & -|\Omega_1||a\rangle\langle b| - |\Omega_1||b\rangle\langle a|. \end{aligned} \tag{C.10}$$

The eigenstates of this Hamiltonian are the dressed states of the present system. They can be written as:

$$|k\rangle = \alpha_k|a\rangle + \beta_k|b\rangle + \gamma_k|c\rangle \ ; \quad k = \pm, 0 \ . \tag{C.11}$$

These eigenstates are given by:

$$\begin{pmatrix} \alpha_k \\ \beta_k \\ \gamma_k \end{pmatrix} = \frac{1}{\sqrt{(|\Omega_2|^2 + \omega_k^2)(\Delta_1 + \Delta_2 + \omega_k)^2 + |\Omega_1|^2\omega_k^2}} \begin{pmatrix} |\Omega_1|\omega_k \\ -\omega_k(\Delta_1 + \Delta_2 + \omega_k) \\ |\Omega_2|(\Delta_1 + \Delta_2 + \omega_k) \end{pmatrix} . \tag{C.12}$$

The corresponding eigenvalues are

$$\omega_k = -\frac{1}{3}A \pm \frac{2}{3}\sqrt{A^2 - 3B}\cos\left[\frac{1}{3}\cos^{-1}\left\{\mp\frac{27C + 2A^3 - 9AB}{2(A^2 - 3AB)^{3/2}}\right\}\right] \tag{C.13}$$

with

$$A = (\Delta_1 + 2\Delta_2), \ B = \Delta_2(\Delta_1 + \Delta_2) - |\Omega_1|^2 - |\Omega_2|^2, \ C = -|\Omega_2|^2(\Delta_1 + \Delta_2) \ . \tag{C.14}$$

In case of two-photon resonance $\Delta_1 = -\Delta_2 = \Delta$ the eigenstates are

$$\begin{pmatrix} \alpha_+ \\ \beta_+ \\ \gamma_+ \end{pmatrix} = \frac{1}{\sqrt{\omega_+^2 + |\Omega_1|^2 + |\Omega_2|^2}} \begin{pmatrix} |\Omega_1| \\ -\omega_+ \\ |\Omega_2| \end{pmatrix}; \qquad \omega_+ = \frac{1}{2}\left[\Delta - \sqrt{\Delta^2 + 4(|\Omega_1|^2 + |\Omega_2|^2)}\right]$$

$$\begin{pmatrix} \alpha_0 \\ \beta_0 \\ \gamma_0 \end{pmatrix} = \frac{1}{\sqrt{|\Omega_1|^2 + |\Omega_2|^2}} \begin{pmatrix} -|\Omega_2| \\ 0 \\ |\Omega_1| \end{pmatrix}; \qquad \omega_0 = 0$$

$$\begin{pmatrix} \alpha_- \\ \beta_- \\ \gamma_- \end{pmatrix} = \frac{1}{\sqrt{\omega_-^2 + |\Omega_1|^2 + |\Omega_2|^2}} \begin{pmatrix} |\Omega_1| \\ -\omega_- \\ |\Omega_2| \end{pmatrix}; \qquad \omega_- = \frac{1}{2}\left[\Delta + \sqrt{\Delta^2 + 4(|\Omega_1|^2 + |\Omega_2|^2)}\right]$$

Utility of the dressed state analysis

The dressed state analysis provides us the exact physical understanding of the process. To start with, we set $\Omega_2 = 0$. Then the eigenvalues for the state $|+\rangle$, $|0\rangle$, and $|-\rangle$ become

$$\omega_\pm = \frac{1}{2}[\Delta \mp \sqrt{\Delta^2 + 4|\Omega_1|^2}], \quad \omega_0 = 0. \tag{C.15}$$

The dressed states under this condition become,

$$\begin{aligned} |+\rangle &= \frac{1}{\sqrt{\omega_+^2 + |\Omega_1|^2}}[|\Omega_1||a\rangle - \omega_+|b\rangle], \\ |0\rangle &= |c\rangle, \\ |-\rangle &= \frac{1}{\sqrt{\omega_-^2 + |\Omega_1|^2}}[|\Omega_1||a\rangle - \omega_-|b\rangle]. \end{aligned} \tag{C.16}$$

Clearly we can see that from the above expressions that the levels $|a\rangle$ and $|b\rangle$ are dressed by the pump filed Ω_1 and the level $|c\rangle$ remains unchanged. For simplicity, if we now consider the case of one-photon resonance, i.e., $\Delta = 0$, then $\omega_+ = -|\Omega_1|$, $\omega_- = |\Omega_1|$ and

$$|+\rangle = \frac{1}{\sqrt{2}}[|a\rangle + |b\rangle], \quad |-\rangle = \frac{1}{\sqrt{2}}[|a\rangle - |b\rangle]. \tag{C.17}$$

These states have been shown in Fig. C.2. Clearly, there are now two levels $|+\rangle$ and $|-\rangle$ separated by a energy difference of $2\hbar|\Omega_1|$, which are the dressed states

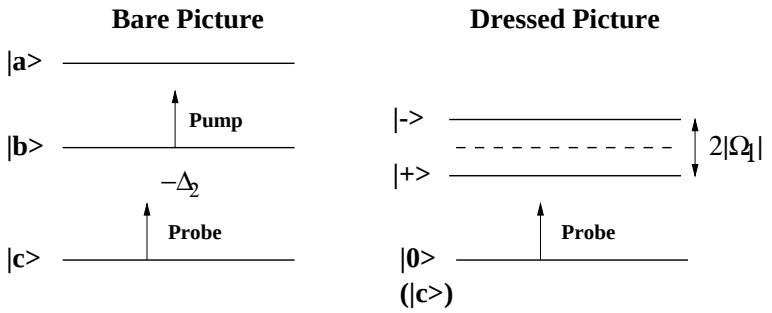

Figure C.2: Dressed picture for Ladder system for resonant pump ($\Delta_1 = 0$).

comprised of the levels $|a\rangle$ and $|b\rangle$. So if now one applies the probe ($\equiv \Omega_2$), then there will be two Autler-Townes peaks in the absorption spectrum separated by $2|\Omega_1|$, corresponding to $|c\rangle \leftrightarrow |\pm\rangle$ transitions, respectively. Note from the expressions for ω_k that the absorption spectrum becomes symmetric about $\Delta_2 = 0$ only if the pump is also resonant ($\Delta_1 = 0$).

Pump-probe interchanged

Here we consider the case, when the pump (probe) field is applied in the $|b\rangle \leftrightarrow |c\rangle$ ($|a\rangle \leftrightarrow |b\rangle$) transition. This is a situation reverse to the case discussed above. Thus we can consider $\Omega_1 \ll \Omega_2$. Then we can expand $\tilde{\rho}_{\alpha\beta}$ in terms of Ω_1 as follows:

$$\tilde{\rho}_{\alpha\beta} = \tilde{\rho}^{(0)}_{\alpha\beta} + \frac{\Omega_1}{\gamma}\tilde{\rho}^{(1)}_{\alpha\beta}, \tag{C.18}$$

then we can get the following steady state solutions:

$$\begin{aligned}
\tilde{\rho}^{(0)}_{aa} &= 0, \\
\tilde{\rho}^{(0)}_{bb} &= \frac{2|\Omega_2|^2\Gamma_{bc}}{\gamma_{cb}(\Gamma^2_{bc}+\Delta^2_2)+4|\Omega_2|^2\Gamma_{bc}}, \\
\tilde{\rho}^{(0)}_{cc} &= \frac{2|\Omega_2|^2\Gamma_{bc}+\gamma_{cb}(\Gamma^2_{bc}+\Delta^2_2)}{4|\Omega_2|^2\Gamma_{bc}+\gamma_{cb}(\Gamma^2_{bc}+\Delta^2_2)}, \\
\tilde{\rho}^{(0)}_{bc} &= \frac{i\Omega_2\gamma_{cb}(\Gamma_{bc}+i\Delta_2)}{4|\Omega_2|^2\Gamma_{bc}+\gamma_{cb}(\Gamma^2_{bc}+\Delta^2_2)}, \\
\tilde{\rho}^{(1)}_{ab} &= \frac{i|\Omega_2|^2\{(\Gamma_{bc}+i\Delta_2)\gamma_{cb}+2\Gamma_{bc}[-i(\Delta_1+\Delta_2)+\Gamma_{ac}]\}}{\{\gamma_{cb}(\Gamma^2_{bc}+\Delta^2_2)+4|\Omega_2|^2\Gamma_{bc}\}\{(\Gamma_{ab}-i\Delta_1)[\Gamma_{ac}-i(\Delta_1+\Delta_2)]+|\Omega_2|^2\}}.
\end{aligned} \tag{C.19}$$

Appendix: D

Coherent control in 'V' systems : Basic equations

We consider the level diagram in Fig. D.1. We assume that the transition between the levels $|a\rangle$ and $|b\rangle$ is dipole-forbidden. The pump (probe) field $\vec{E}_1$ ($\vec{E}_2$) is interacting with the transition $|a\rangle \leftrightarrow |c\rangle$ ($|a\rangle \leftrightarrow |b\rangle$). These field are given by

$$\vec{E}_i = \vec{\mathcal{E}}_i e^{-i\omega_i t} + \vec{\mathcal{E}}_i^* e^{i\omega_i t} \ , \quad (i \in 1,2) \ . \tag{D.1}$$

The Hamiltonian in the dipole approximation can be written as

$$H_0 = \hbar(\omega_a|a\rangle\langle a| + \omega_b|b\rangle\langle b| + \omega_c|c\rangle\langle c|) - \hbar(\vec{d}_{ac}|a\rangle\langle c| + \vec{d}_{bc}|b\rangle\langle c| + \text{c.c.}).(\vec{E}_1 + \vec{E}_2) \ . \tag{D.2}$$

Using the Liouville equation taking all the decays possible into account, we

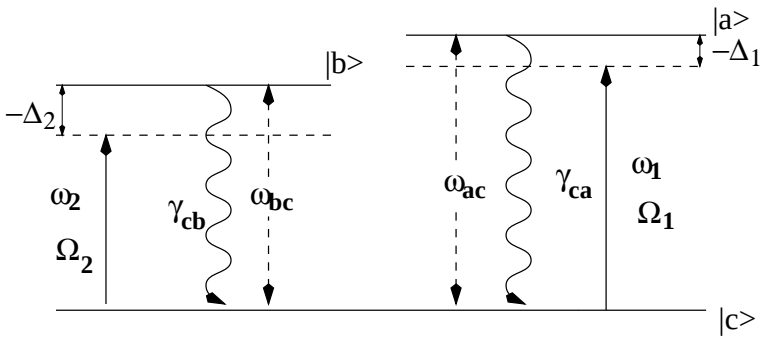

Figure D.1: Level Configuration for a V-system

obtain the following equations for the density matrix elements:

$$\begin{aligned}
\dot{\tilde{\rho}}_{aa} &= -\gamma_{ca}\tilde{\rho}_{aa} + i(\Omega_1\tilde{\rho}_{ca} - \Omega_1^*\tilde{\rho}_{ac}),\\
\dot{\tilde{\rho}}_{bb} &= -\gamma_{cb}\tilde{\rho}_{bb} + i(\Omega_2\tilde{\rho}_{cb} - \Omega_2^*\tilde{\rho}_{bc}),\\
\dot{\tilde{\rho}}_{cc} &= -\dot{\tilde{\rho}}_{aa} - \dot{\tilde{\rho}}_{bb},\\
\dot{\tilde{\rho}}_{ac} &= [i\Delta_1 - \Gamma_{ac}]\tilde{\rho}_{ac} + i[\Omega_1(\tilde{\rho}_{cc} - \tilde{\rho}_{aa}) - \Omega_2\tilde{\rho}_{ab}],\\
\dot{\tilde{\rho}}_{bc} &= [i\Delta_2 - \Gamma_{bc}]\tilde{\rho}_{bc} + i[\Omega_2(\tilde{\rho}_{cc} - \tilde{\rho}_{bb}) - \Omega_1\tilde{\rho}_{ba}],\\
\dot{\tilde{\rho}}_{ab} &= [i(\Delta_1 - \Delta_2) - \Gamma_{ab}]\tilde{\rho}_{ab} + i\Omega_1\tilde{\rho}_{cb} - i\Omega_2^*\tilde{\rho}_{ac},
\end{aligned} \tag{D.3}$$

where we have used the RWA in a rotating frame such that

$$\tilde{\rho}_{ac} = \rho_{ac}e^{i\omega_1 t}, \quad \tilde{\rho}_{ab} = \rho_{ab}e^{i(\omega_1-\omega_2)t}, \quad \tilde{\rho}_{bc} = \rho_{bc}e^{i\omega_2 t}. \tag{D.4}$$

Here we have defined the detunings Δ's and the decay terms Γ's in the following way: $\Delta_1 = \omega_1 - \omega_{ac}$; $\Delta_2 = \omega_2 - \omega_{bc}$; $\Gamma_{ac} = \frac{1}{2}\gamma_{ca} + \gamma_{\rm coll}$; $\Gamma_{bc} = \frac{1}{2}\gamma_{cb} + \gamma_{\rm coll}$; $\Gamma_{ab} = \gamma_{\rm coll}$. The half of pump and probe Rabi frequencies are defined as

$$\Omega_1 = \frac{\vec{d}_{ac}.\vec{\mathcal{E}}_1}{\hbar}; \ \Omega_2 = \frac{\vec{d}_{bc}.\vec{\mathcal{E}}_2}{\hbar}\ . \tag{D.5}$$

In steady state condition ($\dot{\tilde{\rho}}_{\alpha\beta} = 0$), we expand the density matrix elements in terms of the probe field Ω_2 ($\ll \Omega_1$) as

$$\tilde{\rho}_{\alpha\beta} = \tilde{\rho}^{(0)}_{\alpha\beta} + \frac{\Omega_2}{\gamma}\tilde{\rho}^{(1)}_{\alpha\beta}. \tag{D.6}$$

Using above, we have the following perturbative solutions:

$$\tilde{\rho}^{(0)}_{aa} = \frac{2\Gamma_{ac}|\Omega_1|^2}{\gamma_{ca}(\Gamma_{ac}^2 + \Delta_1^2) + 4\Gamma_{ac}|\Omega_1|^2}, \tag{D.7}$$

$$\tilde{\rho}^{(1)}_{bc} = -i\gamma\frac{\{\Gamma_{ab} + i(\Delta_1 - \Delta_2)\}\{\gamma_{ca}(\Gamma_{ac}^2 + \Delta_1^2) + 2\Gamma_{ac}|\Omega_1|^2\} + |\Omega_1|^2\gamma_{ca}(\Gamma_{ac} - i\Delta_1)}{\{\gamma_{ca}(\Gamma_{ac}^2 + \Delta_1^2) + 4\Gamma_{ac}|\Omega_1|^2\}[\{\Gamma_{ab} + i(\Delta_1 - \Delta_2)\}(i\Delta_2 - \Gamma_{bc}) - |\Omega_1|^2]}\ . \tag{D.8}$$

Dressed state analysis

Using the transformation $|\Psi\rangle = \exp[-i\omega_1 t|a\rangle\langle a| - i\omega_2 t|b\rangle\langle b|]|\phi\rangle$ the Schrödinger equation becomes,

$$i\hbar\frac{\partial|\phi\rangle}{\partial t} = H_{\rm eff}|\phi\rangle \tag{D.9}$$

where $H_{\rm eff}$ is the effective Hamiltonian and is given by

$$\begin{aligned}\frac{1}{\hbar}H_{\rm eff} &= -\Delta_1|a\rangle\langle a| - \Delta_2|b\rangle\langle b| - |\Omega_2||c\rangle\langle b| - |\Omega_2||b\rangle\langle c| \\ &\quad -|\Omega_1||a\rangle\langle c| - |\Omega_1||c\rangle\langle a| \end{aligned} \tag{D.10}$$

The dressed states are the eigenfunctions of this Hamiltonian. For the 'V' configuration, the three dressed can be written as :

$$|k\rangle = \alpha_k|a\rangle + \beta_k|b\rangle + \gamma_k|c\rangle \ ; \quad k = \pm, 0 \ . \tag{D.11}$$

So the eigenstates of the Hamiltonian are given by

$$\begin{pmatrix} \alpha_k \\ \beta_k \\ \gamma_k \end{pmatrix} = \frac{1}{N}\begin{pmatrix} -|\Omega_1|(\Delta_2+\omega_k) \\ -|\Omega_2|(\Delta_1+\omega_k) \\ (\Delta_1+\omega_k)(\Delta_2+\omega_k) \end{pmatrix} \ , \tag{D.12}$$

where $N = \sqrt{(\Delta_1+\omega_k)^2(\Delta_2+\omega_k)^2 + |\Omega_1|^2(\Delta_2+\omega_k)^2 + \Omega_1^2(\Delta_2+\omega_k)^2}$. The corresponding eigenvalues are,

$$\omega_k = -\frac{1}{3}A \pm \frac{2}{3}\sqrt{A^2-3B}\cos\left[\frac{1}{3}\cos^{-1}\left(\mp\frac{27C+2A^3-9AB}{2(A^2-3B)^{\frac{3}{2}}}\right)\right] \ , \tag{D.13}$$

where,

$$A = -(\Delta_1+\Delta_2), \quad B = \Delta_1\Delta_2 - |\Omega_1|^2 - |\Omega_2|^2, \quad C = |\Omega_2|^2\Delta_1 + |\Omega_1|^2\Delta_2 \ . \tag{D.14}$$

In case of single-photon as well as two-photon resonance, $\Delta_1 = \Delta_2 = 0$, the eigenvalues reduce to

$$\omega_\pm = \pm\sqrt{\Omega_1^2+\Omega_2^2} \ , \quad \omega_0 = 0 \ , \tag{D.15}$$

and the eigenstates are given by,

$$\begin{aligned}\begin{pmatrix} \alpha_+ \\ \beta_+ \\ \gamma_+ \end{pmatrix} &= \frac{1}{\sqrt{|\Omega_1|^2+|\Omega_2|^2+\omega_+^2}}\begin{pmatrix} -|\Omega_1| \\ -|\Omega_2| \\ \omega_+ \end{pmatrix} \\ \begin{pmatrix} \alpha_0 \\ \beta_0 \\ \gamma_0 \end{pmatrix} &= \frac{1}{\sqrt{|\Omega_1|^2+|\Omega_2|^2}}\begin{pmatrix} -|\Omega_2| \\ |\Omega_1| \\ 0 \end{pmatrix} \\ \begin{pmatrix} \alpha_- \\ \beta_- \\ \gamma_- \end{pmatrix} &= \frac{1}{\sqrt{|\Omega_1|^2+|\Omega_2|^2+\omega_-^2}}\begin{pmatrix} -|\Omega_1| \\ -|\Omega_2| \\ \omega_- \end{pmatrix} \end{aligned} \tag{D.16}$$

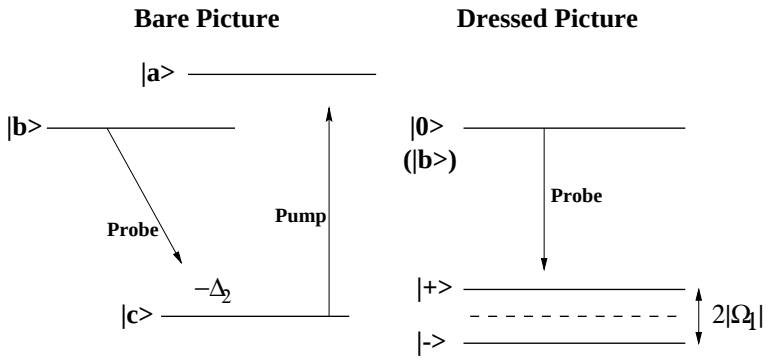

Figure D.2: Dressed state picture of V system for resonant pump field.

Now for $\Omega_2 = 0$, the dressed states become

$$|+\rangle = \frac{1}{\sqrt{2}}(-|a\rangle + |c\rangle) \ , \ |0\rangle = |b\rangle \ , \ |-\rangle = \frac{-1}{\sqrt{2}}(|a\rangle + |c\rangle) \ . \tag{D.17}$$

These dressed states are shown in Fig. D.2. The absorptions in the transitions $|b\rangle \leftrightarrow |\pm\rangle$ produce the two peaks in the absorption spectrum at $\Delta_2 = \pm|\Omega_1|$.

Appendix: E

Pulse propagation in an atomic media

We start with a Gaussian profile of a pulse passing through the medium:

$$\mathcal{E}_{in}(\omega) = \frac{\mathcal{E}_0}{\sigma\sqrt{\pi}} e^{-(\omega-\omega_0)^2/\sigma^2} \ . \tag{E.1}$$

Thus the temporal profile of this pulse can be calculated as

$$\mathcal{E}_{in}(t) = \int_{\infty}^{\infty} d\omega \mathcal{E}_{in}(\omega) e^{-i\omega(t-z/c)} = \mathcal{E}_0 e^{-\sigma^2\tau^2/4} e^{-i\omega_0\tau} \ , \tag{E.2}$$

where $\tau = t - z/c$.

After passing through the atomic medium, the output electric field in time-domain becomes

$$\mathcal{E}_{out}(t) = \int_{\infty}^{\infty} d\omega \mathcal{E}_{in}(\omega) \exp[-i\omega\{t - \frac{z}{c}(1 + 2\pi\chi(\omega)\}] \tag{E.3}$$

where $\chi(\omega)$ is the susceptibility of the dilute medium, such that $|4\pi\chi| \ll 1$.

To integrate the above, we now expand $\chi(\omega)$ in a Taylor's series about the central frequency ω_0 of the input pulse. We expand upto second order derivative of χ. Thus after integration, we obtain

$$\mathcal{E}_{out}(t) = \frac{\mathcal{E}_0}{\sqrt{Q}} \exp[-i\omega_0\{t - \frac{z}{c} - 2\pi\frac{z}{c}\chi(\omega_0)\}] e^{-P^2/4Q} \ , \tag{E.4}$$

where

$$P = \sigma \left\{ t - \frac{z}{c} - 2\pi\frac{z}{c}\chi(\omega_0) - 2\pi\omega_0\frac{z}{c}\left.\frac{\partial\chi}{\partial\omega}\right|_{\omega=\omega_0} \right\} \ , \tag{E.5}$$

$$Q = 1 - 2\pi\frac{z}{c}\sigma^2 \left\{ \frac{\omega_0}{2!}\left.\frac{\partial^2\chi}{\partial\omega^2}\right|_{\omega=\omega_0} + \left.\frac{\partial\chi}{\partial\omega}\right|_{\omega=\omega_0} \right\} \ . \tag{E.6}$$

Clearly, the input and output intensities are given by

$$|\mathcal{E}_{in}(t)|^2 = |\mathcal{E}_0|^2 \exp[-\frac{\sigma^2}{2}(t-\frac{z}{c})^2] , \tag{E.7}$$

$$|\mathcal{E}_{out}(t)|^2 = |\mathcal{E}_0|^2 \frac{1}{\sqrt{QQ^*}} e^{-P^2/2Q} = \frac{|\mathcal{E}_0|^2}{|Q|} \exp\left[-\frac{\sigma^2}{2Q}\left(t-\frac{z}{v_g}\right)^2\right] , \tag{E.8}$$

where

$$v_g = \frac{c}{n_g} , \; n_g = 1 + 2\pi\chi(\omega_0) + 2\pi\omega_0 \left.\frac{\partial\chi}{\partial\omega}\right|_{\omega=\omega_0} \tag{E.9}$$

defines the group velocity.

Clearly, in course of propagation through the atomic medium, the amplitude reduces to $1/|Q|$th of the initial amplitude, width of the output pulse changes to $\sqrt{Q}$th of the initial width, and the velocity changes from c outside the medium to c/n_g inside the medium.

We should emphasize that while passing through the medium, the width of the pulse changes. This is determined by the factor Q, which can be rewritten as

$$Q \approx 1 - iz\kappa , \quad \kappa = \frac{\sigma^2}{2c}\left[\frac{d^2}{d\omega^2}\{\omega\,[1+2\pi\chi(\omega)]\}\right]\Big|_{\omega=\omega_0} . \tag{E.10}$$

Thus the reduced output intensity becomes

$$\frac{|\mathcal{E}_0|^2}{\sqrt{QQ^*}} = \frac{|\mathcal{E}_0|^2}{\sqrt{1+2z\mathrm{Im}\kappa+2|k|^2}} \approx |\mathcal{E}_0|^2(1-z\mathrm{Im}\kappa). \tag{E.11}$$

Appendix: F

Some important issues

Calculation of spontaneous emission rate for hyperfine manifold

The problems we have dealt with in this thesis frequently require the exact values of the spontaneous emission rate from the atomic excited level. The available value A (i.e., the Einstein's A-coefficient) of this rate is defined in terms of $J \rightarrow J'$ transition (All the primed parameters are defined for the ground levels). However, whenever the problem involves the hyperfine structures, the decay rate should be properly calculated. We summarize the required formulae for this from [177] for quick reference.

The A-coefficient is defined by

$$A_{J\rightarrow J'} = \frac{4\omega^3}{3\hbar c^3}.\frac{|(J \parallel D \parallel J')|^2}{2J+1} \,, \tag{F.1}$$

where $(2J+1)$ is the multiplicity factor. The term $|(J \parallel D \parallel J')^2|$ is the reduced matrix element and can be written in terms of the reduced matrix element of the involved hyperfine levels through

$$|\vec{d}_{F,F'}| \equiv |(JIF \parallel D \parallel J'IF')|^2 = (2F+1)(2F'+1) \left\{ \begin{array}{ccc} J & F & I \\ F' & J' & 1 \end{array} \right\}^2 |(J \parallel D \parallel J')|^2 \,. \tag{F.2}$$

The terms J, I, F are self-explanatory. The curly bracketed term is the Wigner $6j$-symbol and can be calculated from the standard tables [177]. We define

$$2\gamma = \frac{4\omega^3}{3\hbar c^3}|(JIF \parallel D \parallel J'IF')|^2 \,. \tag{F.3}$$

Thus, γ can be calculated using the known value of $A_{J\rightarrow J'}$. This helps in calculating the total decay rate $A_{F,F'}$ from the F level to F' level.

Now one has to calculate the dipole matrix elements between the levels $(m_F, m_{F'})$ through the formula

$$\langle JIFm_F|D_q|J'IF'm_{F'}\rangle = (-1)^{F-m_F}(JIF \parallel D \parallel J'IF') \begin{pmatrix} F & 1 & F' \\ -m_F & q & m_{F'} \end{pmatrix} , \quad \text{(F.4)}$$

where $q = \pm 1$ for $m_F - m_{F'} = \pm 1$. The reduced matrix element is the same for a given $F \rightarrow F'$ manifold. The last term is the Wigner $3j$-symbol and can be calculated from the standard table [177]. Thus, when there are multiple decay channels, one can calculate $3j$ symbols for each transition and combining all these, one finds the value of γ from the known value of A. As A has the dimension of frequency (conventionally it is defined as $2\pi\times$ a few MHz), the parameter γ also has the same dimension.

Here we are using the following convention: For $m_F - m_{F'} = \pm 1$, the unit vector for the dipole moment matrix element will be $\hat{\epsilon}_{\mp}$ and the $\sigma_{\pm}$ ($\equiv \hat{\epsilon}_{\pm}$) component of the input electric field interacts with corresponding transition. Note that $\hat{\epsilon}^*_{\pm}.\hat{\epsilon}_{\pm} = 1$.

Zeeman splitting

Having known the value of γ, we can calculate the value of magnetic field required for certain Zeeman splitting, say, $B = n\gamma$, n being any multiplicity factor. We identify this with the Zeeman separation ΔE through the relation

$$\Delta E = -\mu_B g_F m_F M = \hbar B , \quad \text{(F.5)}$$

where M is the magnitude of the applied magnetic field, g_F is the hyperfine Lande' g-factor, and μ_B is the Bohr magneton. Note that the level $m_F = +1$ ($m_F = -1$) shift downward or upward upon application of the magnetic field, depending upon whether g_F is positive (negative) or negative (positive). The term g_F can be calculated from the following formulae.

$$g_J = 1 + \frac{J(J+1) - L(L+1) + S(S+1)}{2J(J+1)} , \quad \text{(F.6)}$$

$$g_F = g_J \times \frac{F(F+1) + J(J+1) - I(I+1)}{2F(F+1)} . \quad \text{(F.7)}$$

Calculation of power of the applied field

Because most often in the thesis, we are dealing with weak and strong fields,

it is very important how much power it refers to. The half of the Rabi frequency is generally defined as a multiple of the parameter γ. Thus it has the dimension of frequency. Further, we know $G = |\vec{d}_{\alpha\beta}||\vec{\mathcal{E}}_0|/\hbar$. Clearly one has to know the dipole moment matrix element $|\vec{d}_{\alpha\beta}|$, so that we can calculate $|\mathcal{E}_0|$. The power of the field is given by the magnitude of the Poynting vector $\vec{S} = (c/4\pi)(\vec{E} \times \vec{B})$ [1] and it can simply expressed as

$$P = \frac{c}{2\pi}|\mathcal{E}_0|^2 \ . \tag{F.8}$$

As we have discussed in this Appendix, the dipole moment matrix element is given by the reduced matrix element $|(J \parallel D \parallel J')|$ multiplied by some number. This reduced matrix element is given by

$$|(J \parallel D \parallel J')| = \sqrt{\frac{3}{2}\left(\frac{\lambda}{2\pi}\right)^2 A\hbar} \ , \tag{F.9}$$

where λ is the transition wavelength. Using all these relations and putting the values of all the relevant parameters in CGS unit, one calculates the power P in erg s^{-1} cm^{-2} unit.

Appendix: G

Analytical calculation for susceptibility in a Doppler-broadened medium

In this appendix, we show how one can integrate the Eq. (3.20). We replace δ and Δ in the expressions for $\bar{\chi}_{\pm}$ by their Doppler-shifed values $\delta_v = \delta + kv_z$ and $\Delta_v = 2B + k_p v_z$. Thus changing the integration variable from v_z to δ_z, we find that the integration in (3.20) takes the following form:

$$\langle \bar{\chi}_{\pm}(\delta_v) \rangle = \frac{1}{\sqrt{2\pi\omega_D^2}} \int_{-\infty}^{\infty} \bar{\chi}_{\pm}(\delta_v) \exp\{-\frac{(\delta_v - \delta)^2}{2\omega_D^2}\} d\delta_v \ . \tag{G.1}$$

The standard form of the error function [175] is given by

$$W(\xi) = \frac{i}{\pi} \int_{-\infty}^{\infty} \frac{e^{-t^2}}{\xi - t} dt \ . \tag{G.2}$$

Comparing the form (G.1) and the above formula, we have the following results for the averages:

$$\langle \bar{\chi}_{\pm}(B) \rangle = \frac{\sqrt{\pi}\alpha_0\gamma^2}{2i\omega_D^2} W(\xi_{\pm}) \ , \tag{G.3}$$

where

$$\begin{aligned} \xi_+ &= \frac{1}{\sqrt{2}\omega_D} \left[-\frac{|\Omega|^2}{\delta - \Delta + 3B + i\Gamma_{fg}} - (\delta + B + i\Gamma_{e-g}) \right] \ , \\ \xi_- &= \frac{-\delta + B - i\Gamma_{e+g}}{\sqrt{2}\omega_D} \ . \end{aligned} \tag{G.4}$$

References

[1] J. D. Jackson, *Classical Electrodynamics* (Wiley, New York, 1962).

[2] P. A. M. Dirac, *The Principles of Quantum Mechanics* (Oxford, 1958).

[3] P. Mandel and E. Wolf, *Optical Coherence and Quantum Optics* (Cambridge University Press, Cambridge, 1995).

[4] G. S. Agarwal, *Quantum Statistical Theories of Spontaneous Emission and their relation to other approaches* (Springer-Verlag, Berlin, 1974).

[5] M. Sargent III, M. O. Scully, and W. E. Lamb, Jr., *Laser Physics* (Addison-Wesley, Massachusetts, 1974), Chapter 2.

[6] C. Cohen-Tannoudji, B. Diu, and F. Laloë, *Quantum Mechanics* (John Wiley and sons, 1977), vol. 2.

[7] L. Allen and J. H. Eberly, *Optical resonance and two-level atoms* (Wiley, New York, 1975).

[8] I. I. Rabi, Phys. Rev. A **51**, 652 (1937).

[9] P. L. Knight and P. W. Milonni, Phys. Rep. **66**, 21 (1980).

[10] S. Swain, in *Advances in Atomic and Molecular Physics*, Eds. D. R. Bates and B. Bederson **16**, 159 (1980).

[11] see [1], Sec. 7.10, p. 309.

[12] B. R. Mollow, Phys. Rev. **188**, 1969 (1969).

[13] W. Hartig, W. Rasmussen, R. Schieder, and H. Walther, Z. Phys. A **278**, 205 (1976).

[14] R. E. Grove, F. Y. Wu, and S. Ezekiel, Phys. Rev. A **15**, 227 (1977).

[15] B. R. Mollow, Phys. Rev. A **5**, 2217 (1972).

[16] S. Haroche and F. Hartmann, Phys. Rev. A **6**, 1280 (1972); S. L. McCall, *ibid.* **9**, 1515 (1974).

[17] F. Y. Wu, S. Ezekiel, M. Ducloy, and B. R. Mollow, Phys. Rev. Lett. **38**, 1077 (1977); M. T. Gruneisen, K. R. MacDonald, and R. W. Boyd, J. Opt. Soc. Am. B **5**, 123 (1988); W. V. Davis, A. L. Gaeta, R. W. Boyd, and G. S. Agarwal, Phys. Rev. A **53**, 3625 (1996).

[18] G. Khitrova, J. F. Valley, and H. M. Gibbs, Phys. Rev. Lett. **60**, 1126 (1988); A. Lezama, Y. Zhu, M. Kanskar, and T. W. Mossberg, Phys. Rev. A **41**, 1576 (1990).

[19] G. S. Agarwal, Phys. Rev. A **19**, 923 (1979).

[20] D. Grandclement, G. Grynberg, and M. Pinard, Phys. Rev. Lett. **59**, 44 (1987); G. Grynberg and P. R. Berman, Phys. Rev. A **39**, 4016 (1989).

[21] G. Yu. Kryuchkyan, Opt. Commun. **54**, 19 (1985); G. S. Agarwal, Y. Zhu, D. J. Gauthier, and T. W. Mossberg, J. Opt. Soc. Am. B **8**, 1163 (1991); Z. Ficek and K. S. Freedhoff, Phys. Rev. A **48**, 3092 (1993).

[22] Q. Wu, D. J. Gauthier, and T. W. Mossberg, Phys. Rev. A **49**, 1519 (1994); **50**, 1474 (1994); C. C. Yu, J. R. Bochinski, T. M. Kordich, and T. W. Mossberg, *ibid.* **56**, 4381 (1997).

[23] R. W. Boyd, M. G. Raymer, P. Narum, and D. J. Harter, Phys. Rev. A **24**, 411 (1981); G. S. Agarwal and R. W. Boyd, *ibid.* **38**, 4019 (1988).

[24] G. S. Agarwal and W. Harshawardhan, Phys. Rev. A **50**, 4465 (1994).

[25] G. S. Agarwal, Progress in Optics **XI** Ed. E. Wolf (Amsterdam, North Holland, 1973), 1.

[26] G. Alzetta, A. Gozzini, L. Moi, and G. Orriols, Nuovo Cimento Soc. B **36**, 5 (1976).

[27] R. M. Whitley and C. R. Stroud Jr., Phys. Rev. A **14**, 1498 (1976).

[28] H. R. Grey, R. M. Whitley, and C. R. Stroud Jr., Opt. Lett. **3**, 218 (1978).

[29] C. Cohen-Tannoudji and S. Reynaud, J. Phys. B. **10**, 2311 (1977).

[30] G. S. Agarwal and S. S. Jha, J. Phys. B **12**, 2655 (1979).

[31] For an excellent review on CPT, see E. Arimondo, in *Progress in Optics* **XXXV** Ed. E. Wolf (North Holland, Amsterdam, 1996), p. 257.

[32] E. Arimondo and G. Orriols, Nuovo Cemento Lett. **17**, 333 (1976).

[33] G. S. Agarwal, Phys. Rev. Lett. **37**, 1383 (1976); S. Swain, Adv. At. Mol. Phys. **16**, 159 (1980).

[34] F. T. Hioe and C. E. Carroll, Phys. Rev. A **37**, 3000 (1988); V. S. Smirnov, A. M. Tumaikin, and V. I. Yudin, Sov. Phys. JETP **69**, 913 (1989).

[35] J. D. Stettler, C. M. Bowden, N. M. Witrol, and J. H. Eberly, Phys. Lett. A **73**, 171 (1979).

[36] P. L. Knight, Comm. At. Mol. Phys. **15**, 193 (1984).

[37] I. V. Jyotsna and G. S. Agarwal, Phy. Rev. A **53**, 1690 (1996).

[38] F. Renzoni, A. Lindner, and E. Arimondo, Phys. Rev. A **60**, 450 (1999).

[39] R. Höller, F. Renzoni, L. Windholz, and J. H. Xu, J. Opt. Soc. Am. B **14**, 2221 (1997).

[40] J. E. Thomas, P. R. Hemmer, S. Ezekiel, C. C. Leiby Jr. R. H. Picard, and C. R. Wills, Phys. Rev. Lett. **48**, 867 (1982); P. L. Knight, Nature **297**, 16 (1982).

[41] A. Aspect, E. Arimondo, R. Kaiser, N, Vansteenkiste, and C. Cohen-Tannoudji, Phys. Rev. Lett. **61**, 826 (1988).

[42] A. Godone, F. Levi, and J. Vanier, Phys. Rev. A **59**, 12 (1999).

[43] K. Bergmann, H, Theuer, and B. W. Shore, Rev. Mod. Phys. **70**, 1033 (1998).

[44] W. Harshawardhan and G. S. Agarwal, Phys. Rev. A **53**, 1812 (1996).

[45] G. S. Agarwal, Phys. Rev. Lett. **71**, 1351 (1993); M. Fleischhauer, *ibid.* **72**, 989 (1994).

[46] K. J. Boller, K. Imamoglu, and S. E. Harris, Phys. Rev. Lett. **66**, 2539 (1991); J. E. Field, K. H. Hann, and S. E. Harris, *ibid.* **67**, 3062 (1991).

[47] S. H. Autler and C. H. Townes, Phys. Rev. **100**, 707 (1955).

[48] J. H. Hertz, K. Hoffman, W. Brunner, H. Paul, G. Ritcher, and H. Steudel, Phys. Lett. A **26**, 156 (1968).

[49] G. S. Agarwal, Phys. Rev. A **55**, 2467 (1997).

[50] Y. Li and M. Xiao, Phys. Rev. A **51**, 4959 (1995).

[51] M. Xiao, Y. Li, S. Jin, and J. Gaebanacloche, Phys. Rev. Lett. **74**, 666 (1995); J. Gaebanacloche, Y. Li, S. Jin, and M. Xiao, Phys. Rev. A **51**, 576 (1995); Y. Li and M. Xiao, Phys. Rev. A **51**, 2703 (1995).

[52] R. R. Moseley, S. Shepherd, D. J. Fulton, B. D. Sinclair, and M. H. Dunn, Phys. Rev. Lett. **74**, 670 (1995); Opt. Commun. **119**, 61 (1995); S Shepherd, D. J. Fulton, and M. H. Dunn, Phys. Rev. A **51**, 2730 (1995).

[53] D. J. Fulton, S. Shepherd, R. R. Moseley, B. D. Sinclair, and M. H. Dunn, *ibid.* **52**, 2302 (1995); J. R. Boon, E. Zekou, D. McGloin, and M. H. Dunn, *ibid.* **59**, 4675 (1998).

[54] G. S. Agarwal, Phys. Rev. A **51**, 2711 (1995).

[55] S. E. Harris, Phys. Rev. Lett. **77**, 5357 (1996).

[56] S. A. Hopkin, E. Usadi, H. X. Chen, and A. V. Durrant, Opt. Commun. **138**, 185 (1997); A. V. Durrant, H. X. Chen, S. A. Hopkin, and J. A. Vaccaro, *ibid.* **151** 136 (1998); M. Mitsunaga, T. Mukai, K. Watanabe, and T. Mukai, J. Opt. Soc. Am. B **13**, 2696 (1998).

[57] Y. Zhao, C. Wu, B. S. Han, M. S. Kim, and E. Awad, Phys. Rev. Lett. **79**, 641 (1997); B. S. Han and M. S. Shahriar, Opt. Lett. **22**, 1138 (1997); K. Yamamoto, K. Ichimura, and N. Gemma, Phys. Rev. A **58**, 2460 (1998); K. Ichimura, K. Yamamoto, and N. Gemma, *ibid.* **58**, 4116 (1998).

[58] M. J. Werner and A. Imamoglu, Phys. Rev. A **61**, 011801 (2000); C. L. Bentley Jr., J. Liu, and Y. Liao, *ibid.* **61**, 023811 (2000).

[59] S. E. Harris, Phys. Rev. Lett. **77**, 5357 (1996).

[60] G. S. Agarwal and R. Boyd, Phys. Rev. A **60**, 2681 (1999).

[61] S. E. Fry, X. Li, D. Nikonov, G. G. Padmabandhu, M. O. Scully, V. A. Smith, K. F. Kittel, C. Wang, R. S. Wilkinson, and S.-Y. Zhu, Phys. Rev. Lett. **70**, 3235 (1993).

[62] E. A. Korsunsky, N. Leinfellner, A. Huss, S, Baluschev, and L. Windholz, Phys. Rev. A **59**, 2302 (1999).

[63] Y. Chen, C. Lin, and I. A. Yu, Phys. Rev. A **61**, 053805 (2000); D. McGloin, M. H. Dunn, and D. J. Fulton, *ibid.* **62**, 053802 (2000).

[64] A. Kasapi, Phys. Rev. Lett. **77**, 5357 (1996).

[65] H. Y. Ling, Y. Li, and M. Xiao, Phys. Rev. A **57**, 1338 (1998); M. Mitsunaga and N. Imoto, *ibid.* **59**, 4773 (1999).

[66] S. E. Harris, Phys. Rev. Lett. **70**, 552 (1993); R. Grobe, F. T. Hioe, and J. H. Eberly, *ibid.* **73**, 3183 (1994).

[67] G. S. Agarwal, Phys. Rev. Lett. **71**, 1351 (1993).

[68] G. S. Agarwal and W. Harshawardhan, Phys. Rev. Lett. **77**, 1039 (1996).

[69] S. E. Harris and Y. Yamamoto, Phys. Rev. Lett. **81**, 3611 (1998).

[70] M. Yan, E. G. Rickey, and Y. Zhu, Phys. Rev. A **64**, 013412 (2001).

[71] S. E. Harris, Phys. Today **50**(7), 36 (1997); J. P. Marangos, J. Mod. Opt. **45**, 471 (1998).

[72] O. Kocharovskaya and Ya. I. Khanin, Sov. Phys. JETP Lett. **48**, 630 (1998).

[73] S. E. Harris, Phys. Rev. Lett. **62**, 1033 (1989).

[74] A. Imamoglu and S. E. Harris, Opt. Lett. **14**, 1344 (1989).

[75] M. O. Scully, S.-Y. Zhu, and A. Gavridiles, Phys. Rev. Lett. **62**, 2813 (1989).

[76] G. S. Agarwal, Phys. Rev. Lett. **67**, 980 (1991).

[77] J. Gao, H. Z. Zhang, H. F. Cui, Z. X. Guo, Y. Jiang, W. Q. Wang, X. G. Jin, and D. J. Li, Opt. Commun. **110**, 590 (1994).

[78] L. M. Narducci, H. M. Doss, P. Ru, M. O. Scully, S.-Y. Zhu, and C. H. Kittel, Opt. Commun. **81**, 379 (1991).

[79] S. E. Fry, X. Li, D. Nikonov, G. G. Padmabandu, M. O. Scully, V. A. Smith, K. F. Tittel, C. Wang, R. S. Wilkinson, and S.-Y. Zhu, Phys. Rev. Lett. **70**, 3235 (1993).

[80] A. S. Zibrov, M. D. Lukin, D. E. Nikonov, L. Hollberg, M. O. Scully, V. L. Velichansky, and H. G. Robinson, Phys Rev. Lett. **75**, 1499 (1995).

[81] G. G. Padmabandu, G. R. Welch, I. N. Shubin, E. S. Fry, D. E. Nikonov, M. D. Lukin, and M. O. Scully, Phys. Rev. Lett. **76**, 2053 (1996).

[82] G. S. Agarwal, Phys. Rev. A **44**, 28 (1991).

[83] S. Menon and G. S. Agarwal, Phys. Rev. A **59**, 740 (1999).

[84] O. Kocharovskaya, Phys. Rep. **219**, 175 (1992); P. Mandel, Contemporary Phys. **34**, 235 (1993); M. O. Scully, Quantum Opt. **6**, 203 (1994); M. O. Scully and M. Fleischhauer, Science **263** , 337 (1994).

[85] S. P. Tewari and G. S. Agarwal, Phys. Rev. Lett. **56**, 1811 (1986).

[86] S. E. Harris, J. E. Field, and A. Imamoglu, Phys. Rev. Lett. **64**, 1107 (1990).

[87] S. P. Tewari and G. S. Agarwal, Phys. Rev. Lett. **66**, 1797 (1991).

[88] K. Hakuta, L. Marmet, and B. P. Stoicheff, Phys. Rev. Lett. **66**, 596 (1991); Phys. Rev. A **45**, 5152 (1992).

[89] G. Z. Zhang, K. Hakuta, and B. P. Stoicheff, Phys. Rev. Lett. **71**, 3099 (1993); G. Z. Zhang, M. Kasturagwa, K. Hakuta, R. I. Thompson, and B. P. Stoicheff, Phys. Rev. A **52**, 1594 (1993).

[90] M. Jain, G. Y. Gin, and S. E. Harris, Opt. Lett. **18**, 998 (1993).

[91] M. Jain, H. Xia, G. Y. Yin, A. J. Merriam, and S. E. Harris, Phys. Rev. Lett. **77**, 4326 (1996).

[92] H. Schmidt and A. Imamoglu, Opt. Lett. **21**, 1936 (1996).

[93] P. R. Hemmer, D. P. Katz, J. Donoghue, M. Cronin-Golomb, M. S. Shahriar, and P. Kumar, Opt. Lett. **20**, 982 (1995); M. D. Lukin, P. R. Hemmer, M. Löffler, and M. O. Scully, Phys. Rev. Lett. **81**, 2675 (1998).

[94] M. D. Lukin, M. Fleischhauer, A. S. Zibrov, H. G. Robinson, V. L. Velichansky, L. Höllberg, and M. O. Scully, Phys. Rev. Lett. **79**, 2959 (1997).

[95] M. O. Scully, Phys. Rev. Lett. **67**, 1855 (1991); M. O. Scully and S.-Y. Zhu, Opt. Commun. **87**, 134 (192).

[96] A. S. Zibrov, M. D. Lukin, L. HÏlberg, D. E. Nikonov, M. O. Scully, H. G. Robinson, and L. V. Velichansky, Phys. Rev. Lett. **76**, 3935 (1996).

[97] O. Kocharovskaya, P. Mandel, and M. O. Scully, Phys. Rev. Lett. **74**, 2451 (1991); M. Löffler, D. E. Nikonov, O. Kocharovskaya, and M. O. Scully, Phys. Rev. A **56**, 5014 (1997).

[98] M. O. Scully and M. Fleischhauer, Phys. Rev. Lett. **69**, 1360 (1992); M. Fleischhauer and M. O. Scully, Phys. Rev. A **49**, 1973 (1994).

[99] L. Brillouin, *Wave propagation and group velocity* (Academic, New York, 1960).

[100] S. E. Harris, J. E. Field, and A. Kasapi, Phys. Rev. A **46**, 29 (1992).

[101] A. Kasapi, M. Jain, G. Y. Yin, and S. E. Harris, Phys. Rev. A **74**, 2447 (1995).

[102] L. V. Hau, S. E. Harris, Z. Dutton, and C. H. Behroozi, Nature **397**, 594 (1999).

[103] M. M. Kash, V. A. Sautenkov, A. S. Zibrov, L. Hollberg, G. R. Welch, M. D. Lukin, Y. Rostovtsev, E. S. Fry, and M. O. Scully, Phys. Rev. Lett. **82**, 5229 (1999).

[104] D. Budker, D. F. Kimball, S. M. Rochester, and V. V. Yashchuk, Phys. Rev. Lett. **83**, 1767 (1999).

[105] O. Schmidt, R. Wynands, Z. Hussein, and D. Meschede, Phys. Rev. A **53**, 27 (1996).

[106] M. G. Payne and L. Deng, Phys. Rev. A **64**, 031802 (2001).

[107] M. Xiao, Y.-Q. Li, S.-Z Lin, and J. Gae-Banacloche, Phys. Rev. Lett. **74**, 666 (1995).

[108] M. Scalora, R. J. Flynn, S. B. Reinhardt, R. L. Fork, M. J. Bloemer, M. D. Tocci, C. M. Bowden, H. S. Ledbetter, J. M. Bendickson, J. P. Dowling, and R. P. Leavitt, Phys. Rev. E **54**, 1078 (1996).

[109] M. S. Bigelow, N. N. Lepeshkin, and R. W. Boyd, Phys. Rev. Lett. **90**, 113903 (2003).

[110] M. Artoni, G. C. la Rocca, F. S. Cataliotti, and F. Bassani, Phys. Rev. A **63**, 023805 (2001).

[111] U. Leonhardt and P. Piwnicki, Phys. Rev. Lett. **84**, 822 (2000).

[112] J. Fiurasek, U. Leonhardt, and R. Parentani, Phys. Rev. A **65**, 011802 (2002).

[113] M. D. Lukin and A. Imamoğlu, Phys. Rev. Lett. **84**, 1419 (2000).

[114] M. Fleischhauer and M. D. Lukin, Phys. Rev. Lett. **84**, 5094 (2000).

[115] M. D. Lukin, S. F. Yelin, and M. Fleischhauer, Phys. Rev. Lett. **84**, 4232 (2000).

[116] C. Liu, Z. Dutton, C. H. Behroozi, and L. V. Hau, Nature **409**, 490 (2001).

[117] D. F. Phillips, A. Fleischhauer, A. Mair, R. L. Walsworth, and M. D. Lukin, Phys. Rev. Lett. **86**, 783 (2001).

[118] O. Kocharovskaya, Y. Rostovtsev, and M. O. Scully, Phys. Rev. Lett. **86**, 628 (2001).

[119] R. Grobe, F. T. Hioe, and J. H. Eberly, Phys. Rev. Lett. **73**, 3183 (1994).

[120] C. G. B. Garrett and D. E. McCumber, Phys. Rev. A **1**, 305 (1970).

[121] D. L. Fisher and T. Tajima, Phys. Rev. Lett. **71**, 4338 (1993).

[122] S. Chu and S. Wong, Phys. Rev. Lett. **48**, 738 (1982).

[123] A. M. Akulshin, S. Barreiro, and A. Lezama, Phys. Rev. Lett. **83**, 4277 (1999).

[124] E. Picholle, C. Montes, C. Leycuras, O. Legrand, and J. Botineau, Phys. Rev. Lett. **66**, 1454 (1991).

[125] E. L. Bolda, J. C. Garrison, and R. Y. Chiao, Phys. Rev. A **49**, 2938 (1994).

[126] E. L. Bolda, Phys. Rev. A **54**, 3514 (1996).

[127] L. J. Wang, A. Kuzmich, and A. Dogariu, Nature **406**, 277 (2000).

[128] M. Artoni, I. Carusotto, G. C. La Rocca, and F. Bassani, Phys. Rev. Lett. **86**, 2549 (2001); I. Carusotto, M. Artoni, G. C. La Rocca, and F. Bassani, *ibid.* **87**, 064801 (2001).

[129] C. Spielmann, R. Szipöcs, A. Stingl, and F. Krausz, Phys. Rev. Lett. **73**, 2308 (1994).

[130] R. Y. Chiao, Phys. Rev. A **48**, 34 (1993); R. Y. Chiao and J. Boyce, Phys. Rev. Lett. **73**, 3383 (1994).

[131] M. W. Mitchell and R. Y. Chiao, Am. J. Phys. **66**, 14 (1998).

[132] A. M. Steinberg and R. Y. Chiao, Phys. Rev. A **49**, 2071 (1994).

[133] G. Deiner, Phys. Lett. A **223**, 327 (1996).

[134] A. Kuzmich, A. Dogariu, L. J. Wang, P. W. Milonni, and R. Y. Chiao, Phys. Rev. Lett. **86**, 3925 (2001). J. Peatross, S. A. Glasgow, and M. Ware, Phys. Rev. Lett. **84**, 2370 (2000).

[135] D. Bortman-Arbiv, A. D. Wilson-Gordon, and H. Friedmann, Phys. Rev. A **63**, 043818 (2001).

[136] K. Kim, H. S. Moon, C. Lee, S. K. Kim, and J. B. Kim, Phys. Rev. A **68**, 013810 (2003).

[137] G. S. Agarwal, T. N. Dey, and S. Menon, Phys. Rev. A **64**, 053809 (2001).

[138] Md. A. I. Talukder, Y. Amagishi, and M. Tomita, Phys. Rev. Lett. **86**, 3546 (2001).

[139] M. Farady, Phil. Trans. R. Soc. **XIX**, 1 (1846).

[140] L. D. Landau and E. M. Lifshitz, and L. P. Pitaevski, *Electrodynamics of Continuous media* (Pargamon, Oxford, 1984).

[141] D. A. Van Baak, Am. J. Phys. **64**, 724 (1996).

[142] J.-P. Connerade, J. Phys. B: At. Mol. Phys. **16**, 399 (1983).

[143] G. S. Agarwal, P. Anantha Lakshmi, J.-P. Connerade, and S. West, J. Phys. B **30**, 5971 (1997).

[144] S. Wielandy and A. L. Gaeta, Phys. Rev. Lett. **81**, 3359 (1998).

[145] D. Budker, V. Yashchuk, and M. Zolotorev, Phys. Rev. Lett. **81**, 5788 (1998); D. Budker, D. F. Kimball, S. M. Rochester, and V. V. Yashchuk, Phys. Rev. Lett. **85**, 2088 (2000).

[146] V. A. Sautenkov, M. D. Lukin, C. J. Bednar, I. Novikova, E. Mikhailov, M. Fleischhauer, V. L. Velichansky, G. R. Welch, and M. O. Scully, Phys. Rev. A **62**, 023810 (2000).

[147] I. Kanorsky, A. Weis, J. Wurster, and T. W. Hänsch, Phys. Rev. A **47**, 1220 (1992).

[148] P. Jungner, T. Fellman, B. Stahlberg, and M. Lindberg, Opt. Commun. **73**, 38 (1989); K. H. Drake and W. Lange, *ibid.* **66**, 315 (1988); P. Avan and C. Cohen-Tannoudji, J. Physique Lett. **86**, L85 (1975); S. Giraud-Cotton, V. P. Kaftandjian, and L. Klein, Phys. Rev. A **32**, 2211 (1985); F. Schuller, M. J. D. Macpherson, and D. N. Stacey, Opt. Commun. **71**, 61 (1989).

[149] M. Yamamoto and S. Murayama, J. Opt. Soc. Am. **69**, 781 (1979); F. Schuller, R. B. Warrington, K. P. Zetie, M. J. D. Macpherson, and D. N. Stacey, Opt. Commun. **93**, 169 (1992); G. Nienhuis, and F. Schuller, *ibid.* **151**, 40 (1998).

[150] M. Fleischhauer, A. B. Matsko, and M. O. Scully, Phys. Rev. A **62**, 013808 (2000).

[151] I. Novikova, A. B. Matsko, V. A. Sautenkov, V. L. Velichansky, G. R. Welch, and M. O. Scully, Opt. Lett. **25**, 1651 (2000).

[152] D. Budker, D. F. Kimball, S. M. Rochester, V. V. Yashchuk, and M. Zolotorev, Phys. Rev. A **62**, 043403 (2000); D. Budker, D. F. Kimball, V. V. Yashchuk, and M. Zolotorev, *ibid.* **65**, 055403 (2002).

[153] T. Isayama, Y. Takahashi, N. Tanaka, K. Toyoda, K. Ishikawa, and T. Yabuzaki, Phys. Rev. A **59**, 4836 (1998).

[154] G. Labeyrie, C. Miniatura, and R. Kaiser, Phys. Rev. A **64**, 033402 (2001).

[155] A. B. Matsko, I. Novikova, M. O. Scully, and G. Welch, Phys. Rev. Lett. **87**, 133601 (2001).

[156] D. Budker, D. F. Kimball, S. M. Rochester, and V. V. Yashchuk, Phys. Rev. Lett. **83**, 1767 (1999).

[157] A. K. Patnaik and G. S. Agarwal, Opt. Commun. **179**, 195 (2000); *ibid.* **199**, 109 (2001).

[158] D. Budker, W. Gawlik, D. F. Kimball, S. M. Rochester, V. V. Yashchuk, and A. Weis, Rev. Mod. Phys. **74**, 1153 (2002).

[159] F. Renzoni, W. Maichen, L. Windholz, and E. Arimondo, Phys. Rev. A **55**, 3710 (1997).

[160] S. Franke-Arnold, M. Arndt, and A. Zeilinger, J. Phys. B **34**, 2527 (2001).

[161] B. S. Ham and P. R. Hemmer, Phys. Rev. Lett. **84**, 4080 (2000).

[162] G. L. J. A. Rikken and E. Raupach, Phys. Rev. E **58**, 5081 (1998).

[163] G. L. J. A. Rikken and E. Raupach, Nature (London) **390**, 493 (1997).

[164] M. Vallet, R. Ghosh, A. Le Floch, T. Ruchon, F. Bretenaker, and J.-Y. Thépot, Phys. Rev. Lett. **87**, 183003 (2001).

[165] D. L. Portigal and E. Burstein, J. Phy. Chem. Solids **32**, 603 (1971); see also V. A. Markelov, M. A. Novikov, and A. A. Turkin, JETP Lett. **25**, 378 (1977).

[166] M. P. Groenewege, Mol. Phys. **5**, 541 (1962).

[167] N. B. Baranova, Yu. V. Bogdanov, and B. Ya. Zel'dovich, Opt. Commun. **22**, 243 (1977); N. B. Baranova and B. Ya. Zel'dovich, Mol. Phys. **38**, 1085 (1979).

[168] G. Wagnière and A. Meier, Chem. Phys. Lett. **93**, 78 (1982); G. Wagniére, *ibid.* **110**, 546 (1984).

[169] L. D. Barron and J. Vrbancich, Mol. Phys. **51**, 715 (1984).

[170] P. Kleindienst and G. H. Wagniére, Chem. Phys. Lett. **288**, 89 (1998); N. K. Kalugin, P. Kleindienst, and G. H. Wagniére, Chem. Phys. **248**, 105 (1999).

[171] G. L. J. A. Rikken, J. Fölling, and P. Wyder, Phys. Rev. Lett. **87**, 236601 (2001).

[172] G. L. J. A. Rikken and E. Raupach, Nature **405**, 932 (2000).

[173] I. Carusotto, M. Artoni, G. C. La Rocca, and F. Bassani, Phys. Rev. Lett. **87**, 064801 (2001).

[174] J. J. Sakurai, *Modern quantum mechanics* (Addison-Wesley, Massachusetts, 1999), chap. 4.

[175] M. Abramowitz and I. A. Stegun, *Handbook of Mathematical Functions*,(Dover Publication, New York, 1972).

[176] M. Born and E. Wolf, *Principles of Optics*, 7th Ed. (Cambridge University Press, Cambridge, 1999), p. 630.

[177] I. I. Sobel'man, *Atomic Spectra and Radiative Transitions*, 2nd Ed. (Springer Verlag, Berlin, 1992), Sec. 9.3.6.

[178] W. J. Brown, J. R. Gardner, D. J. Gauthier, and R. Vilaseca, Phys. Rev. A **56**, 3255 (1997).

[179] M. O. Scully and M. S. Zubairy, *Quantum Optics* (Cambridge University Press, Cambridge, 1997), chapter 1.

[180] W. K. Wootters and W. H. Zurek, Nature (London) **299**, 802 (1982).

[181] D. Dieks, Phys. Lett. A **92**, 271 (1982).

[182] P. J. Bussey, Phys. Lett. A **90**, 9 (1982).

[183] N. Gisin, Phys. Lett. A **242**, 1 (1998).

[184] H. P. Yuen, Phys. Lett. A **113**, 405 (1986).

[185] P. W. Milonni and M. L. Hardies, Phys. Lett. A **92**, 321 (1982).

[186] L. Mandel, Nature (London) **304**, 188 (1983).

[187] C. E. Shannon and W. Weaver, *The Mathematical Theory of Communication*, (University of Illinois Press, Urbana, IL, 1963), p. 108.

[188] B. Schumacher, Phys. Rev. A **51**, 2738 (1995).

[189] V. Bužek and M. Hillery, Phys. Rev. A **54**, 1844 (1996).

[190] N. Gisin and S. Massar, Phys. Rev. Lett. **79**, 2153 (1997).

[191] R. F. Werner, Phys. Rev. A **58**, 1827 (1998).

[192] D. Bruß, A. Ekert, and C. Macchiavello, Phys. Rev. Lett. **81**, 2598 (1998).

[193] V. Bužek and M. Hillery, Phys. Rev. Lett. **81**, 5003 (1998) (For a review, see V. Bužek and M. Hillery, e-print: quant-ph/9801009) ; M. Keyl and R. F. Werner, J. Math. Phys. **40**, 3283 (1999) ; N. J. Cerf, J. Mod. Opt. **47**, 187 (2000).

[194] M. Koashi and N. Imoto, Phys. Rev. Lett. **81**, 4264 (1998).

[195] N. J. Cerf, A. Ipe, and X. Rottenberg, Phys. Rev. Lett. **85**, 1754 (2000) ; N. J. Cerf and S. Iblisdir, Phys. Rev. A **62**, 040301(R) (2000).

[196] H. Barnum, C. M. Caves, C. A. Fuchs, R. Jozsa, and B. Schumacher, Phys. Rev. Lett. **76**, 2818 (1996).

[197] M. Hillery and V. Bužek, Phys. Rev. A **56**, 1212 (1997); D. Bruß, D. P. DiVincenzo, A. Ekert, C. A. Fuchs, C. Macchiavello, and J. A. Smolin, *ibid.* **57**, 2368 (1998).

[198] C. Simon, G. Weihs, and A. Zeilinger, J. Mod. Opt. **47**, 233 (2000).

[199] C. Simon, G. Weihs, and A. Zeilinger, Phys. Rev. Lett. **84**, 2993 (2000).

[200] J. Ye, D. W. Vernooy, and H. J. Kimble, quant-ph/9908007.

[201] J. Kempe, C. Simon, and G. Weihs, Phys. Rev. A **62**, 032302 (2000).

List of Publications

I. Papers in Journals and Books:

1. *Improving the Fidelity of Quantum Cloning by Field-Induced Inhibition of the Unwanted Transition*, Shubhrangshu Dasgupta and G. S. Agarwal, Phys. Rev. A **64**, 022315 (2001).

2. *Coherent Medium as a Polarization Splitter of Pulses*, G. S. Agarwal and Shubhrangshu Dasgupta, Phys. Rev. A **65**, 053811 (2002).

3. *Laser Induced Breakdown of the Magnetic Field Reversal Symmetry in the Propagation of Unpolarized Light*, G. S. Agarwal and Shubhrangshu Dasgupta, Phys. Rev. A **67**, 023814 (2003).

4. *Magneto-optical Rotation of Spectrally Impure Fields and its Nonlinear Dependence on Optical Density*, G. S. Agarwal and Shubhrangshu Dasgupta, Phys. Rev. A **67**, 063802 (2003).

II. In Proceedings/Abstracts of International and National Conferences:

1. *Improvement of Fidelity of of Quantum Cloning using a Control Field*, S. Dasgupta, "International Conference on Perspectives in Theoretical Physics", p. 43, held at Physical Research Laboratory, Ahmedabad, India, 8-12, Jan., 2001.

2. *Novel Coherence Effects in a Four-level System Induced by Extra Control Field*, S. Dasgupta, "Proceedings of the DAE-BRNS National Laser Symposium", p. 486, held at Indian Institute of Technology, Kharagpur, India, 22-24 Dec., 2003.

III. Invited Talk in Delivered in Conferences/Workshops:

1. *Deutsch-Jozsa Algorithm*, "SERC School on Quantum Information and Quantum Optics", held at Physical Research Laboratory, Ahmedabad, India, 1-14 Feb., 2003.